Mesomeric Tuning At Bi Centres & The Reuse Of A Waste Product From Cage Synthesis

by

Toren Hynes

Submitted in partial fulfilment of the requirements

for the degree of Master of Science

at

Dalhousie University

Halifax, Nova Scotia

October 2022

Contents

List of Figures

Abstract

Over the past decade, there has been a great interest in using the main group elements to do transition metal-like chemistry. One method to tune their reactivity is by using ancillary ligands, which, despite being widely used to tune transition metal reactivity, has only recently been applied to the main group elements. Furthermore, most of the recent developments in main group chemistry have focused on phosphorus, boron, fluorine, and silicon, due to them being NMR active. By contrast, the chemistry of the 5th and 6th row main group elements is relatively underexplored. Our research group seeks to use ancillary ligands on heavy main group elements, thereby forcing them to adopt non-VSEPR geometries and enabling new, useful reactivity. The first half of this thesis will investigate the use of a new class of tuneable tridentate ligands to see how substituent bulk affects the structure and reactivity of the resulting bismuth compounds.

This thesis will also address the issue of chemical waste. Synthetic chemistry has made major improvements to our life over the past century, yet the reactions used to make said products often produce by-products. Reuse of by-products is cheaper and more environmentally friendly than discarding it and is one of the 12 principles of green chemistry. In the second part of this thesis, we will examine methods used to turn a waste product from our lab's polymer chemistry into an N-centered electrophile and a weakly coordinating cation, both of which we hope will be useful synthetic reagents.

List of Abbreviations and Symbols

°C	degree Celsius
Å	angstrom
AcOH	acetic acid
APCI	atmospheric pressure chemical ionization
Ar	aryl
BArF	Tetrakis[3,5-bis(trifluoromethyl)phenyl]borate
C_6D_6	benzene-d_6
$CDCl_3$	chloroform-D
cm	centimeter
DCE	1,2-dichloroethane
DCM	dichloromethane
DFT	density functional theory
Dipp	2,6-diisopropylphenyl
dppe	1,2-Bis(diphenylphosphino)ethane
dppf	1,1′-Bis(diphenylphosphino)ferrocene
ESI	electrospray ionization
Et	ethyl
Et_2O	diethyl ether
EtOAc	ethyl acetate
eV	electron volt
FT	Fourier transform
HMPA	hexamethylphosphoramide
HOMO	highest occupied molecular orbital
hv	irradiation
Hz	hertz
^{i}Pr	isopropyl
IR	infrared
J	coupling constant
kcal	kilocalorie
kg	kilogram
KIE	kinetic isotope effect
LUMO	lowest unoccupied molecular orbital
M	molar
Me	methyl
MeCN	acetonitrile
MeOTf	methyl triflate
MeO	methoxy
Mes	mesityl (2,4,6-trimethylphenyl)
mmol	millimole
MO	molecular orbital
MS	mass spectrometry
NBO	natural bond orbital
^{n}Bu, Bu	butyl group

nm	nanometer
NMR	Nuclear magnetic resonance
ONf	nonaflate
OTf	triflate
Ph	phenyl
Pn	pnictogen
ppm	parts per million
^{t}Bu	*tert*-butyl
TES	triethylsilyl
TESCl	triethylchlorosilane
THF	tetrahydrofuran
TMS	trimethylsilyl
TMSCl	trimethylchlorosilane
UV	ultraviolet
Vis	visible spectrum
VSEPR	valence shell electron-pair repulsion
XRD	X-ray diffraction
X	A leaving group, such as halide or triflate
α	alpha
β	beta
γ	gamma
δ	shift
π	pi

Acknowledgements

I would like to thank Dr. Saurabh Chitnis for being my supervisor for both my honours project (Fall 2019-Spring 2020) and my MSc. Completing an honours degree and an MSc during a global pandemic was not a trivial matter, and I am grateful for Dr. Chitnis's dedication to his work and his excellent mentoring throughout this challenging time. I would also like to thank Dr. Alex Speed for being a member of my research committee and all the expertise he has provided to me over the years.

I would also like to thank all the members of the Chitnis group, past and present. In particular, I would like to thank Nick Murphy, who I mentored in the summer of 2022, for making Ph_3PNCl, Ph_3PNI, Ph_3PNOTf, and for performing the reactions of Ph_3PNCl with the P_2N_6 cages. I would also like to thank Joe Bedard for synthesizing the P_2N_6 cages used in this work, Maxwell Lohoar for performing the reactions involving the PNP cations, Anastasiia Kutulska for her unwavering support, and Marcus Kindervater for being my mentor in the summer of 2019.

Finally, I would like to thank Dr. Mike Lumsden for assistance with NMR experiments, Dr. Katherine Marczenko, Dr. Karlee Bamford, and Dr. Jason Masuda for XRD, Mr. Xiao Feng for mass spectrometry, Mr. Ryan MacKinnon for keeping the hot plates working, Dr. Marc Whalen for being an excellent TA supervisor, and Dr. Alex Speed for providing various chemicals which contributed to this work.

Chapter 1: Introduction

1.1 Current Transition Metal Catalysis

For decades, transition-metal based compounds have been important workhorses for performing challenging organic syntheses.[1] One of the best-known examples of this is the Suzuki coupling, a reaction that forms carbon-carbon bonds under particularly mild conditions with the help of a palladium catalyst,[2] Another transition metal-catalyzed reaction, which is especially important in pharmaceutical and agrochemistry, is the Buchwald-Hartwig coupling. Usually catalyzed by palladium, it is one of the most powerful ways of making anilines.[3] Other examples include molybdenum and ruthenium-based catalysts, widely used to make macrocycles via olefin metathesis, and rhodium-based catalysts used for hydrogenation of olefins.[4] In more everyday life, rhodium, platinum, and palladium metal are widely used in vehicle catalytic converters to convert harmful carbon monoxide and nitrous oxides to carbon dioxide, nitrogen, and oxygen.[5] Finally, transition metal catalysts are widely used to turn small molecules into more valuable and useful larger ones. Examples include the Monsanto acetic acid process, which converts methanol and carbon monoxide into acetic acid using a square-planar rhodium based catalyst, the Smidt process, used to turn ethylene into acetaldehyde via a $[PdCl_4]^{2-}$ catalyst, and catalytic deuteration, which uses a tantalum catalyst, deuterium, and benzene to make the important NMR solvent, C_6D_6.[4]

While all the reactions previously mentioned are useful and important, all of them rely on second- and third-row transition metals. These metals are generally not very abundant, which tends to make them expensive.[6] Also, they are often quite poisonous,

requiring careful purification of final synthesized products, and resulting in soil contamination along major highways.[7] As a result, transition metal chemists have started moving away from the second- and third-row transition metals to explore the chemistry of the first-row transition metals, which are generally more abundant and less expensive. Nickel has been successfully used for both C-C and C-N cross-couplings in the Suzuki-Miyaura, Negishi, and Buchwald-Hartwig reactions, as it has multiple stable oxidation states and is capable of easily undergoing oxidative addition.[8] Copper has been successfully used to activate C-H bonds in heterocycles,[9] while iron catalyzes the world's most important reaction: the Haber-Bosch process, which consumes 10% of the world's energy and converts nitrogen and hydrogen into ammonia.[10] In recent years, homogenous iron catalysts have been shown to perform a wide variety of useful reactions, such as hydrodefluorination of aryl/vinyl fluorides, intramolecular hydroamination, hydrosilylation of carbonyl compounds, and hydroboration.[11] Finally, cobalt has been shown to be capable of catalyzing various cross-coupling and cycloaddition reactions.[12]

1.2 Tuning Main Group Element Centres

Homogenous catalysis can occur in several different ways, including redox catalysis, Lewis acid catalysis, and Lewis base catalysis. Transition metals are widely used in redox catalysis because they have five d-orbitals that are relatively close in energy (narrow HOMO/LUMO gap), allowing for easy and reversible changes in oxidation state.[13] By contrast, p-block elements have much wider s/p orbital energy gaps (wide HOMO/LUMO gap), which, *in general*, makes redox catalysis difficult for main group elements.[14]

The shape of main-group molecules can often be explained using the VSEPR model. In its simplest form, this model assumes ligands and lone pairs are regions of increased electron density around an element centre. Because electrons are negatively charged and repel one another, according to VSEPR, the most stable geometry of a molecule (the ground state) is the one where all the ligands and lone pairs are as far apart from one another as possible.[15] Therefore, forcing a molecule into a non-VSEPR geometry is expected to unlock new electronic structures, and hence change the reactivity, of a main group compound.[16, 17] One of the most effective ways to accomplish this is to use a chelating "pincer" type ligand. A pincer-type ligand (Figure 1) can affect the geometric structure in two ways. Firstly, it can hold multiple donors a predictable distance from each other, making the ligand less likely to fall off and helping to constrict the geometry compared to electronically similar monodentate ligands. Secondly, if those donors are connected using a rigid linker (as opposed to a flexible one), they can enforce a particular geometry around an element centre. A final benefit of pincer ligands is that the compounds made using them tend to be more thermally stable than those using labile ligands.[17, 18] These ligands are most often installed using either salt elimination reactions or acid/base chemistry.[16] While the use of pincer ligands is common in transition metal chemistry to change the energies of the d orbitals – and hence the metal's reactivity – the use of pincer ligands is still quite unusual in main-group compounds.

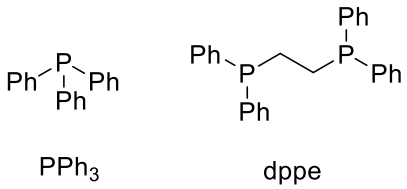

Figure 1. Triphenylphosphine (left), a common monodentate ligand, and dppe (right), a common bidentate pincer ligand.

The Chitnis research group specializes in main-group inorganic chemistry, with a particular emphasis on the chemistry of the pnictogens. The group's two focus areas are macromolecular "cage" chemistry, involving the synthesis of polymers and metal-(in)organic frameworks whose backbone is comprised of phosphorus and nitrogen-containing cages, and small molecule chemistry, mainly centered around bismuth. The Chitnis group is interested in bismuth because in addition to being the heaviest member of the pnictogens, it is also the heaviest naturally occurring non-radioactive element, which should enable it to readily access several stable oxidation states. Although the elements that surround it are toxic, bismuth has very low toxicity,[19] and is relatively abundant in the Earth's crust considering how deep in the periodic table it lies. Being that bismuth is a pnictogen, most of its compounds are pyramidal, like ammonia and triphenylphosphine. However, using the appropriate ligands, bismuth can be pushed into a planar, T-shaped geometry instead. When this is done, the symmetry around the metal centre changes from C_{3v} to C_{2v}, which results in a change in the electronic structure (Figure 2). Most notably, one of the p orbitals becomes nonbonding. This allows the metal centre to act as a Lewis base, which is quite normal for pnictogen compounds, but also as a Lewis acid, which is not something that is typically expected for pnictogens.

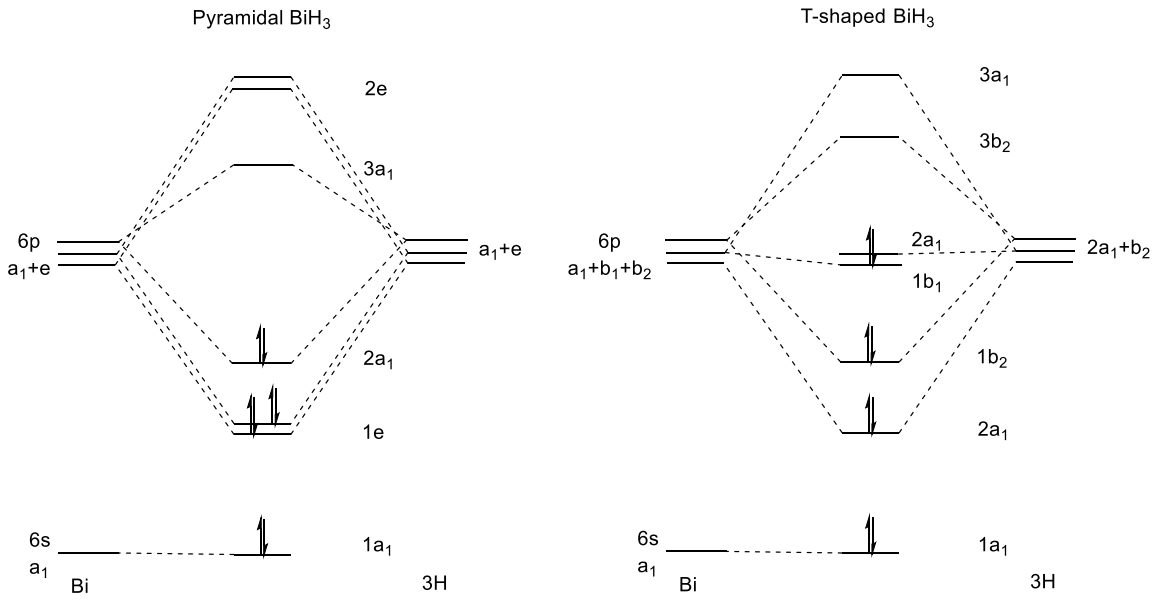

Figure 2. The MO diagram for a pyramidal BiH_3 (left) compared to a T-shaped BiX_3 (right). Note the creation of two new nonbonding orbitals in the T-shaped geometry.

In addition to the MO diagram suggesting that a planar, T-shaped Bi compound might exhibit Lewis amphoteric behaviour, it also suggests that this compound might have the potential to do redox chemistry without decomposing, because both the $1b_1$ and the $2a_1$ molecular orbitals (MO's) are nonbonding. This is similar to what is observed in transition metals, where the d orbitals are similar in energy and readily accessible for redox chemistry.[12]

Although research involving geometric distortions of main group elements is still in its infancy, compounds featuring low oxidation state p-block elements with a narrow HOMO/LUMO gap have been shown to participate in redox reactions usually performed by transition metals – as predicted by the MO diagram in Figure 2. Critically, the key steps required for a successful catalytic cycle (oxidative addition/reductive elimination) have been performed stoichiometrically by a variety of p-block elements.[14, 20]

1.3 Planar Pnictogen Compounds

1.3.1 Phosphorus

One of the earliest examples of a compound featuring a planar, T-shaped pnictogen was based on a diaminoketone ONO ligand. When this was combined with PCl_3 (Figure 3), it made a compound that was formally P (III), however, resonance structures can be drawn where the phosphorus is a P (I), with *two* lone pairs on phosphorus.[17] This compound is capable of catalytically hydrogenating azobenzene using aminoborane as a transfer agent, via a P(III)/P(V) pathway (Figure 5). It is also capable of coordinating to amines by making a new P-N bond (Figure 4).

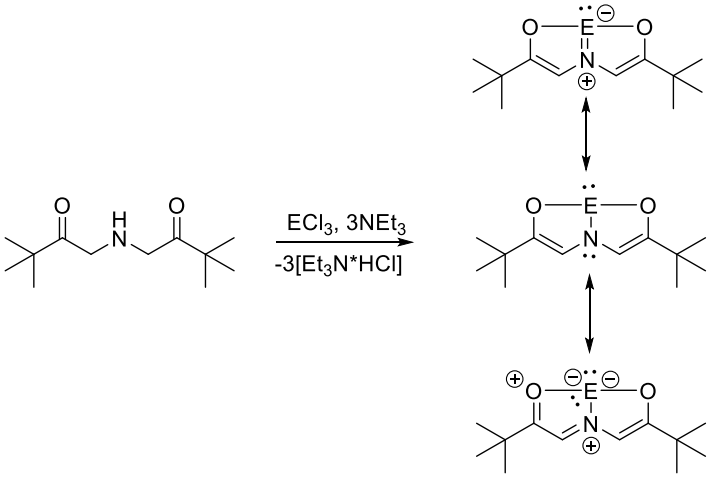

Figure 3. Synthesis of a planar phosphine based on an ONO ligand. Resonance structures show how the phosphorus shows characteristics of both a P(III) and a P (I).

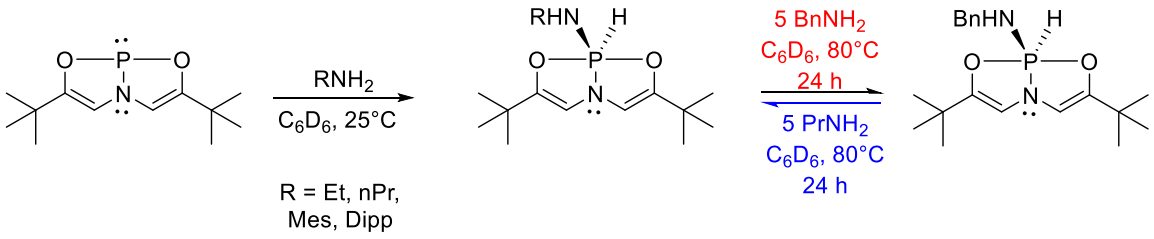

Figure 4. Reactivity of the planar phosphine with primary amines, activating them and forming a new P-N and P-H bond.

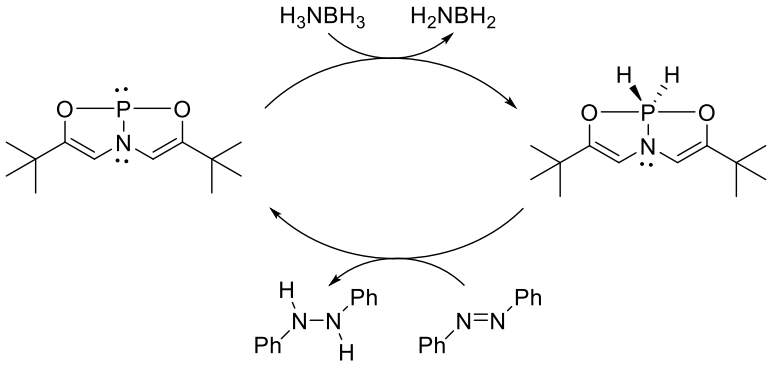

Figure 5. Catalytic reduction of azobenzene using the ONO phosphine as a catalyst and aminoborane as a hydrogen source.

A pair of planar diphosphorus compound based on thioanisole were first reported about 30 years ago by Baccolini and co-workers. Both have two sulfur atoms bonded to one phosphorus atom, and are air stable, being synthesized via a Friedel Crafts reaction (Figure 6).[21] Unfortunately, no further reactivity studies were attempted.

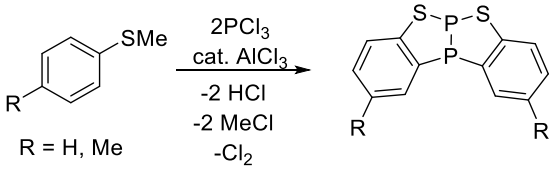

Figure 6. Synthetic protocol used by Baccolini et al. to synthesize an air stable planar diphosphine.

A NPN ligand, similar in structure to the ONO described previously, but with the heterobicyclic core of the thioanisole ligand mentioned previously, also managed to make

a planar phosphine, which could accept H_2 from aminoborane (Figure 7). It also reacted slowly with ammonia, making a new P-N bond. Unlike the ONO compound, where the oxygens of the enol stayed attached to the phosphorus when the P-N bond formed, in this complex, the ammonia substituted for the enamine, resulting in it falling off and eventually tautomerizing into an imine.[22]

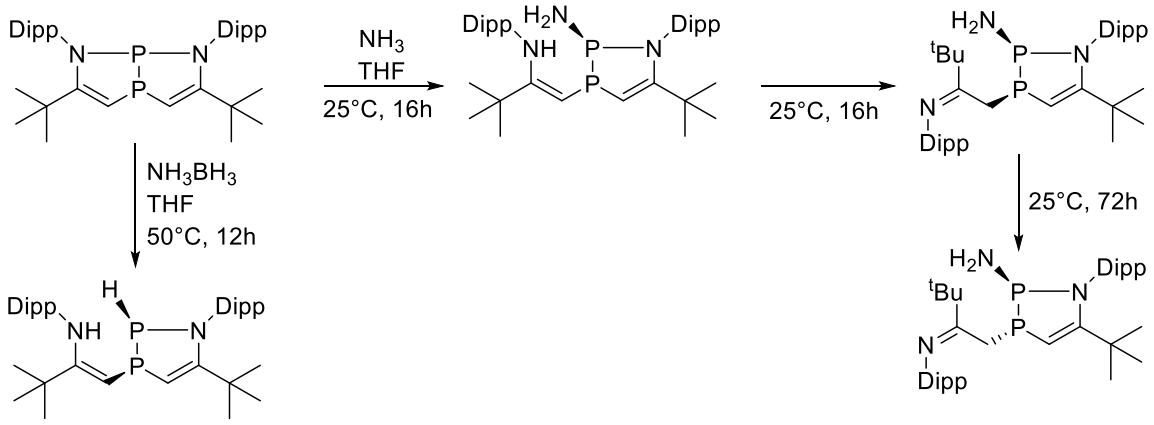

Figure 7. Reactivity of a phosphine based on an NPN ligand, with ammonia and aminoborane. Ammonia results in addition of NH_2 to the phosphine, with the proton going on the amine. Eventually, tautomerization to an imine occurs. Aminoborane instead adds H_2 across the P-N bond.

Another ONO phosphine, this one based on an aryl backbone (Figure 8), could activate the O-H and N-H bonds of water and ammonia via oxidative addition, which is similar to what had been observed with the phosphine in Figure 4. This compound did not appear to have a very high degree of P (I) character, as, despite showing amphoteric reactivity with KO^{t}Bu and MeOTf, the reaction occurred in different locations. The reaction with KO^{t}Bu at the phosphorus to give an anionic complex, while MeOTf methylated the central nitrogen atom. A compound with greater P (I) character would be expected to have been methylated at the phosphorus centre. Reaction with HCl generated the P (V) compound. Halogen sources also oxidized the phosphorus. Taken together,

these results strongly suggest that this compound had much more P (III) than P (I) character.[16, 17]

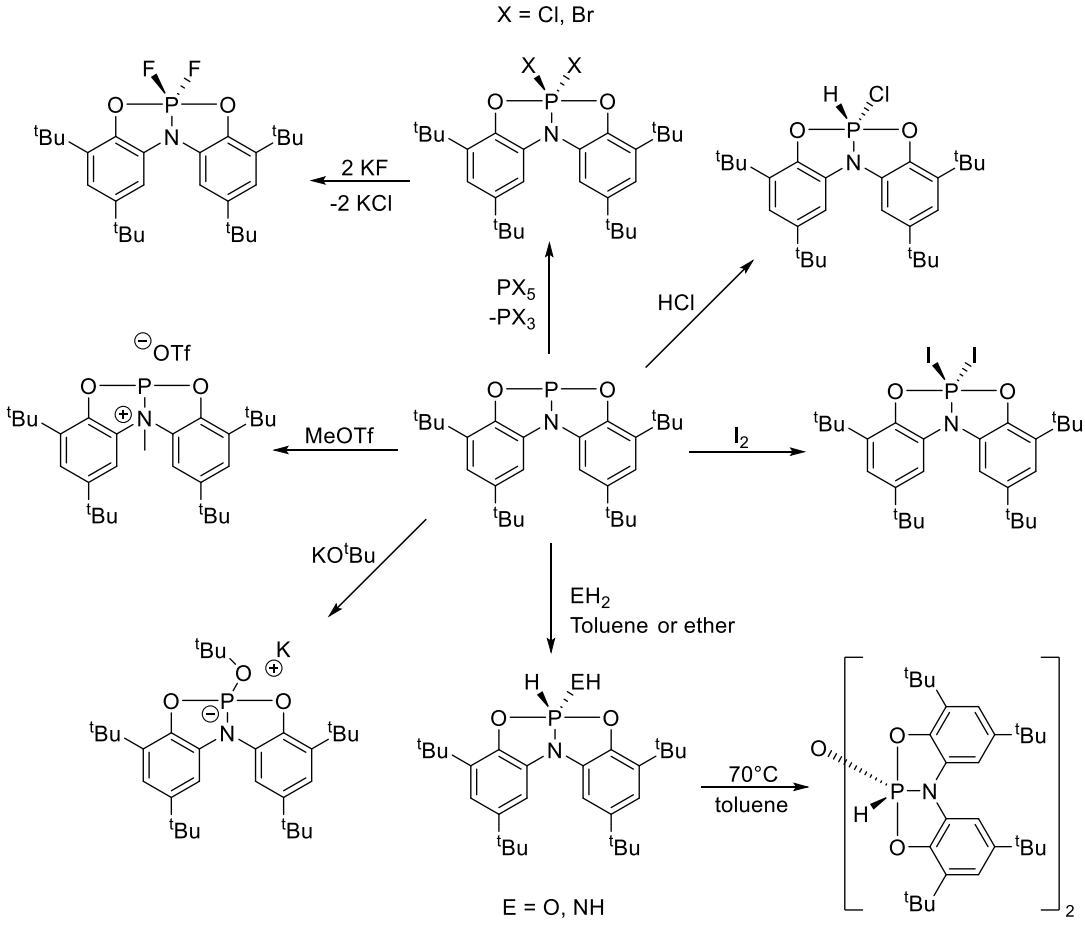

Figure 8. Various reactions of a distorted phosphine based on an ONO ligand, showing reactivity with nucleophiles, electrophiles, acids, water, amines, and halides.

In 2018, Uhl et al. used a ligand based on a silylated distyrene (Figure 9). This forced the geometry to become nearly T-shaped, resulting in significant ring strain in the two 5-membered rings containing the phosphine. The compound reacted with XeF_2, resulting in oxidation from P (III) to P (V) as in the ONO compound, but, due to the high ring strain, it was also able to react with two equivalents of sulfur and selenium, causing one the rings to expand.[23]

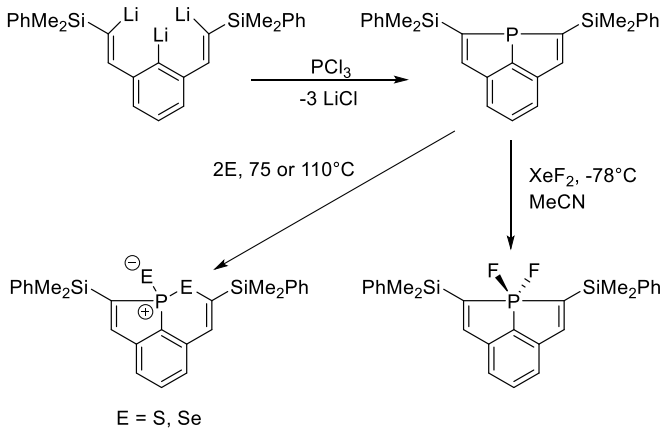

Figure 9. Synthesis of a planar phosphine based on a CCC ligand from a trilithium salt, and subsequent reactions of that phosphine with sulfur, selenium, and XeF_2.

Wang et al. recently made an NNN aryl ligand with a tethered backbone (Figure 10). While the CCC ligand resulted in a "hard" P (III) centre (Figure 9), the NNN ligand created a planar, T-shaped pnictogen centre which showed characteristics of being in both the +1 and +3 oxidation states simaltaneously, similar to the behaviour observed with the first ONO ligand. No reactivity studies were performed with these compounds, but when they were reduced using potassium metal, they formed an anionic radical where the T-shaped geometry around the pnictogen centre was preserved. [24]

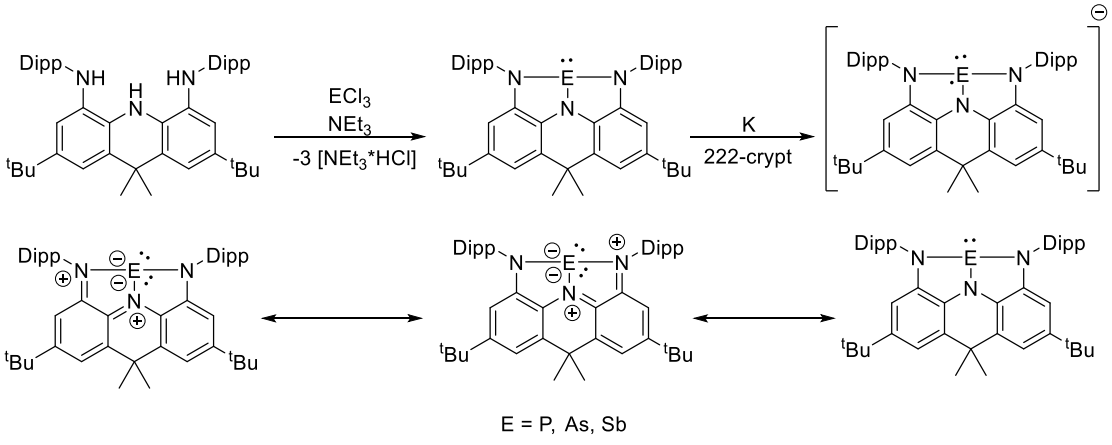

Figure 10. Using a tethered triaryl ligand to synthesize a compound with a planar, T-shaped pnictogen centre. These compounds could be reduced to an anionic radical

without losing planarity. Resonance structures showing partial Pn (I) character are also shown.

Another NNN aryl ligand, this one based on diphenylamine and lacking the tethered backbone of the previous NNN aryl ligand (Figure 11), activated amines, giving the corresponding P (V) amide hydride compounds. This reaction was like that observed for the ONO phosphine mentioned previously, but unlike the ONO phosphine, the reaction was reversible. The amine would attach to the phosphorus at room temperature but would fall off when the reaction mixture was heated to 80°C. Additionally, the compound was capable of catalyzing hydroboration of imines (Figure 12).[16]

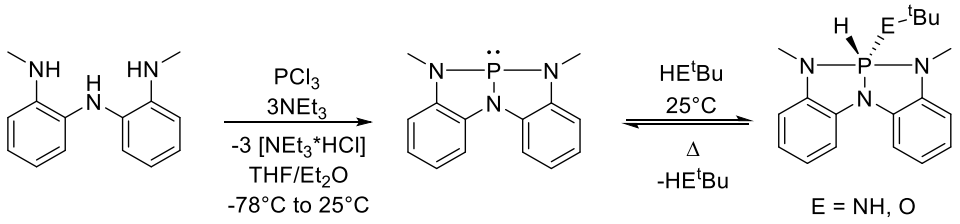

Figure 11. Installing phosphorus using PCl_3 onto a ligand based on diphenylamine. The resulting compound can activate amines and alcohols.

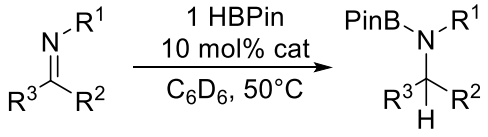

Figure 12. Protocol for hydroboration of imines using the phosphorus complex from Figure 11 as a catalyst.

Introducing a main group element into a small ring can also change its geometry via ring strain. This method was used by Radosevich for making a biphillic catalyst (Figure 13), which could carry out a wide variety of useful reactions, including the formation of heterocycles, reductive coupling of boronic acids and nitroaromatics, installation of sulfenyl groups onto indoles, and the Wittig reaction (Figure 14).[17]

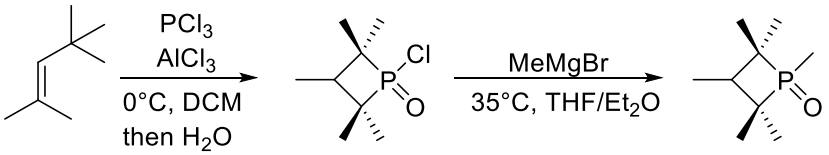

Figure 13. Synthesis of the strained phosphine oxide by Radosevich et al.

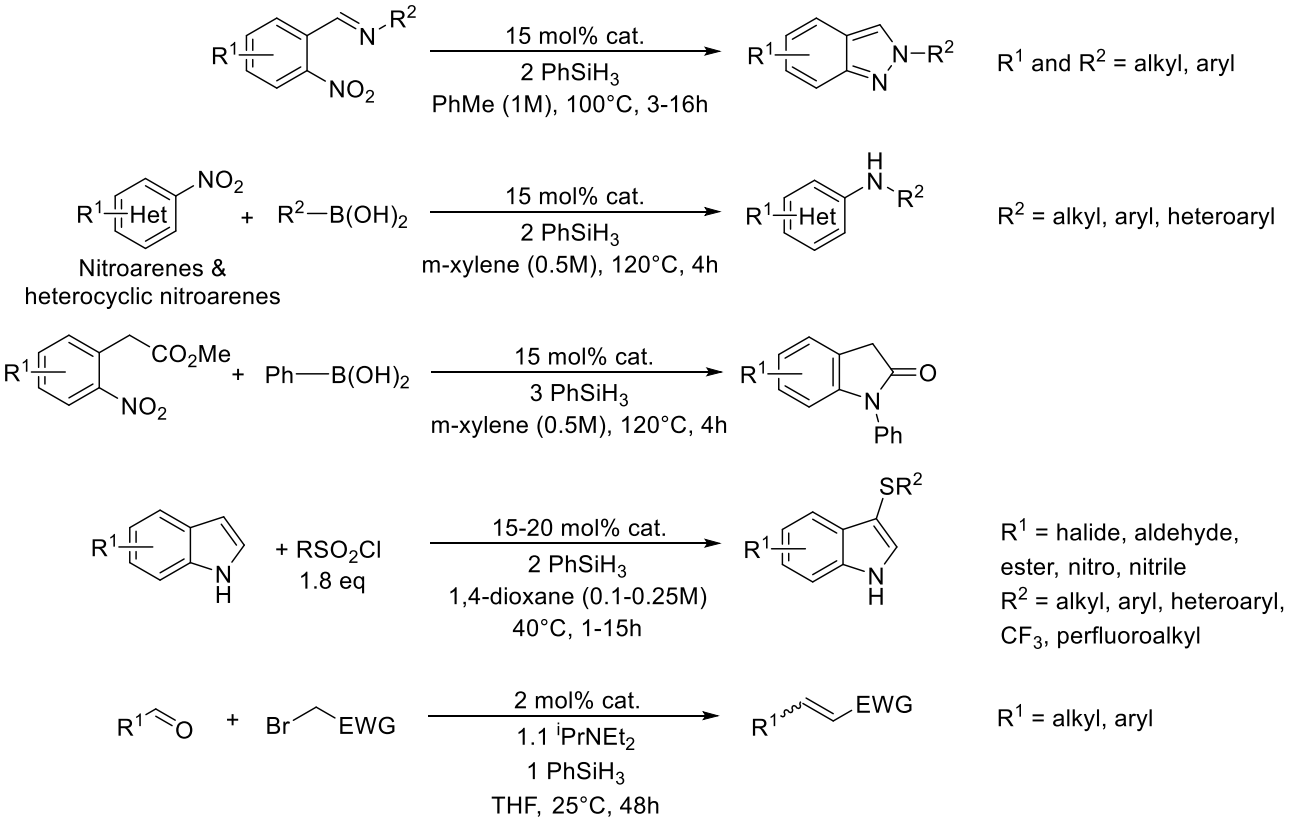

Figure 14. A variety of reactions involving the transfer of hydride from phenylsilane to various organic substrates, catalyzed by the strained phosphine oxide.

1.3.2 Arsenic, Antimony, and Bismuth

Most of the examples, up to this point, have involved the geometric distortion of a phosphorus centre using a ligand, largely because ^{31}P is NMR-active, facilitating product characterization. However, phosphorus is relatively small.[25] And, as a result, distorting it is quite challenging when compared to heavier elements. In a study of a series of pnictogen compounds by the Chitnis lab involving an NNN aryl-based pincer ligand

(Figure 15), the phosphorus and arsenic compounds were both pyramidal, as predicted by VSEPR. The antimony compound was a pyramidal dimer in the solid state and in solution at low temperatures, however, as the temperature of the solution was raised, the geometry around the Sb went from pyramidal to planar. The heaviest pnictogen, bismuth, adopted a planar geometry, both in solution and in the solid state.[26]

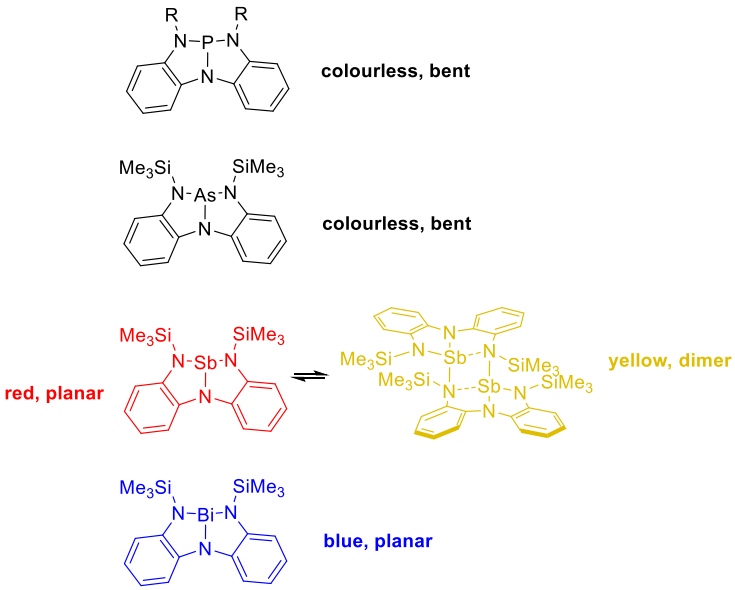

Figure 15. The structures of several Pn (III) compounds, where the heavier elements prefer to adopt a planar geometry, while the lighter ones prefer to be pyramidal. The colours of the figures are representative of the actual colours of the compounds.

This trend is entirely consistent with that observed for a series of compounds based on an NCN ligand (Figure 16): where nitrogen, phosphorus, and antimony show fluxional behaviour, Sb and Bi have hypervalent bonding patterns. This series of compounds also shows that low oxidation states become more favourable as one goes down the periodic table. Where N, P, and As are clearly all in the +3 oxidation state, Sb and Bi are firmly in the +1 oxidation state.[16]

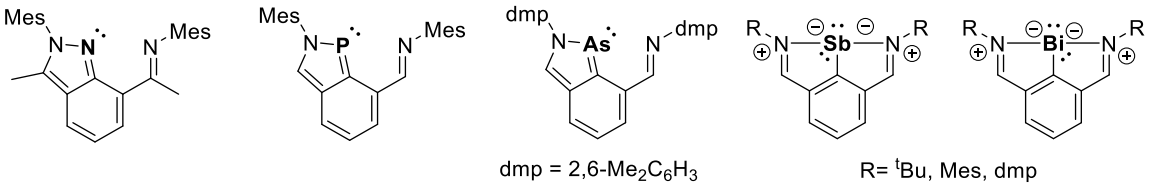

Figure 16. The structure of several pnictogen compounds based on the same ligand, showing how the heavier pnictogens are more willing to adopt lower oxidation states.

These compounds were made from a dihalide, which was reduced to a dihydride using $LiBHEt_3$ (Figure 17). This dihydride, being unstable, lost H_2, making Sb (I) and Bi (I) compounds. Additionally, the Bi (I) compound could perform catalytic hydrogenation at very low catalyst loading (1 mol %) with aminoborane as the hydrogen source, reducing azoarenes and nitroarenes to diphenylhydrazines and hydroxylamines respectively (Figure 18). This latter reaction is especially interesting given that transition metal catalysts do not typically form N-arylhydroxylamines selectively. Additionally, unlike many transition metal complexes, these reaction conditions tolerate weak bonds (such as C-I bonds) and halogenated solvents. Interestingly, the rate of the reaction is determined by the concentration of catalyst, aminoborane, and water, suggesting the substrate is not directly involved in the rate-limiting step. Although the active species is suspected to be a monomeric Bi (III) dihydride (as seen in Figure 17), such a species could never be observed experimentally. A cationic monohydride was observable via ESI-MS during catalysis, but since mass spectrometry does not reveal connectivity, it is unclear that a metal-bound hydride was formed, or a nitrogen atom was protonated.[27] It was also capable of electrocatalytic generation of hydrogen from acetic acid, something that is quite unusual for a main group element-based catalyst (Figure 18). This reaction initially involves breaking the O-H bond of two molecules of acetic acid, forming hydrogen gas and a 7-coordinate Bi (III) diacetate species. This species can subsequently

be reduced by adding two electrons.[16] Meanwhile, the Sb (I) compound added to the double bond of methyl maleimide, forming a new six-membered ring, and reversibly activating the C=C bond (Figure 19). This reaction relies on a formal Sb (I)/Sb (III) redox couple and is assisted by the ligand. [16]

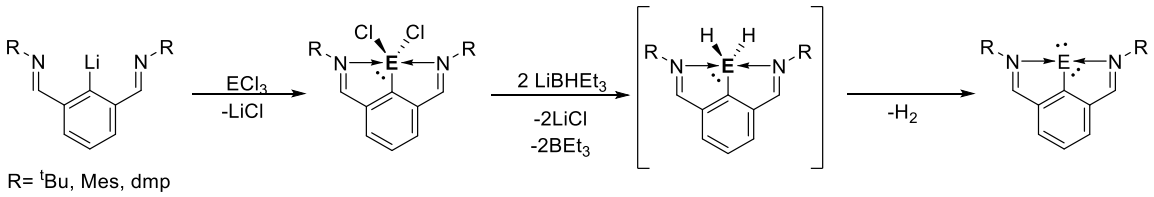

Figure 17. Reaction scheme showing how the planar Bi (I) compound was made, via dihalide and dihydride intermediates.

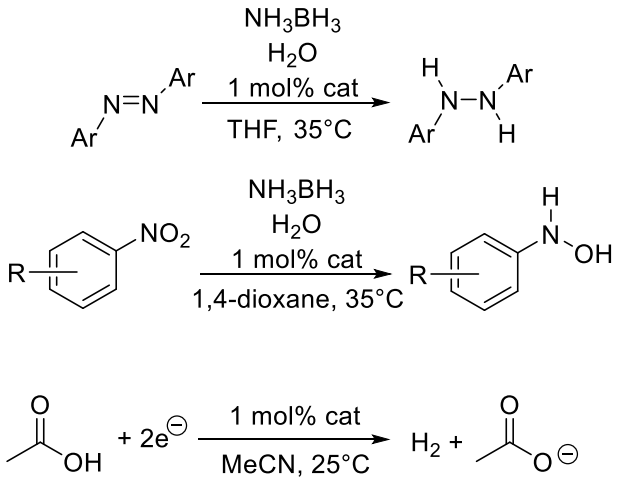

Figure 18. Three examples of reactions that the Bi (I) compound can perform: transfer hydrogenation of azobenzene, transfer hydrogenation of nitroarenes, and electrochemical catalytic formation of hydrogen gas.

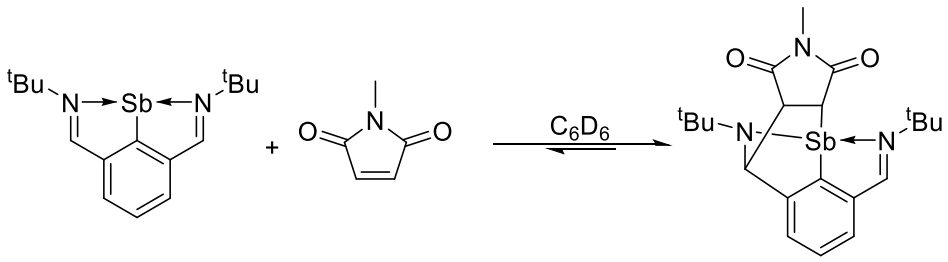

Figure 19. A scheme showing how the Sb (I) compound can activate a dienophile via a [3+2] cycloaddition.

While the hydrogenation mentioned previously used the Bi (I)/Bi (III) redox cycle, bismuth is also capable of accessing a stable Bi (V), similar to its lighter cousins. A bis-anionic aryl catalyst featuring a linking sulfonyl/sulfoximine group helps stabilize the Bi (V) state by donating electron density to the metal centre (Figure 20), while the electron-withdrawing nature of the sulfone helps ensure the bismuth is sufficiently electrophilic to enable the transmetalation and reductive elimination steps of the catalytic cycle. This bismuth compound was successful at enabling catalytic fluorination of arylboronic esters, and, with a slight modification, could also be used for converting arylboronic acids to aryl triflates and nonaflate, enabling the formation of C(sp^2)-O bonds under unusually mild conditions.[28] Usually these bonds are made via the hydrolysis of potentially explosive diazonium salts, due to the lack of a readily available source of O^+.[29]

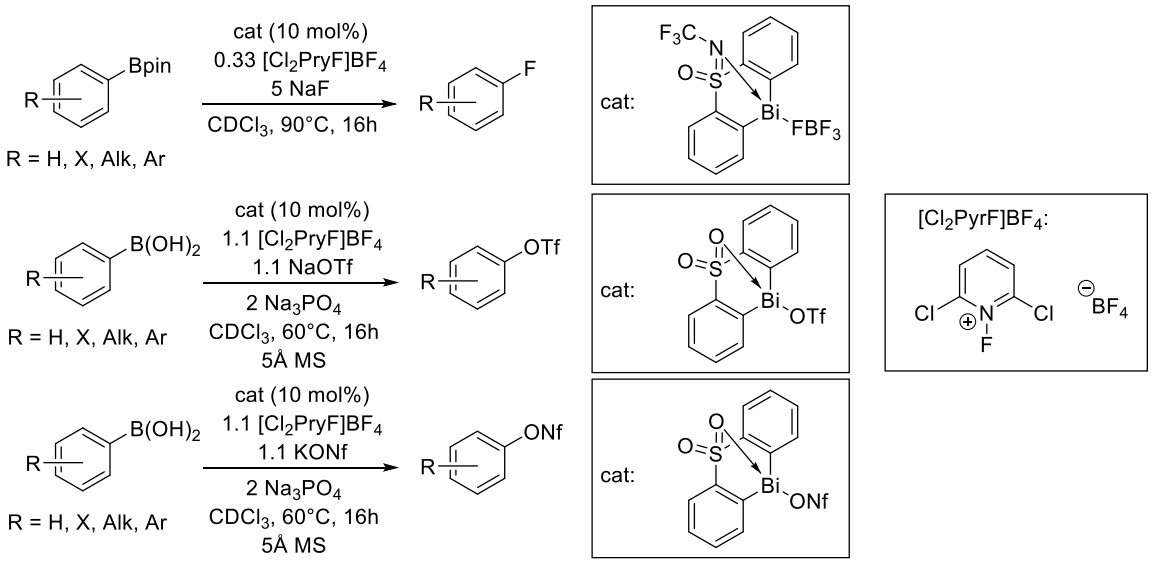

Figure 20. Using a Bi (III)/Bi (V) redox cycle to perform aryl fluorination and triflation reactions.

1.4 NNN and NCN Bismuth Compounds

1.4.1 The NNN Bismuth Compound

The Chitnis lab has worked on many planar bismuth compounds over the years. The first compound the lab created was based on a silylated *ortho*-diminobiphenyl amine (Figure 21), which will henceforth be known as the N_3TMS_2 Bi compound. When this compound was reacted with $BiCl_3$, it immediately made an intensely coloured blue solution, which is unusual, given that most Bi (III) compounds, such as triphenylbismuth, are colourless. X-ray crystallography revealed that this compound had a T-shaped planar geometry around the bismuth centre (Figure 21), which was unprecedented at the time for bismuth in this oxidation state, representing a distortion away from the typically expected pyramidal geometry (AX_3E) for such species.[30]

Figure 21. XRD-determined structure (left) and Lewis structure (right) of the N_3TMS_2 Bi compound made by the Chitnis lab, showing its planarity. Hydrogen atoms omitted for clarity.

The intense colour was the result of a ligand π orbital to metal 6p orbital charge-transfer band, which is not typically something observed in Bi, as the high energy difference between the HOMO and LUMO of pyramidal Bi in the +3 oxidation state makes ligand-to-metal charge-transfer energetically prohibitive. Additionally, just as predicted, this compound was able to act as both a Lewis acid with triethylphosphine oxide and pyridine N-oxide, as well as acting as a Lewis base with tungsten pentacarbonyl, using *the same 6p orbital* (Figure 22). NBO analysis confirmed that the occupancy of this 6p orbital was 0.99, which explained much of this unusual behaviour.

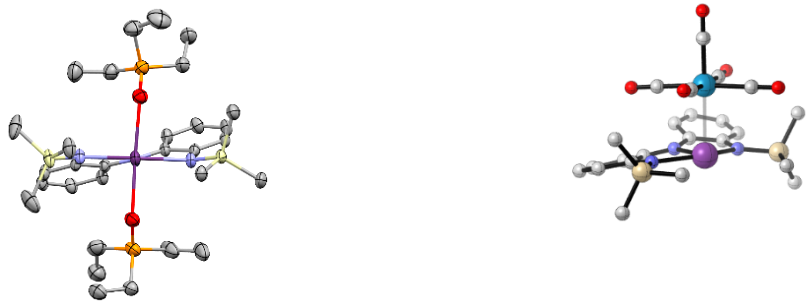

Figure 22. XRD-determined structure of the N_3TMS_2 Bi compound, coordinated to triethylphosphine oxide (left), and the. DFT-calculated structure of the same compound coordinated to tungsten pentacarbonyl (right). Hydrogen atoms have been omitted for clarity.

1.4.2 Attempts to go from Bi (III) to Bi (I)

Seeing our success with the X_3-type NNN ligand, our group wondered whether a similar framework could be used to construct an L_2X-type ligand, where two of the outer nitrogens were replaced by phosphines (Figure 23). The L and X designations in ligands refer to whether the ligand is a neutral lone pair electron donor (L-type, for example triphenylphosphine) or an anionic lone pair electron donor (X-type, for example CH_3^-). Going from an X_3 to an L_2X-type ligand would potentially enable the bismuth to be reduced from a Bi (III) to a Bi (I), which make it much more electron-rich and potentially lead to some interesting catalytic applications, as seen in work by Wang et al.[27] This ligand was relatively easy to synthesize and put on bismuth (Scheme 1), however, when reduction was attempted using various reducing agents (including phenylsilane, magnesium, lithium triethylborohydride, sodium borohydride, and potassium) the relatively weak Bi-N bond broke, resulting in the formation of free ligand and bismuth metal.[31]

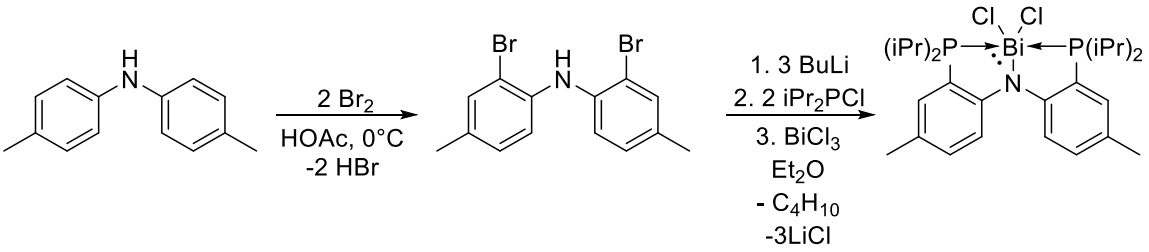

Figure 23. Synthesis of the PNP bismuth dichloride.

Nevertheless, the compound had some utility, for the chlorides could be replaced by triflates or BArF (Figure 24), which resulted in a very Lewis acidic cation capable of abstracting chloride from DCM and polymerizing THF (Scheme 2). It is likely this dication would be a powerful Lewis acid catalyst for various transformations.[31]

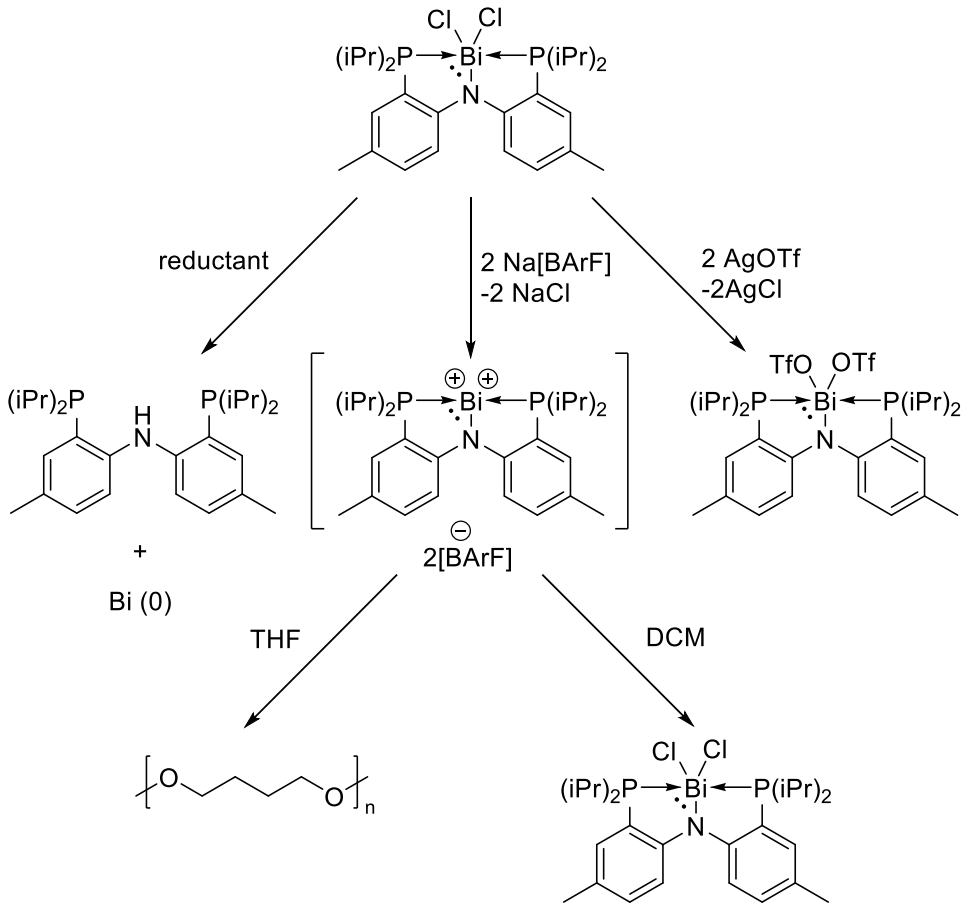

Figure 24. Various reactions of the PNP bismuth dichloride, including reduction and anion exchange.

To compensate for the weakness of the Bi-N bond, our group started to pursue research on another L_2X-type ligand (part of Toren Hynes' honours project), this one based on a xylene framework, and known as the PCP ligand (Figure 25). It was hoped that this ligand would enable the isolation of Bi (I) species due to the greater strength of the Bi-C bond. While ligand synthesis was ultimately successful, installing the bismuth was not possible, resulting in the formation of metallic deposits.

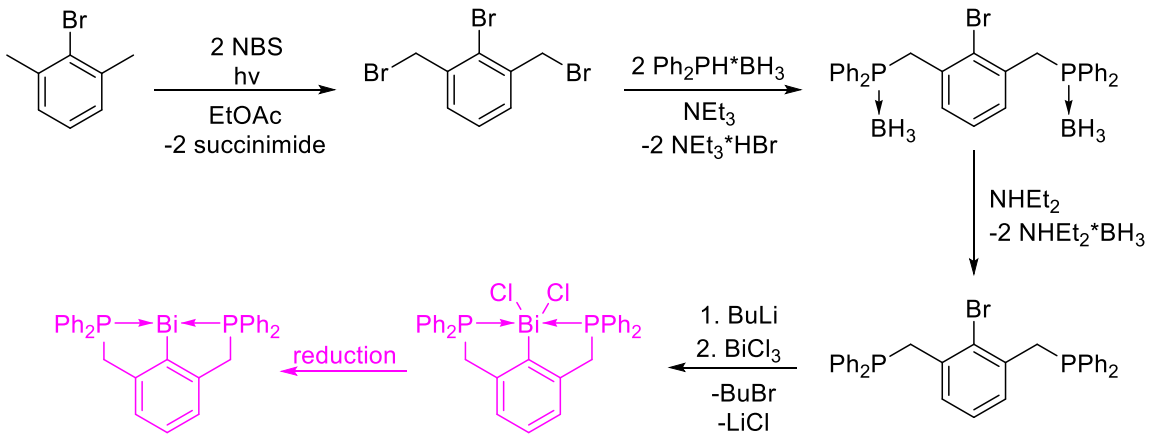

Figure 25. Synthesis of the PCP ligand from 2-bromo-m-xylene, and attempted installation of the ligand onto Bi metal.

1.4.3 A new type of Bi (III) Compound

With our group's limited success using L_2X ligands, we decided to go back to using X_3 ligands, combining the strength of the Bi-C bond with the proven success of the Bi-N bonds. Replacing the central Bi-N bond should result in a boost in Lewis acidity at the Bi centre, as the metal would have one less π donor nearby. Our interest in studying the NCN ligand grew after a large screening using DFT showed that an aniline based NCN ligand (Figure 27) did indeed offer an unusually high fluoronium ion affinity (FIA+), suggesting that it was a rather strong Lewis base. The fluoronium ion affinity is a measure of how much energy is released when an F^+ ion binds to a Lewis base in the gas phase, and is a measure of Lewis acidity, much like the fluoride ion affinity (FIA-) is a common computational measure used to estimate the strength of Lewis acids. In practice, the FIA+ could be measured by dissolving the Lewis base in a solvent such as acetonitrile, adding a source of F^+ such as N-fluoropyridinium tetrafluoroborate or SelectFluor, and measuring how much energy is released. Since this is a more realistic approximation of typical solution-state Lewis base behaviour, the values that will be

reported here are the fluoronium ion transfer energies from N-fluoropyridinium to the Lewis base of interest, with the model solvent being dichloromethane, and will be referred to as the fluoronium transfer energy (FTE; Figure 26). A higher FTE means a compound is a better Lewis base, which means the metal centre is more electron rich and should be better able to participate in oxidative addition in a redox catalytic cycle. Most importantly (Figure 27), the DFT results line up with predictions: $BiPh_3$ is a stronger Lewis base than $Bi(NMe_2)_3$ due to carbon's lower electronegativity, introducing electron-withdrawing substituents makes the N_3TMS_2 Bi compound a weaker Lewis base (while electron-donating substituents have the opposite effect), and Bi (III) compounds are weaker Lewis bases than Bi (I) compounds due to lower electron density around the metal centre.

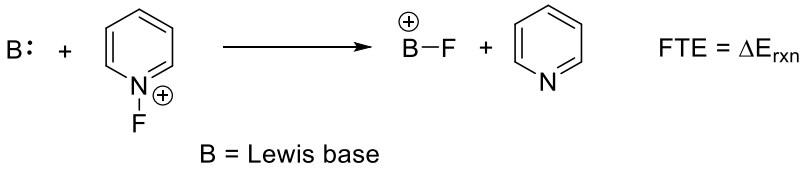

Figure 26. A general schematic of the fluoronium transfer energy (FTE), where B is a generic Lewis base.

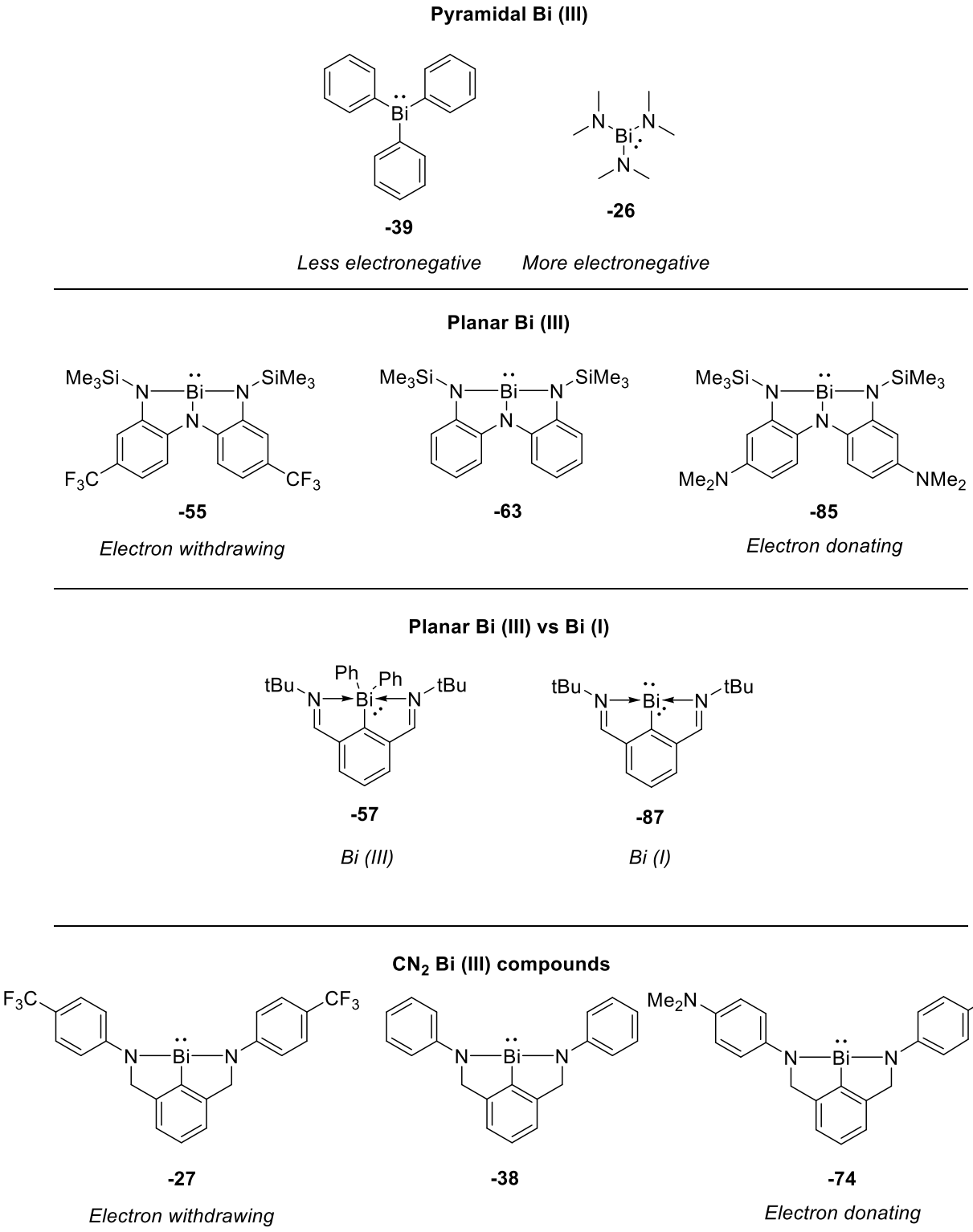

Figure 27. The energy released (kcal/mol) when F^+ is transferred from N-fluoropyridinium to the shown compounds.

Although a very similar imine-based NCN ligand had been reported by Wang et al (Figure 17).[27] and had found success in catalytic hydrogenations, this ligand was an L_2X donor. We could find no examples in the literature of a Bi (III) compound where the two nitrogens were X donors (making an X_3 ligand) and thought that it might be worthwhile comparing the reactivity of a Bi (III) compound with that of a structurally similar Bi (I) compound, where the only difference would be the oxidation state of the metal centre.

1.5 Reuse of a Synthetic Waste Product

Green chemistry is pollution prevention at the molecular level. It consists of 12 principles: elimination of waste, improving atom economy, designing a less hazardous synthesis, designing safer chemicals, using safer solvents and auxillaries, improving energy efficiency, using renewable feedstocks, eliminating derivatives, using catalysts when possible, designing reagents and products so they degrade, effective monitoring for pollution prevention, and designing safer chemistry to prevent accidents.[32]

One of the research goals in the Chitnis lab involves making aminophosphine polymers based on cages (Figure 28). These polymers are attractive for two reasons: first, polymers based on cages are predicted to have interesting material properties but are not widely used because it is difficult to make organic cages. Secondly, the phosphorus-nitrogen bonds in these polymers are expected to hydrolyse over time in the environment, which is desirable from a green chemistry point of view.

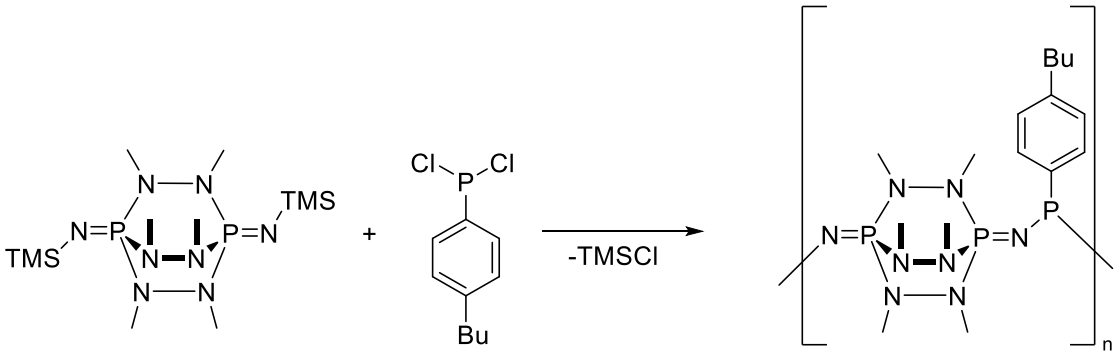

Figure 28. The general structure of the poly(cage)mers made by Bedard et al.

An important reaction in the synthesis of these polymers involves the oxidation of phosphorus and nitrogen containing cages using trimethylsilyl azide, in order to make the cages more reactive (Figure 27).[33] This activation, however, requires a large excess of trimethylsilyl azide to proceed, which must be quenched after the reaction is done, for it can be explosive if improperly stored. The quenching is done using triphenylphosphine, forming N-trimethylsilyl triphenylphosphanimine (Figure 30). As our research group has been performing cage chemistry for the past two years, a large amount of this chemical has built up. Instead of throwing it away, our group has investigated methods of turning this compound into a synthetically useful substance.

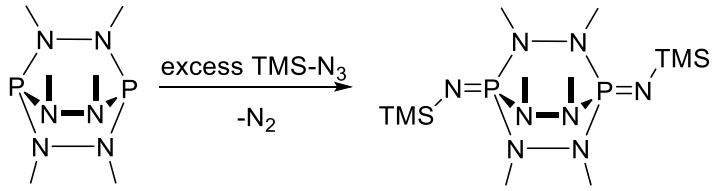

Figure 29. The Staudinger reaction used to activate the P-N cages prior to their polymerization.

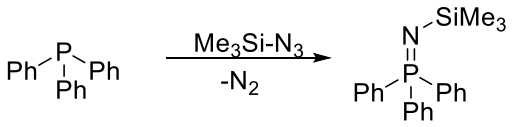

Figure 30. Synthetic protocol used to make Ph_3PNTMS.

Chapter 2: Mesomeric Tuning at Bi Centres

2.1 Contributions

Dr. Saurabh Chitnis is thanked for performing the DFT calculations for the reduction mechanism. Dr. Katherine Marczenko is thanked for performing XRD on $BiCN_2Dipp_2$. Dr. Jason Masuda is thanked for performing XRD on the $BiCN_2TMS_2$ and $BiCN_2TES_2$ dimers. Dr. Alex Speed is thanked for providing $SOCl_2$.

2.2 Ligand Synthesis

The first attempt an NCN ligand consisted of deprotonating aniline itself and reacting it with *m*-xylylene dibromide in an S_N2 fashion, following a literature procedure.[34] This compound could them be deprotonated using methyllithium (Figure 28). While the synthesis of this ligand worked alright, reacting this compound with bismuth chloride resulted in a product that was not very soluble, likely due to the compound's extensive planarity, resulting in extensive π-stacking.

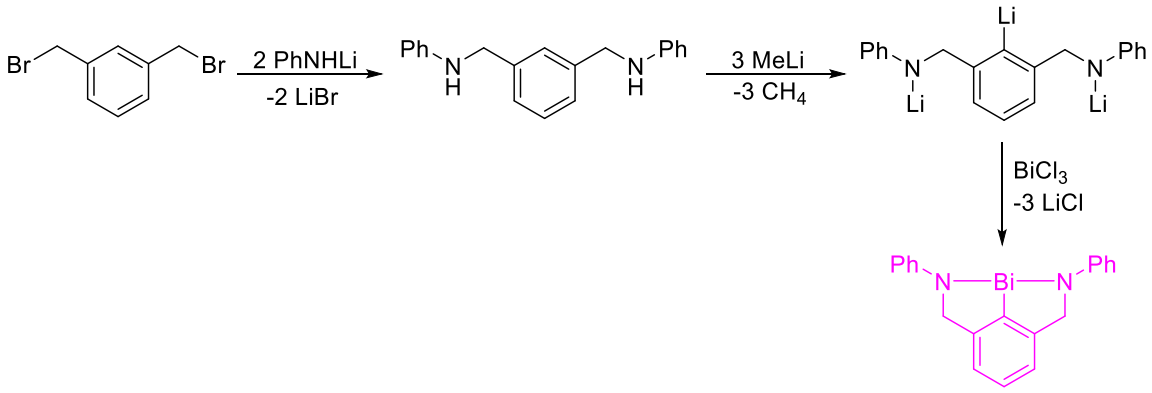

Figure 31. Synthesis of the aniline based NCN ligand and attempts to install the ligand onto bismuth.

In order to try and solve the solubility problems we switched from using aniline to 2,6-diisopropylaniline (Dipp aniline), which would help break up the π-stacking and

improve solubility. The synthesis of this ligand was essentially identical to that of the aniline-based ligand, and the trilithium salt was successfully made. When this was reacted with bismuth chloride (Figure 32), it did not make the expected Bi (III) compound. Instead of being colourless as would be expected for a Bi (III) species, the solution immediately became dark green, and the NMR spectrum showed evidence of an aldimine peak at 10.81 ppm (Figure 31), suggesting that reduction from Bi (III) to Bi (I) had taken place. This was confirmed by X-ray crystallography (Figure 33), which clearly showed that the length of the C-N bonds (1.31Å) was closer to the DFT-calculated length of a double bond (1.29Å), than a single bond (1.43Å). Additionally, a peak was visible at 4.54 ppm, which we suspect corresponds to dihydrogen gas. Unfortunately, it was not possible to isolate pure material in bulk from this reaction for further characterization, despite several attempts, which included conducting and monitoring the reaction at low temperature. In all cases, multiple products were detected, including bismuth metal and free ligand, resulting in a heterogenous reaction mixture.

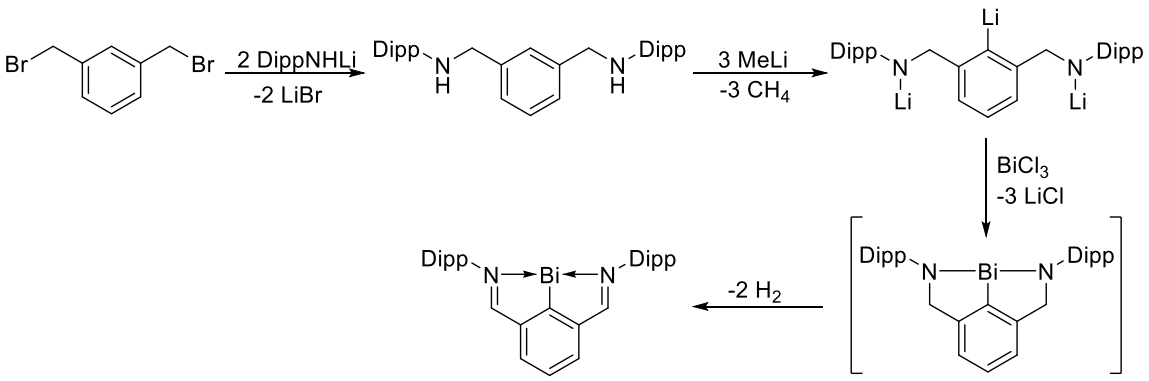

Figure 32. Synthetic scheme used to make the Dipp NCN Bi (III) compound, which unexpectedly lost H_2 to make a Bi (I) compound.

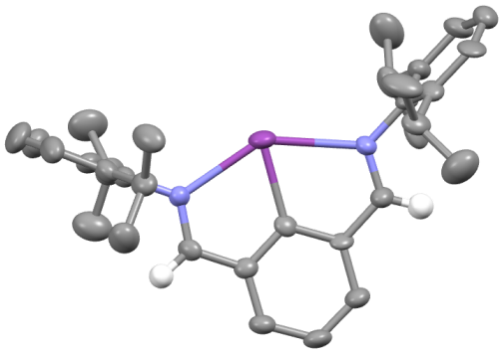

Figure 33. XRD crystal structure of the Bi (I) compound resulting from spontaneous reduction of the Bi (III) compound. All hydrogen atoms, except the aldimine ones, removed for clarity.

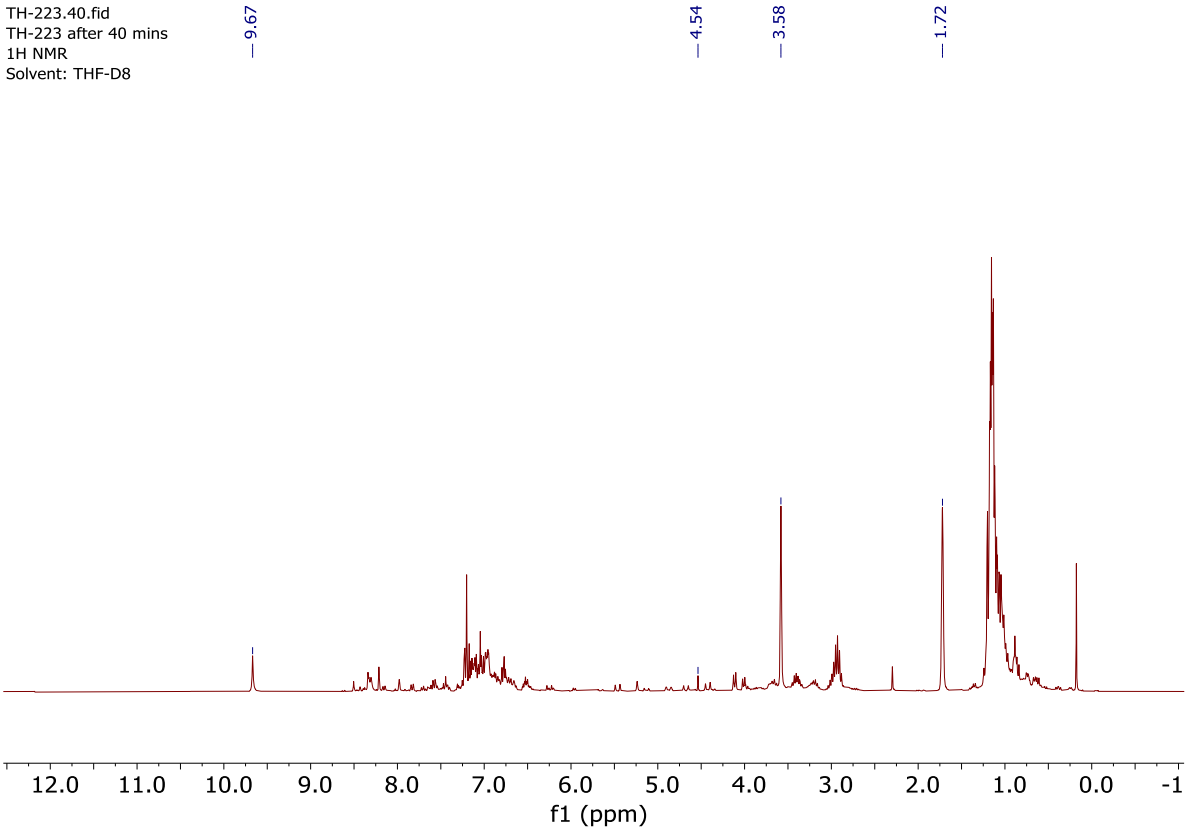

Figure 34. ^{1}H NMR spectrum of the crude reaction mixture containing $BiCl_3$ and the lithium salt in thf-d8. The picked resonances correspond to the aldimine peaks (9.67 ppm), dihydrogen (4.54 ppm), and solvent peaks (thf-d8).

Mass spectrometry also confirmed the presence of the Bi (I) compound. The most intense peak had the mass expected for the $[M+CH_3]^+$ ion, from activation of acetonitrile

in the instrument (Figure 35). Analogous activation of alkyl halides has been reported before for Bi (I) complexes.

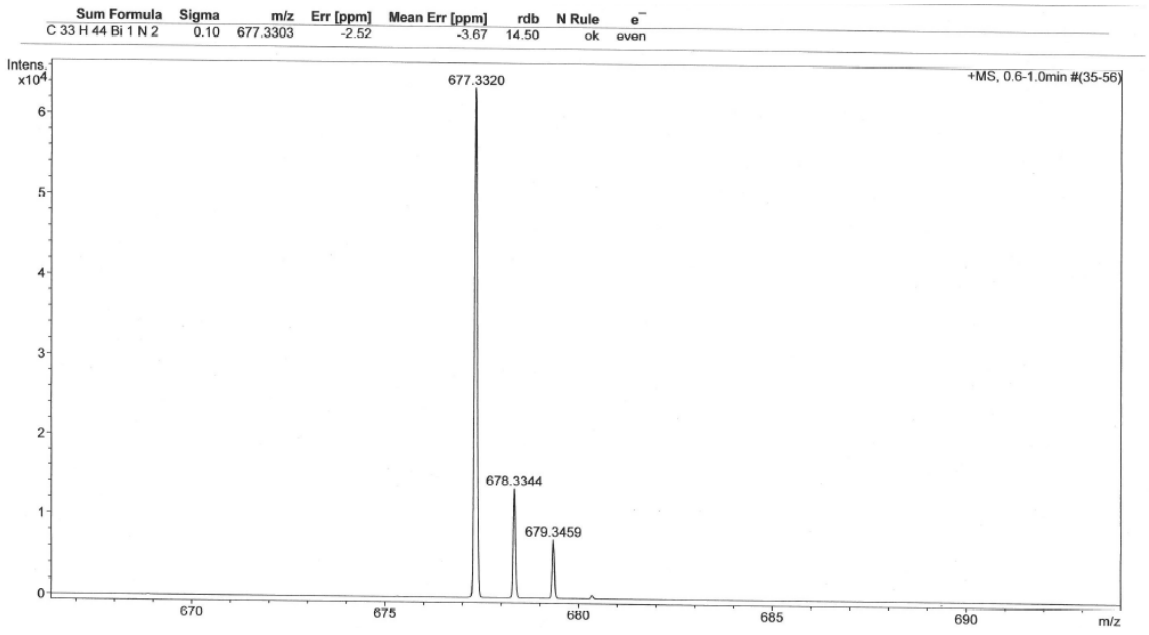

Figure 35. High-resolution ESI mass spectrum of the peak at 677.3 m/z, originating from the crude reaction mixture containing $BiCl_3$ and the lithium salt. The compound has picked up a methyl group from acetonitrile.

An attempt was made to react bismuth chloride with the dilithium salt (Figure 36), but bismuth was not capable of activating the aryl C-H bond, even when it was given extra energy via UV irradiation. Instead, the compound decomposed, forming a precipitate of Bi metal.

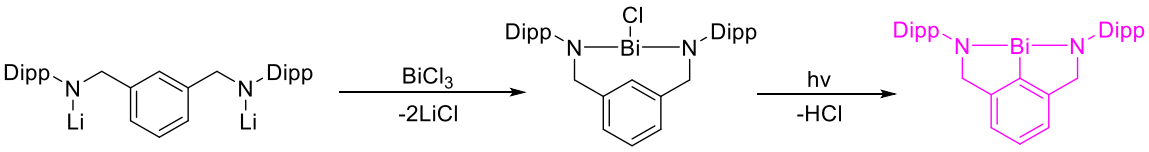

Figure 36. Attempted aryl C-H activation by Bi, starting from the dilithium Dipp salt.

With the ligand acting as a potential source of H_2, we next tried to see whether the H_2 could be "trapped" by using an easily hydrogenable compound, in this case

azobenzene (Figure 37). Unfortunately, no evidence of hydrogenation was visible, despite running the reaction on a stoichiometric scale.

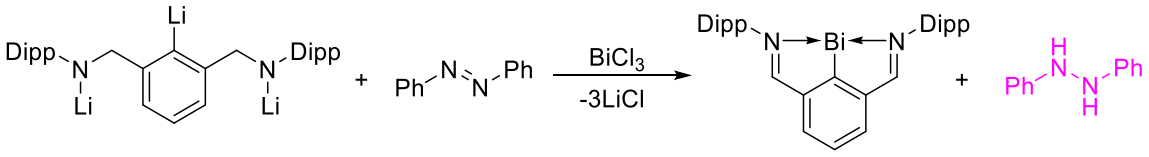

Figure 37. Attempted use of the Dipp based Bi (III) compound for hydrogenation of azobenzene.

This same lithium salt was also reacted with PCl_3, $AsCl_3$, and $SbCl_3$. With both phosphorus and arsenic, a precipitate of poor solubility was formed, and mass spectrometry showed very little, if any, product formation. We attribute this behaviour to the smaller sizes of P and As, which made it difficult for them to bond to all three sites on this chelating ligand. As a result, the product formed oligomers. With antimony, the NMR looked very similar to that of the bismuth compound, with aldimine peaks at 8.74 and 8.00 ppm (Figure 38), so we think that the same autoreduction behaviour occurred.

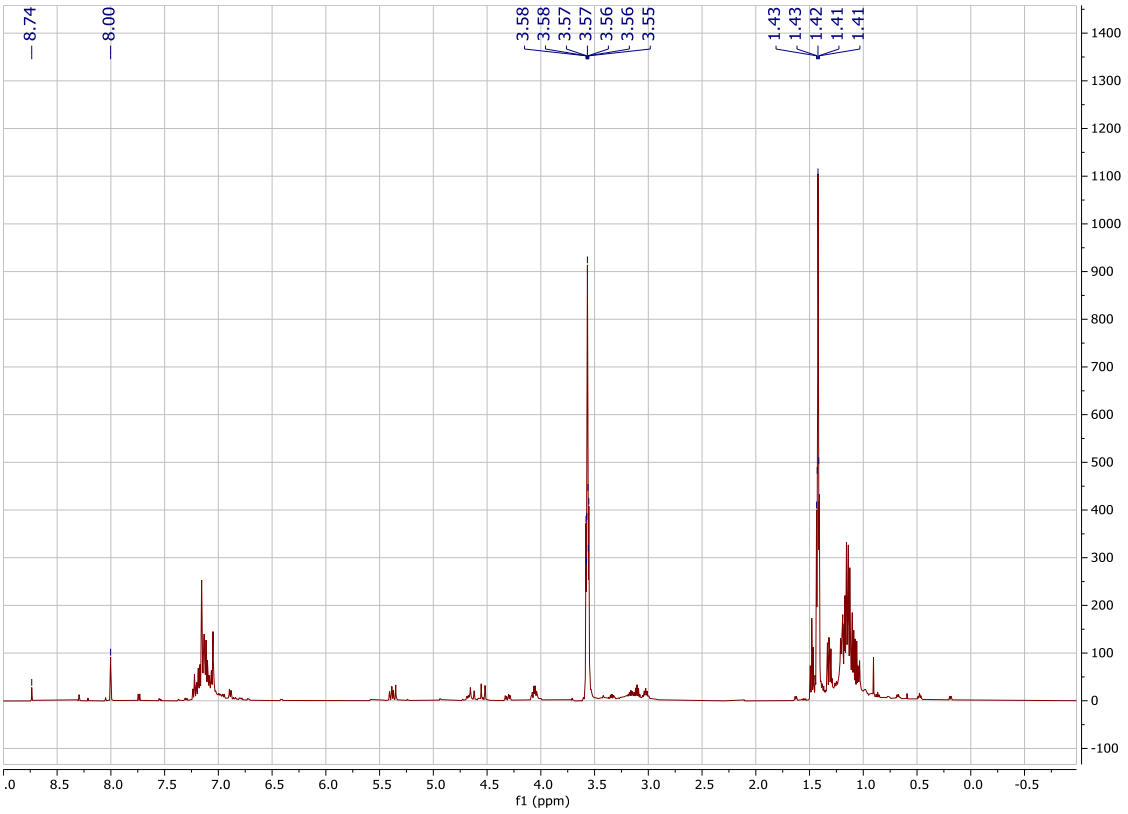

Figure 38. ^{1}H NMR of the reaction product between $Li_3CN_2Dipp_2$ and $SbCl_3$. The peaks at 8.00 and 8.74 correspond to aldimine peaks, while those at 3.57 and 1.42 correspond to THF.

2.3 Understanding Autoreduction

2.3.1 DFT Calculations of Potential Mechanisms

To understand how the bismuth compound reduced itself from Bi (III) to Bi (I), we performed some DFT studies, and came up with three potential mechanisms (Figure 39). To help reduce computational cost, we decided to use 2,6-dimethylphenyl instead of Dipp. Proposed mechanism A (grey lines; Figure 36) starts with the aryl backbone deprotonating a benzyl group, followed by two 1,2-proton shifts to the aryl carbon next to the remaining benzyl group, and concludes in H_2 being eliminated from the benzyl group and the aryl ring. In proposed mechanism B (red lines), one of the amines deprotonates

an adjacent benzyl carbon, a hydride is removed from the other benzyl carbon by the metal, followed by H_2 loss between the bismuth and the amine. Proposed mechanism C (blue lines) involves the metal removing a hydride from each benzyl carbon, followed by reductive elimination at the metal centre. The mechanism is similar to the catalytic cycle proposed by Wang et al.[27]

Based on energetics, Mechanism A can be ruled out. An intermediate that is 24 kcal/mol higher in energy than the reactant is not consistent with a reaction that proceeds rapidly at room temperature, as the activation barrier of this reaction would be necessarily higher than 24 kcal/mol. Assuming the kinetics are not prohibitive, mechanisms B and C are both energetically feasible, as the intermediates are only moderately high in energy. In fact, the only major difference between these two mechanisms is whether the N-centred HOMO or the Bi-centred LUMO drives the initial reactivity. Although at first glance mechanism C seems unlikely, as no hydrogenation of azobenzene was observed experimentally, it cannot be fully discounted. It remains possible that the active catalyst in Cornella et al.'s paper is not the bismuth dihydride, but rather some other species. Wang's catalyst also had relatively small *t*-butyl groups on the nitrogens, whereas our bismuth compound had larger Dipp groups, which might make the metal centre too sterically shielded to react with azobenzene even if the bismuth dihydride were to be formed. Therefore, based on the data we have obtained, it is not possible to distinguish between these two mechanisms. It is also possible that intermolecular mechanisms are involved, but it was not possible to investigate these due to the size of the system, the complexity of the potential intermediates, and the effects of solvation, especially if ionic species are involved.

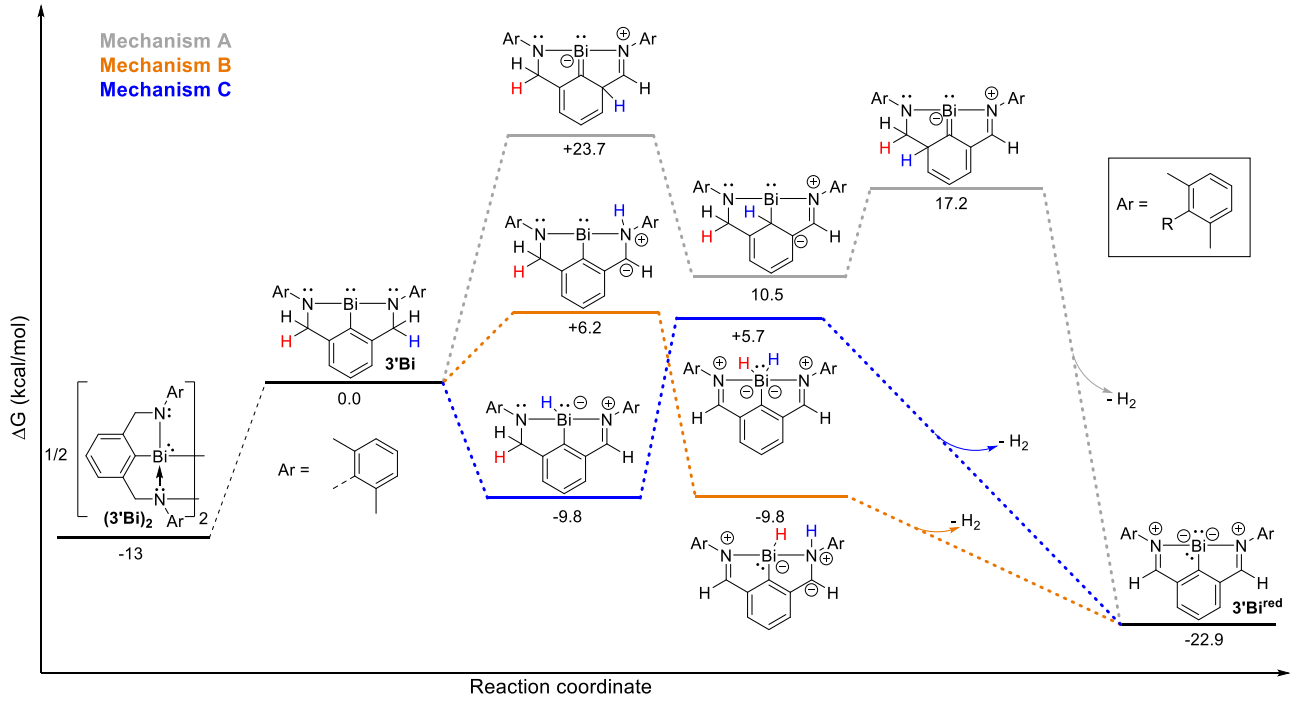

Figure 39. Three proposed mechanisms for the observed spontaneous reduction of the Bi (III) compound to the Bi (I) compound. Ar = 2,6-dimethylphenyl

2.3.2 Comparing Our Mechanisms to the Literature

The intermediates for mechanisms B and C are particularly interesting given the work performed by Cornella et al, where a very similar bismuth compound catalyses the transfer of dihydrogen from aminoborane to azobenzene. In particular, they assume that the ligand is inert, and the active species is a bismuth dihydride (intermediate 2, mechanism B). However, our DFT calculations suggest that this may not be feasible, given that this would involve forming an intermediate that is +28.6 kcal/mol higher in energy than the starting material – and the activation barrier could easily be even higher in energy than this. This is not consistent with a reaction that the authors have found to proceed overnight at 35-50°C.[27] An alternative mechanism for this reaction involves the transfer of a hydride from the BH_3 of aminoborane to bismuth, with Bi acting as a Lewis acid. Additionally, a proton from the NH_3 of aminoborane migrates to one of the imines,

making an intermediate that's a bismuth hydride and a protonated imine (intermediate 2, mechanism C). This intermediate is only moderately higher in energy than the starting materials (+13.1 kcal/mol), which is accessible at 35-50°C, provided that the kinetics are not prohibitive. Therefore, we propose that the catalytic cycle proceeds as shown in Figure 40, proceeding not via a Bi (I)/Bi (III) redox cycle, but via Lewis acid catalysis.

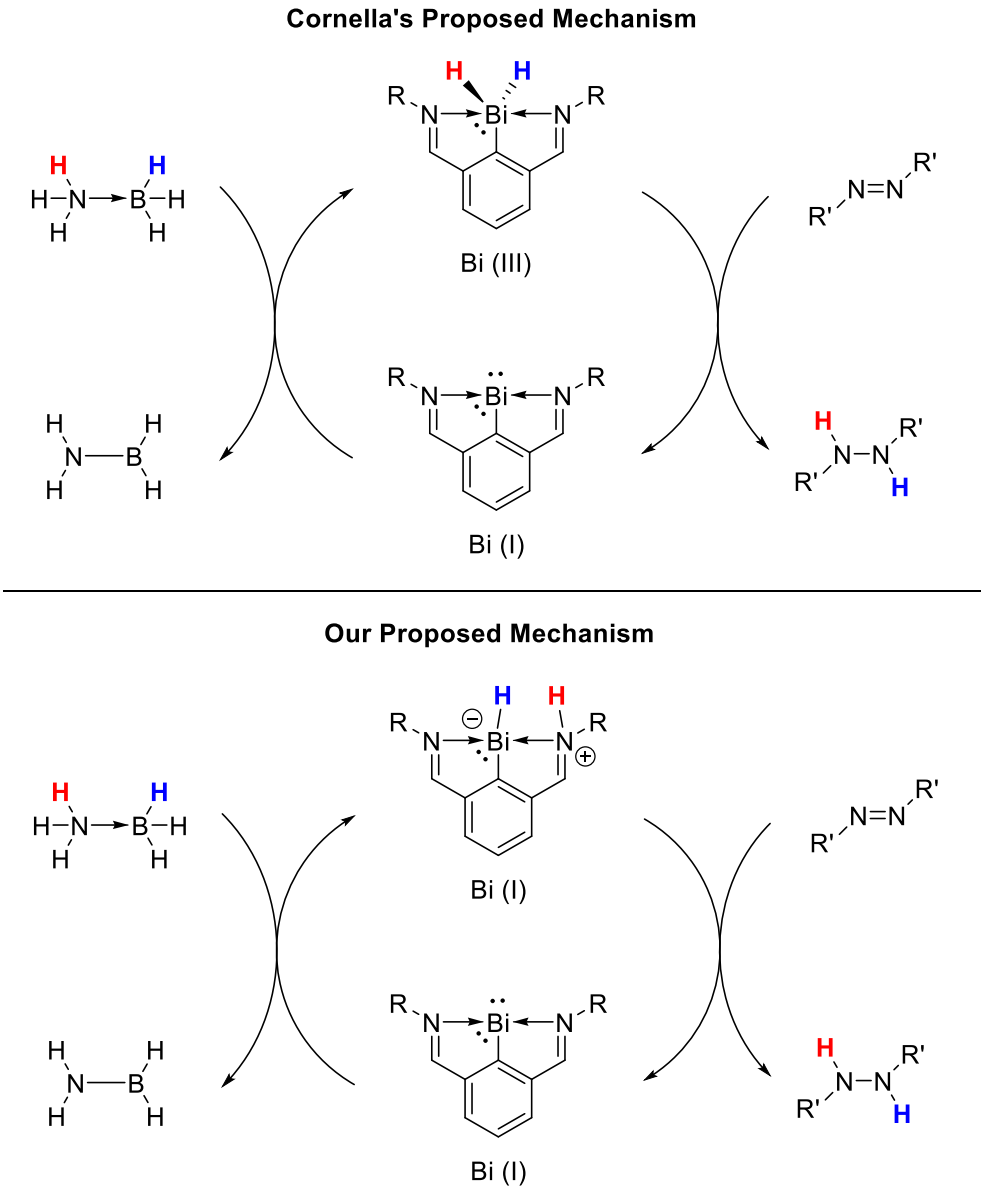

Figure 40. The redox mechanism for catalytic transfer hydrogenation proposed by Cornella et al. (top) and our proposed mechanism for the same reaction (bottom), relying on Lewis acid catalysis.

Even though our research does not suggest that the bismuth dihydride is an active species in Cornella's catalytic cycle, that does not mean it cannot be formed as a transient species. It is entirely possible that when Dostal's bismuth dichloride is reduced with lithium triethylborohydride that is proceeds via formation of this dihydride (Figure 17, page 15), or that it is formed as an intermediate when our Bi (III) compound autoreduces

itself to a Bi (I), as our DFT calculations prove that it is energetically accessible. There is no reason that the active catalytic species needs to be one of the intermediates when going from the Bi (III) to the Bi (I) species, even though both reactions involve the loss of H_2 from a bismuth compound.

2.3.3 Attempted Experimental Verification of Our Mechanisms

We also made a deuterated analogue of our Dipp NCN ligand to learn more about the autoreduction process. This compound was synthesized from isophthaloyl chloride, which was reduced to the tetradeuterated benzyl alcohol by using sodium borodeuteride and BF_3. This could then be converted to the dichloride by using HBr in acetic acid, which reacted with the lithiated aniline in the usual matter. Deprotonation using methyllithium was also performed as with the non-deuterated compound (Figure 41). While this compound did indeed undergo autoreduction, the reduction occurred very quickly, and the complexity of the NMR spectrum was such that the only easily assignable peak was that of the benzyl or aldimine peak in the deuterium NMR, so getting a kinetic isotope effect was not possible. We also tried to figure out whether the autoreduction mechanism was unimolecular or bimolecular by trying to find HD when a 50:50 mix of tetradeutero ligand and normal ligand were employed. Unfortunately, due to low solubility of HD, the results of this experiment were not conclusive.

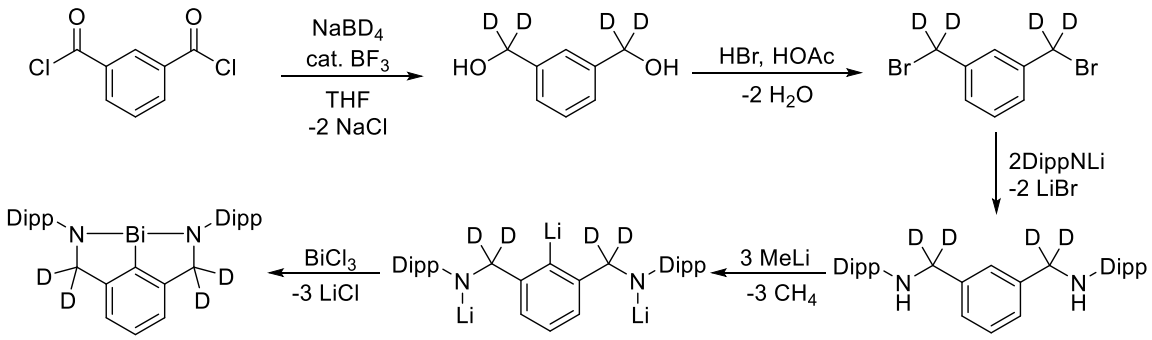

Figure 41. Synthetic method used when making the tetradeuterated Dipp Bi (III) NCN compound.

2.4 Electronic Modification of the Ligand

To help understand more about the mechanism of autoreduction, our next order of business was to try modifying the aryl groups on the ligand. Our initial attempt involved deprotonating bis-(3,5-trifluoromethyl)aniline using BuLi and reacting it with *m*-xylylene dibromide, as had been done for the Dipp compound (Figure 42). When this failed to produce any product, we tried combining the aniline itself with the dibenzyl bromide, using K_2CO_3 as the base. We attribute the failure of this reaction, as well as the previous one, to the electron-poor nature of the aniline, which made it very non-nucleophilic and hence unwilling to participate in the required S_N2 reaction with the dibenzyl bromide.

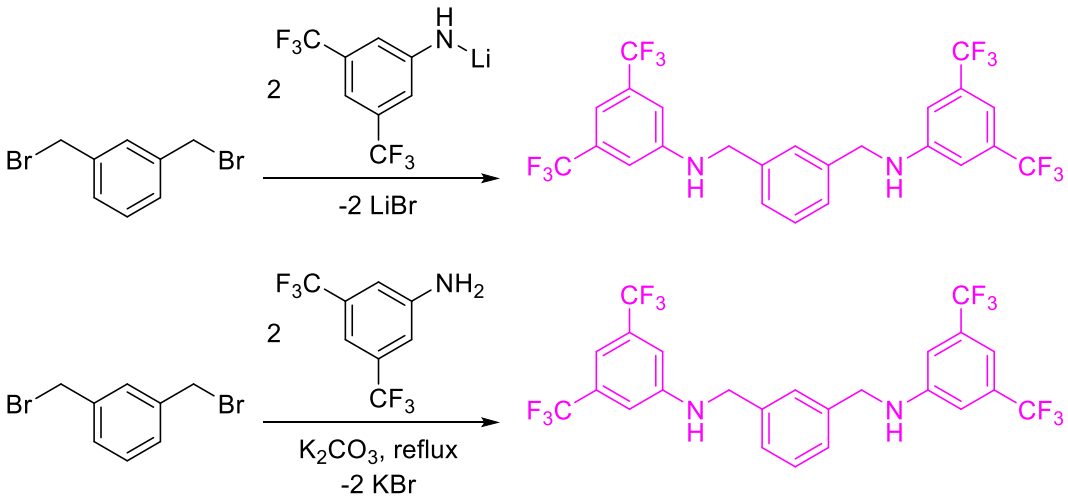

Figure 42. Two synthetic routes that were attempted when making a bis(3.5-trifluoromethyl)phenyl NCN ligand, one involving lithiation, the other the neutral aniline and KBr.

The only route that was successful involved the reaction of the aniline with the isophthalaldehyde with $Ti(OEt)_4$ to make the imine, which could then be reduced using $NaBH_4$ (Figure 43). Unfortunately, it was impossible to achieve triple deprotonation of the diamine, possibly due to the poor electron density around the anilines inhibiting the chelation required to direct the aryl C-H bond activation.

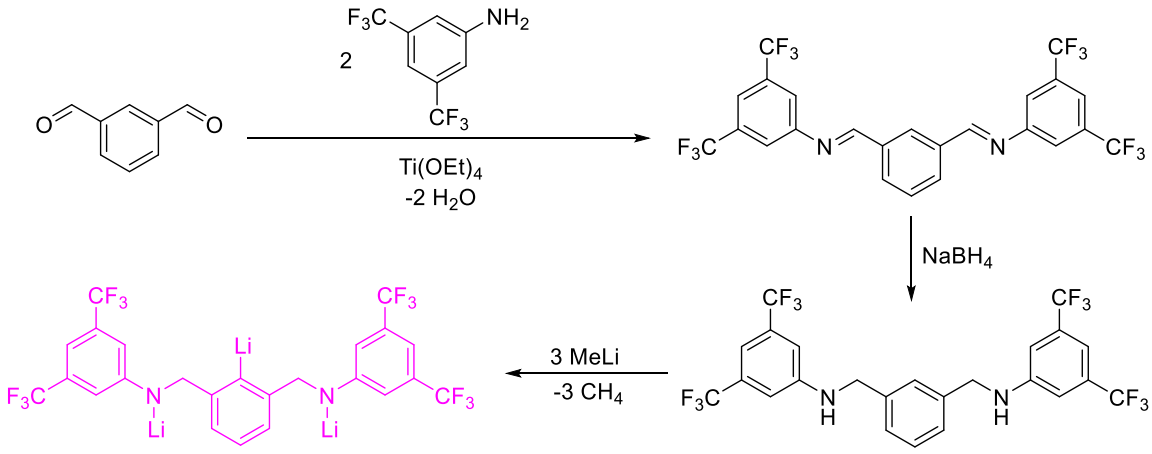

Figure 43. Synthesis of the bis(3,5-trifluoromethyl)phenyl NCN ligand via an imine condensation. Triple deprotonation was attempted, but unsuccessful.

With the limited success of the bis-(3,5-trifluoromethyl)aniline, we decided to try another electron-poor aniline: perfluoroaniline. Initial attempts involved an imine condensation using a Dean-Stark setup to remove the water. When this proved unsuccessful, the aniline was activated by using $SOCl_2$ (Figure 44). Unfortunately, this resulted in a mixture of products as the reaction did not proceed to completion. The reaction was more successful when the non-activated aniline was used via the $Ti(OEt)_4$ route, but yields were still limited, and the sodium borohydride reduction was not very successful.

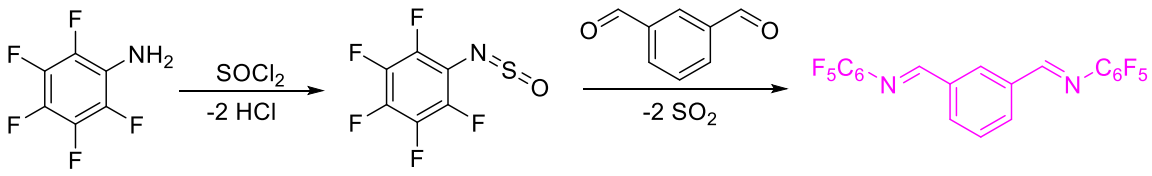

Figure 44. Activating perfluoroaniline with thionyl chloride to try and make it more reactive during imine condensation.

An electron-rich aniline (p-dimethylaminoaniline) was also tried, but this compound made a very planar bismuth complex which was not very soluble, making it unsuitable for the chemistry we desired. We also synthesized the trilithium salt with 3,5-dimethylaniline replacing the Dipp group but gave up on this when we realized that its chemistry was not significantly different from that of the Dipp compound, also resulting in spontaneous reduction to the Bi (I) compound.

2.5 Preventing Autoreduction

Since autoreduction was proving to be a significant problem with all the bismuth compounds we had made to date, we decided to try and use chelating anilines, namely 2-methoxyaniline and 2,6-dimethoxyaniline. According to DFT, these chelating anilines

would make autoreduction thermodynamically unfavourable (Figure 45). While synthesis of these ligands via the lithiation route worked alright, triple deprotonation of the central carbon of the aryl backbone was not successful. We think this failure may arise from the methoxy groups on the anilines acting as chelating directors, directing *ortho*-lithiation onto the aniline rings instead of onto the central aryl ring as intended.

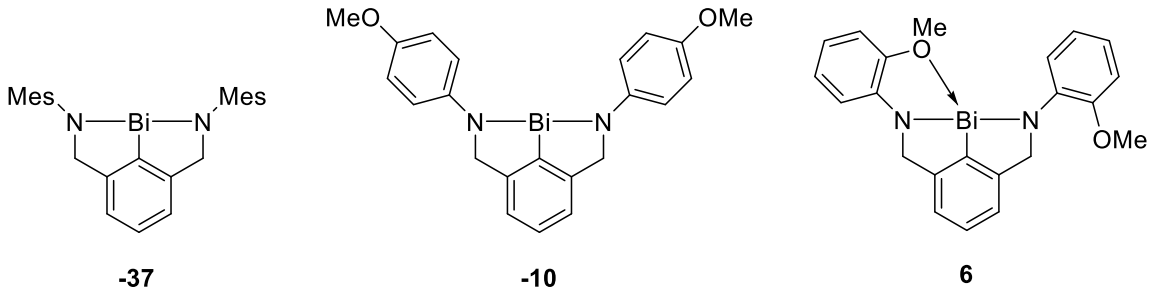

-37 **-10** **6**

Figure 45. Energies of reduction (kcal/mol) for three different CN_2-style bismuth compounds, showing how chelation makes autoreduction less favourable.

Another potential solution was to replace the two benzyl hydrogens with one oxygen, thereby going from an amine-based ligand to an amide-based ligand. These ligands were not difficult to make from the aniline and isophthaloyl chloride, with triethylamine as the base, and they could be deprotonated with MeLi in a similar manner as the Dipp based ligands (Figure 46). Unfortunately, the bismuth compounds made from these lithium salts had extremely poor solubility, making their characterization and separation from lithium chloride nearly impossible.

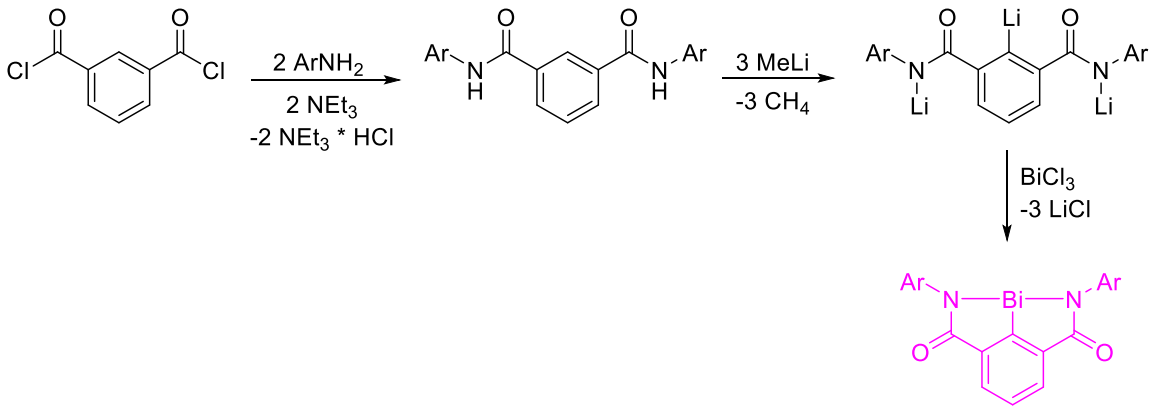

Figure 46. Synthetic protocol used to make the amide-based ligands, and their attempted installation onto Bi.

Finally, we tried replacing the two benzylic protons with methyl groups. While making the alkyl chloride from the appropriate alcohol was not especially difficult (Figure 47), this tertiary alkyl halide was essentially completely unreactive towards substitution by lithiated anilines and tended to perform dehydrohalogenation instead. We also tried making the bromide using HBr in acetic acid, but this compound was so reactive towards dehydrohalogenation that it tended to eliminate HBr spontaneously, making it very difficult to handle and purify.

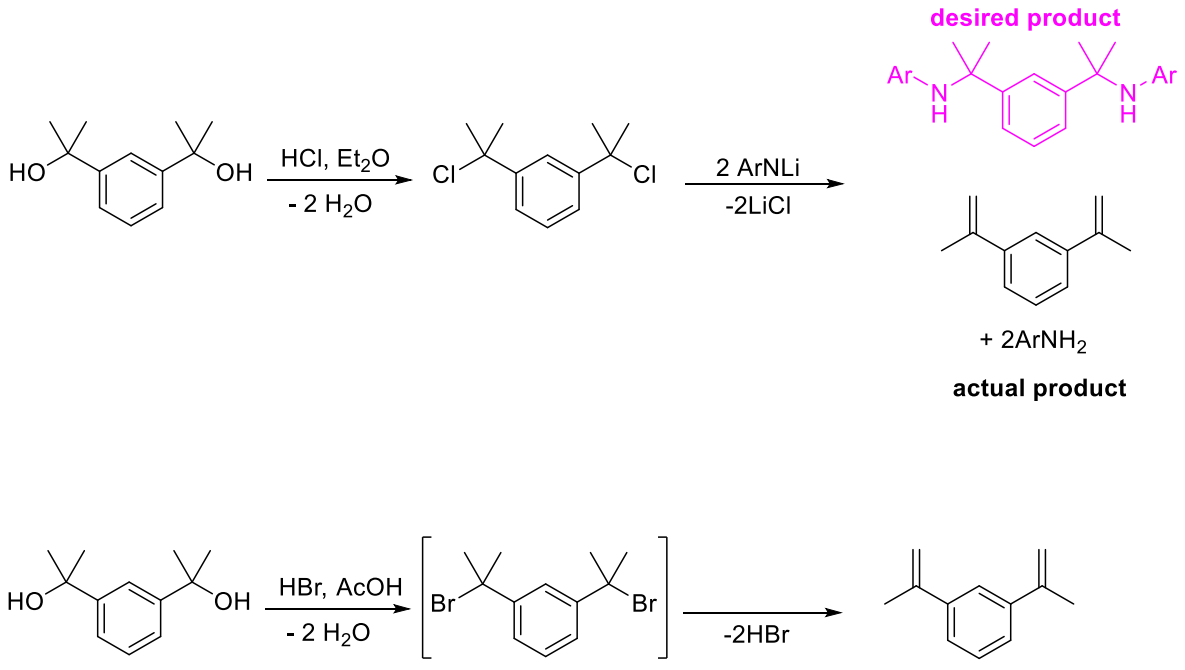

Figure 47. Trying to make a tetramethyl NCN ligand from a tertiary alcohol via an alkyl chloride (top) and attempting to synthesize the alkyl bromide (bottom).

In an attempt to get around this problem, we tried starting from the amine, which was easily made via hydrolysis of a commercially available isocyanate (Figure 48). The lithium salt of this amine did successfully react with chlorosilanes, however, when these silylamines were deprotonated, their lithium salts showed extremely poor solubility, limiting their usefulness. Why the solubility of these trilithium salts was so poor relative to the trilithium salts where the benzyl positions had protons remains a mystery. It is possible that due to steric bulk, they did not manage to dimerize, which might have made them more ionic and less soluble. Alternatively, it is possible that the increased bulk of four methyl groups in the benzyl position increased steric bulk around the ipso carbon so much that the methyllithium was unable to reach the desired aryl proton. A final possibility is that the aryl ring has become so electron rich that it is very difficult to deprotonate.

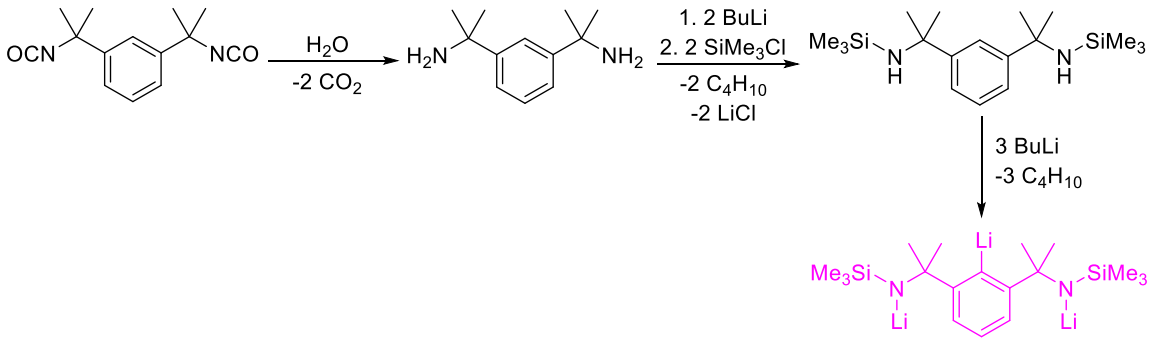

Figure 48. Synthesis of an NCN ligand that cannot lose H_2 from a commercially available isocyanate. Everything was successful except for deprotonation of the ligand.

A final attempt involved starting with 1,3-diacylbenzene and performing an imine condensation, followed by reaction with MeLi to install the second methyl group (Figure 49). Although the formation of the imine proved successful, according to ESI-MS, the product of the reaction did not appear to be methylated. It is possible that the methyllithium struggled to add to the imine due to the steric bulk of the Dipp groups blocking the carbonyl carbon.

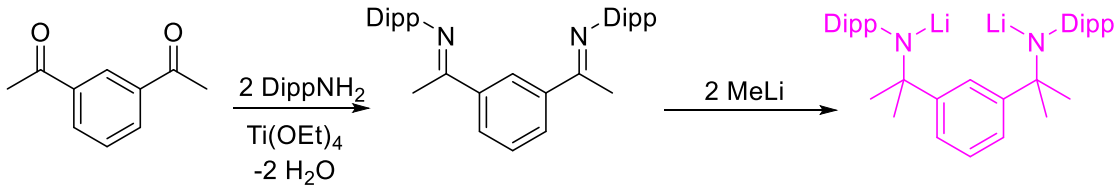

Figure 49. Trying to make a tetramethyl NCN ligand that can't lose H_2 by doing an imine condensation, followed by a methylation.

2.6 Silane-based ligands

With the challenges surrounding the aniline-based ligands, we decided to change course and use silane-based ligands, since they had been successful with the N_3TMS_2 compound. The ligand synthesis was straightforward: it could be made by combining the chlorosilane with *m*-xylylenediamine using triethylamine as the base (Figure 50).

However, better yields were obtained if the amine was first deprotonated using 2 equivalents of BuLi before the chlorosilane (either trimethylchlorosilane or triethylchlorosilane) was added, as the similar basicity of triethylamine and *m*-xylylenediamine meant that much of the latter turned into its insoluble hydrochloride salt, which was unavailable for reaction with the chlorosilane. Deprotonation could be performed in the same manner as for the aniline-based ligands, using either MeLi or BuLi. The trilithium salts were not isolated, and $BiCl_3$ was added directly to the solution at -78°C (Figure 47). Analysis of the NMR (Figure 51) did indeed reveal that a single major compound had formed, but the compound showed much lower symmetry than would be expected.

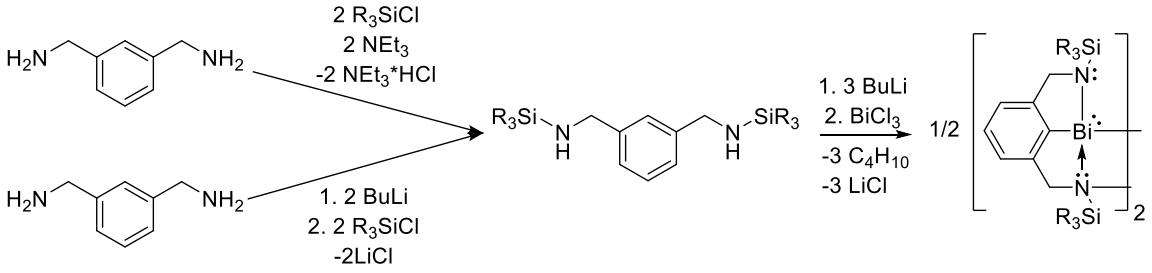

Figure 50. Synthetic protocol used to make the silane-based NCN Bi (III) compounds.

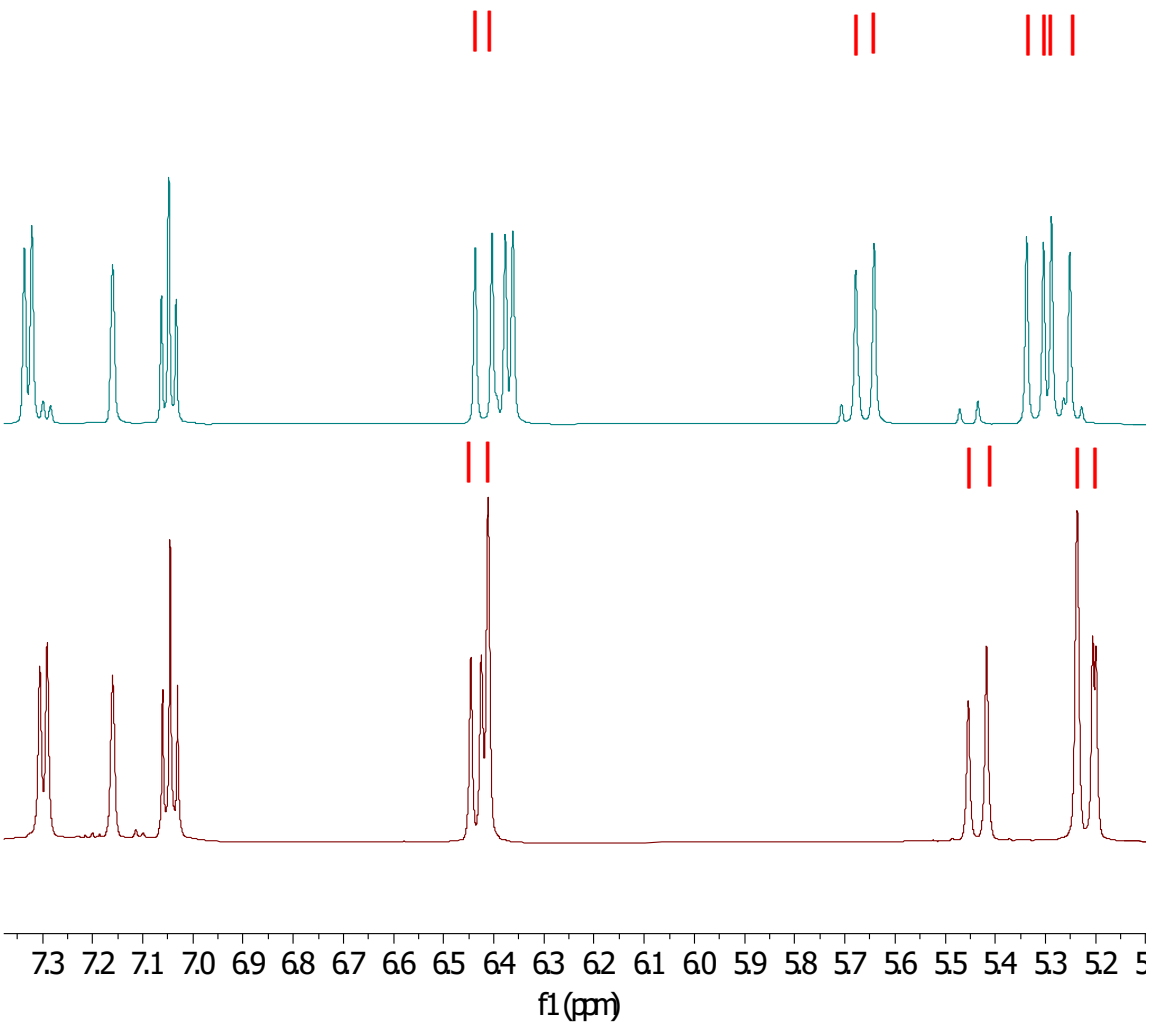

Figure 51. NMR spectrum showing the benzyl peaks (marked with a red vertical line) of the TES bismuth dimer (top) and the TMS dimer (Bottom)

There were three aromatic resonances, four distinct resonances for the benzyl protons, and two non-equivalent silyl groups. If the compounds were monomeric, only two aromatic protons would be observed, all four benzyl protons would be equivalent, and the two silyl groups would also be equivalent. Similarly, the ^{13}C NMR spectrum also showed twice the anticipated number of resonances in both cases. Combined, these features suggested the presence of a dimer. In order to confirm this, single crystals were grown by cooling concentrated solutions in hexanes, and X-ray crystallography

confirmed the presence of dimers in the solid state (Figure 52), which is consistent with our observations in solution NMR. Owing to differences in steric bulk, the TMS dimer showed a *syn* configuration, with the two sets of silyl arms being on the same side of the molecule and the aromatic rings being co-planar, whereas the TES dimer showed an *anti* configuration. To determine whether these differences were due to intrinsic thermodynamic features or crystal packing effects, DFT calculations were performed on isolated dimers in the gas phase to determine their conformational preferences. These calculations show that for the TMS compound, the *syn* conformation is 4 kcal/mol more stable than the *anti* configuration. Conversely, for the TES compound, the *anti* configuration is 0.6 kcal/mol more stable than the *syn* configuration, likely due to the increased steric bulk of the TES groups compared to the TMS. Since these calculations were done on isolated molecules, and their results are consistent with those observed in the crystal structure, we believed the differences in conformations are due to intrinsic thermodynamic stability rather than lattice effects. A thorough investigation of the bond lengths revealed that the compound was not well described as two weakly bonded, planar monomers. Rather, it was more accurately described as a bimetallic complex where each Bi (III) centre is *pyramidal*, bound to two ligand equivalents via short covalent bonds. Each bismuth centre also features one longer dative bond with one of the ligand arms. Specifically, in both compounds, the Bi_1-N_1 bond (ca. 2.186 Å in both) is similar in length to the Bi_1-N_2' bond [2.232(3) Å in $(BiCN_2TMS)_2$, 2.255(3) Å in $(BiCN_2TES)_2$], and these bonds are considerably shorter than the Bi_1-N_2 bond [2.849(3) Å in $(BiCN_2TMS)_2$, 2.843(4) Å in $(BiCN_2TES)_2$]. We infer therefore that the Bi_1-N_2 bonds are dative in nature, while the Bi_1-N_1 and Bi_1-N_2' bonds are electron-sharing covalent bonds.

The calculated Wiberg bond indices also show lower values for the longer bonds (0.15-0.16), suggesting that they exhibit significant dative character, whereas the analogous values for Bi_1-N_1 and Bi_1-N_2' bonds are significantly greater (0.51-0.60) and indicative of a higher degree of covalency.

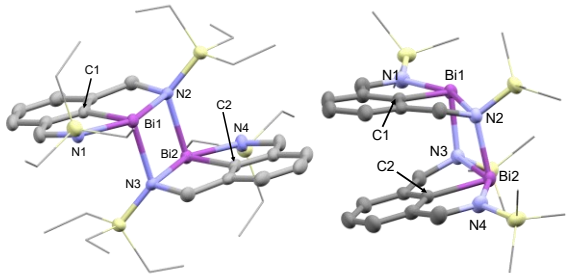

Figure 52. XRD structure of the TES bismuth dimer (left), and the TMS bismuth dimer (right). Hydrogen atoms are omitted for clarity.

The monomer itself could not be isolated in bulk for either the TES or the TMS bismuth compounds, despite the addition of various coordinating compounds including benzonitrile, triethylphosphine oxide, triphenylphosphine, pyridine, pyridine N-oxide, HMPA, trimethylphosphine, tributylphosphine, DPPF, and DPPE, which were intended to inhibit up dimer formation by coordinating to the bismuth centre and sterically preventing said dimerization. However, the TMS and the TES monomers were both detectable in the mass spectrometer using APCI ionization (Figure 53), suggesting that they are stable compounds in the gas phase. The peaks observed at 571.2372 m/z and at 487.1433 m/z were within error of the expected massed of the TES and TMS monomer, respectively. Additionally, peaks were observed at 1159.4777 m/z and 991.2899 m/z; these are within error of the expected masses of the TES and TMS dimers, respectively, coordinated to H_3O^+. We did not obtain high-resolution mass spectrometry on the peak at 973.3, however, we suspect that this peak corresponds to TMS dimer coordinated to H^+.

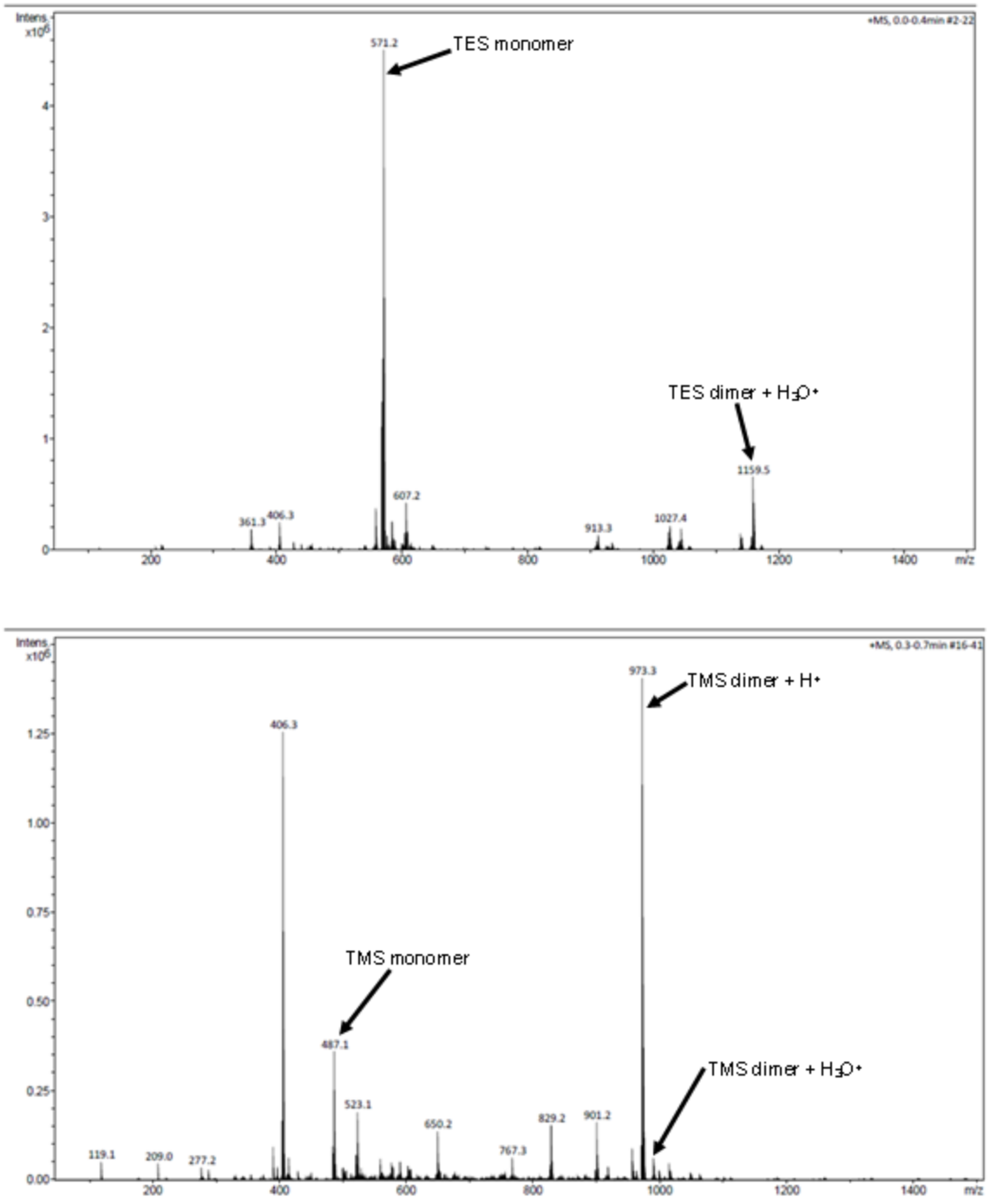

Figure 53. APCI mass spectra of the TES dimer (top) and the TMS dimer (bottom), showing that the monomer can be formed under the conditions of mass spectrometry. All spectra taken in DCM. Peaks of the monomer and dimer are indicated.

The rapid dimerization observed at room temperature of the CN_2Bi compounds is quite in contrast to the N_3Bi compounds previously reported, which did not show any

evidence of dimerization even at -80°C. A DFT analysis (Figure 54) reveals that in the N_3Bi compound's HOMO is a combination of the arene backbone and a highly polarized Bi-N π-bond, arising from strong N→Bi π-donation. By contrast, the HOMO in the CN_2Bi compounds is a combination of the N lone pairs and the benzyl C-H bonds. This explains both why the CN_2Bi compounds readily lose H_2, and why they are prone to dimerization, which is best explained by HOMO/LUMO quenching due to the Bi centre being very electrophilic. Nucleophilicity of the N atoms does not appear to be the decisive factor, as the HOMO energy of the CN_2Bi complexes is lower than that of the N_3Bi complexes by about 0.4 eV. Therefore, we suspect that analogous HOMO/LUMO quenching does not occur with the N_3Bi compounds for few reasons. Firstly, the Bi is not as electrophilic in these compounds, due to the LUMO being higher in energy. Secondly, the HOMO in N_3Bi is heavily delocalized, reducing its nucleophilicity. Finally, dimerization in the N_3Bi compounds would force all four silyl groups to be in proximity, inducing a large amount of steric strain, while in the CN_2Bi compounds, only two silyl groups must be in close proximity.

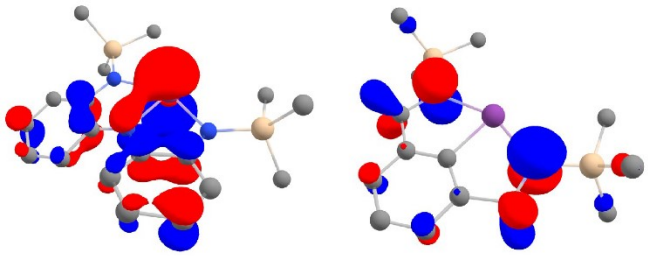

Figure 54. HOMO shape and energy of the N_3TMS_2 Bi compound (left) and the CN_2TMS_2 monomer (right).

To try to prevent dimerization, we decided to increase the bulk of the silanes to triisopropyl and diphenyl *tert*-butyl. Our rationale was that the silylamines were the only

ones that were successful at creating a stable Bi (III) compound, so we thought that the increased electron density around nitrogen due to Si's low electronegativity might be partly responsible for the success of these ligands. Bulkier silylamines would have similar electronic properties as TMS and TES, but their greater steric bulk would make dimerization more difficult. While the synthesis of the lithium salts was successful, attempting to react bismuth chloride with these bulkier silanes resulted in the same autoreduction behaviour observed with the Dipp-based ligand. This shows that while these Bi (III) compounds can be formed, they are very Lewis acidic and therefore unstable. Stabilization is performed either by dimerization or by the loss of H_2 (Figure 55). Which one occurs depends on the size of the groups attached to the amines. While N-substitution does not appreciably change the thermodynamics of dehydrogenative reduction, increasing steric bulk on the nitrogens greatly hinders dimerization. For smaller N-groups (TMS, TES) dimerization is favoured thermodynamically, whereas larger groups (Dipp) favour the loss of H_2.

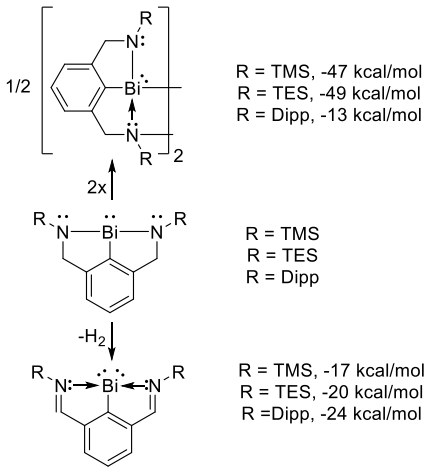

Figure 55. Calculated ΔG_{rxn} values for the dimerization or dehydrogenation of planar $[CN_2]Bi$ compounds. For the dimerization pathway, the most stable conformation was used for the thermodynamic calculation.

We next tried to determine the stability of the dimers by heating them in an NMR tube to 80°C. Both compounds gradually decomposed to form the Bi (I) species, as evidenced by the formation of aldimine peaks. Some bismuth metal and free ligand also formed, possibly via a competing pathway that completely reduced the bismuth back to its metallic form. For the TES dimer (Figure 56), significant decomposition was evident after 100 minutes of heating, and decomposition was essentially complete overnight.

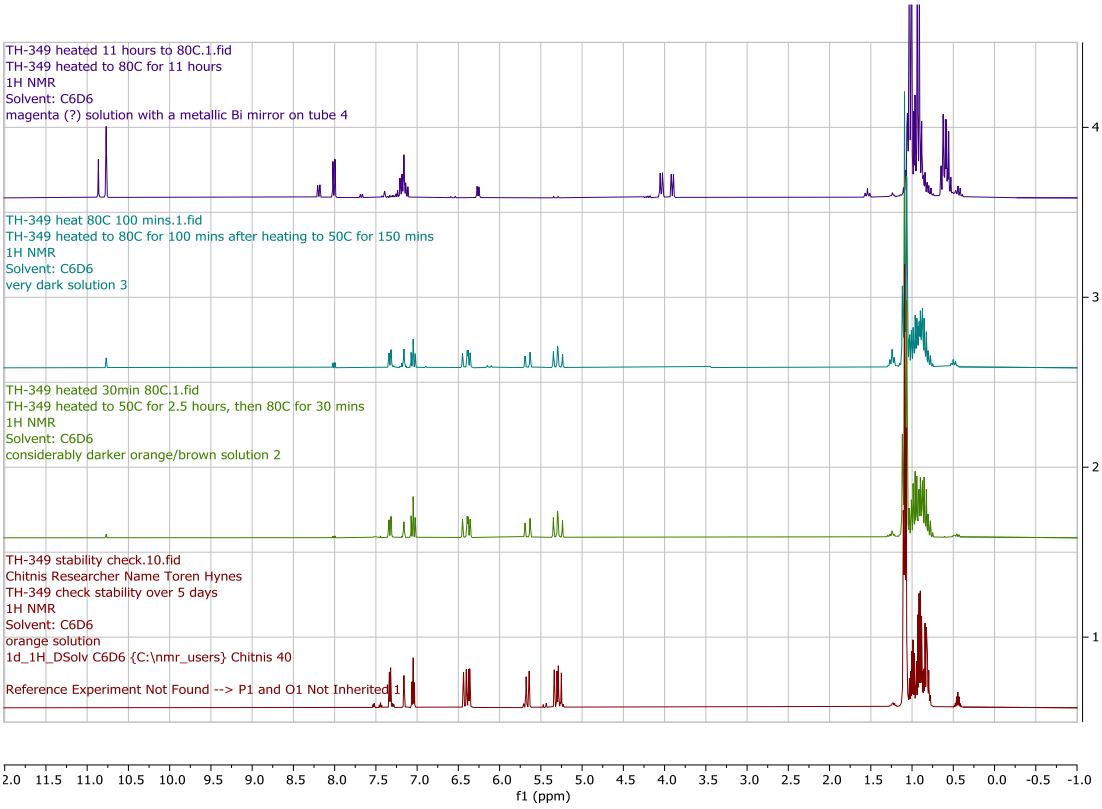

Figure 56. ^{1}H NMR spectra of the TES Bi dimer, dissolved in C_6D_6 and heated to 80°C. Peaks between 10.5 and 11.0 ppm correspond to the aldimine in the Bi (I) compound, while those around 4.0 and 0.5 ppm correspond to free ligand.

The TMS dimer (Figure 57) showed similar reactivity to the TES dimer when heated, however, the rate of reaction was much slower. Although the energy of dimerization was essentially identical for the TMS and TES compounds (-47 and -49 kcal/mol, respectively), the rate of decomposition was much slower for the TMS

compound. Even after 48 hours, the compound was not fully decomposed. This may be due to the TMS dimer having some π stacking interactions between the aryl rings, which might make for a slightly higher activation barrier of monomerization.

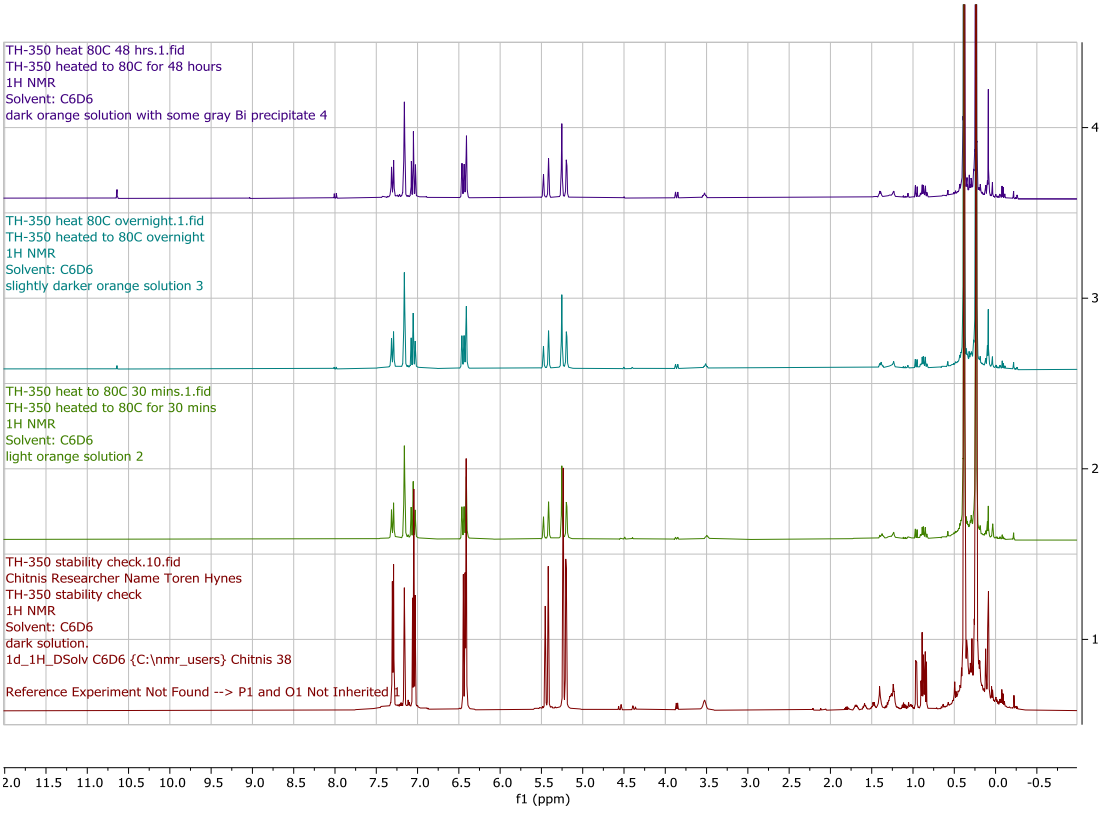

Figure 57. ^{1}H NMR spectra of the TMS Bi dimer, dissolved in C_6D_6 and heated to 80°C. The peak around 10.7 ppm corresponds to the aldimine in the Bi (I) compound.

In a final attempt to determine whether any Bi (III) monomer could be captured in solution, the TMS and TES Bi compounds were combined in a 1:1 stoichiometry in an NMR tube and heated to 80°C (Figure 58). No scrambling was observed, even over several days, however, the TES compound appeared to be undergoing slow decomposition to a Bi (I) species, as well as precipitating a mirror of Bi metal on the NMR tube. This does not mean that the Bi (III) monomer cannot be formed in solution or that the proposed autoreduction mechanisms are incorrect, however, because the

monomeric Bi (III) species is thermodynamically stable in the gas phase and observable via mass spectrometry. Rather, assuming mechanisms B and C are correct, it is likely that monomerization is the rate-determining step, and that any Bi (III) monomer that is formed quickly decomposes to Bi (I).

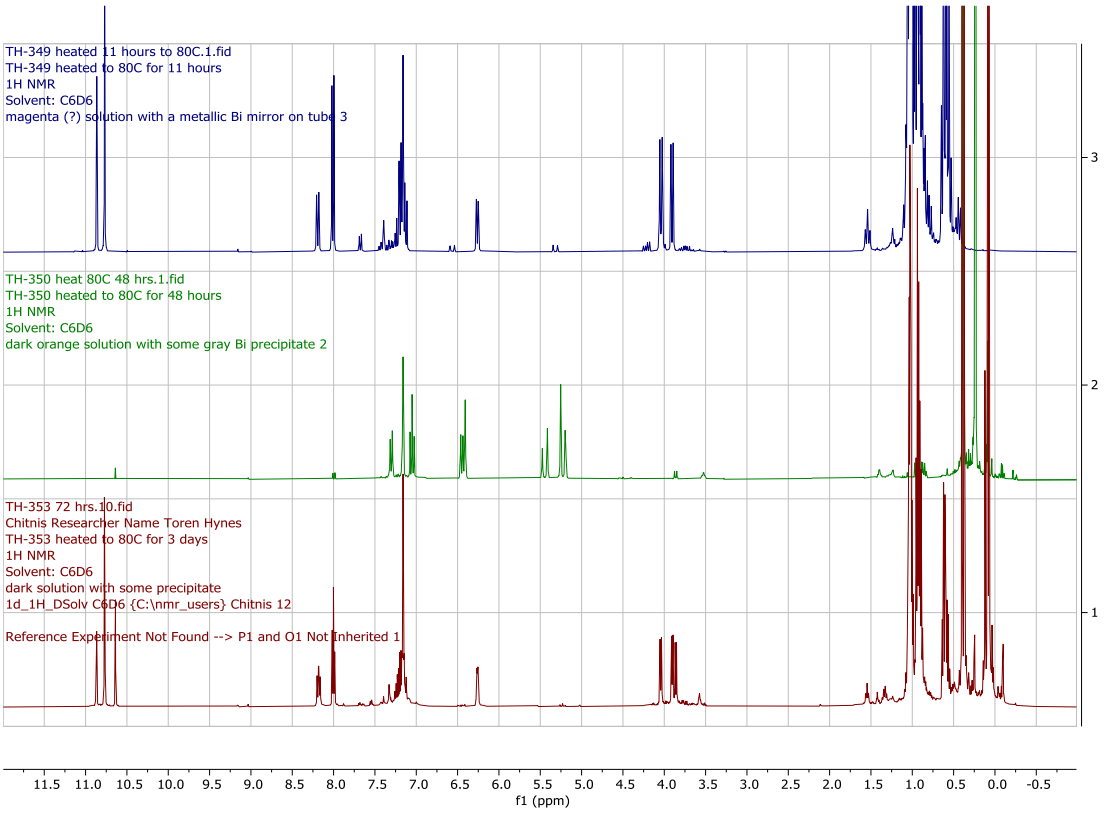

Figure 58. ^{1}H NMR spectra of the TES Bi dimer (top), TMS Bi dimer (middle) and TES + TMS Bi dimer (bottom). All compounds were dissolved in C_6D_6 and heated to 80°C for the indicated times. The peaks around 10.5 to 11.0 ppm correspond to the aldimine in the Bi (I) compound.

2.7 Experimental

2.7.1 Synthetic Procedures

All manipulations were performed using standard Schlenk and glovebox techniques under an atmosphere of dry nitrogen. Solvents were dried over

Na/benzophenone (tetrahydrofuran, pentanes, hexanes, diethyl ether, toluene, benzene-d6) or over calcium hydride (dichloromethane, acetonitrile, 1,2-difluorobenzene, dichloromethane-d2, acetonitrile-d3, chloroform-d) and distilled prior to use. Reaction glassware was baked in a 130°C oven for at least 1 h prior to use and assembled under nitrogen while hot. Melting points were obtained for samples sealed in glass capillaries and are uncorrected.

2.7.2 Solution Nuclear Magnetic Resonance

NMR spectra are referenced to tetramethylsilane (^{1}H, ^{13}C), or $CFCl_3$ (^{19}F), on a Bruker AV-300 spectrometer or a Bruker AV-500 spectrometer with residual solvent used for chemical shift calibration. Samples for NMR spectroscopy were prepared and sealed inside the glovebox with Parafilm before removal into ambient atmosphere.

2.7.3 Vibrational Spectroscopy

Infrared spectra were obtained on a Bruker instrument between KBr plates with the sample dropcast as a thin film.

2.6.4 UV-Vis spectroscopy

UV-VIS spectra were obtained on a cordless SpectroVis Plus spectrometer using a glass cuvette.

2.7.5 Single-crystal XRD

Single crystals diffraction experiments were performed on a Bruker APEX-II CCD diffractometer or D8 Venture diffractometer. Reflections were integrated using the

APEX 3 software[35] and solved using SHELXT[36] and refined using SHLEXL[37] with the Olex2 software GUI.

2.7.7 Mass spectrometry

Electro-Spray Ionization (ESI) and Atmospheric Pressure Chemical Ionization (APCI) spectra were obtained on a Bruker micrOTOF instrument.

2.7.8 Elemental Analysis

Elemental analyses were preformed using samples packaged inside a glovebox. Combustion analysis was performed using an Elementar Unicube instrument in CHN/S mode. Note that the journal requirements of ±0.40% accuracy for all elements have recently been critically re-evaluated.[38]

2.7.9 Reagents

Bismuth(III) chloride was purchased from Oakwood Chemicals and purified by vacuum sublimation (10^{-2} mbar, 200°C) prior to use. Chlorotrimethylsilane (TMSCl), chlorotriethylsilane (TESCl), and m-xylylenediamine were purchased from TCI America and used as received. ^{n}BuLi was purchased from Millipore Sigma and used as received. Titanium (IV) ethoxide, 2,6-diisopropylaniline, isophthaloyl chloride, and isophthalaldehyde were purchased from Oakwood and used as received. Triethylamine was purchased from Sigma-Aldrich and used after drying over 4Å molecular sieves. Sodium borohydride and sodium borodeuteride were purchased from Sigma Aldrich and used as received. HCl in Et_2O was purchased from Sigma Aldrich and used as received.

2.7.10 Computational Methods

All calculations were done using the Gaussian 16 Suite.[39] The PBE1PBE hybrid functional (with D3BJ dispersion correction) and the def2-TZVP basis set (with associated pseudopotentials) were used in all cases except for the dimerization energies, where the def2-SVP basis set (with associated pseudopotentials) was needed for practical reasons.[40] In all cases vibrational frequency calculations showed zero negative frequencies for the optimized structures. Basis set superposition error effects on dimerization energies were not considered since these are known to be quite small when triple-zeta basis sets are employed.[41]

2.7.11 Representative Synthesis of $PnCN_2Dipp_2$

The precursor lithium salt, $Li_3CN_2Dipp_2$, was prepared following literature procedures.[34, 42] $Li_3CN_2Dipp_2$ (1.423g, 3mmol) was dissolved in 20 mL of THF. The solution was cooled to -78°C, and $BiCl_3$ (0.946g, 3 mmol) dissolved in THF (20 mL) was added dropwise. For the other pnictogens, the relevant pnictogen chloride was used. The reaction was allowed to warm to 25°C, and stirred for 1 hour, then the solvent was removed under reduced pressure. The residue was extracted with hexane (20 mL), which was then filtered, concentrated, and cooled to grow crystals. None of these compounds were isolated in bulk. For the Bi compound, only a few crystals were selected to confirm connectivity (see manuscript discussion). The tetradeuterated $BiCN_2Dipp_2$ was synthesized in the exact same way, except for the substitution of the deuterated trilithium salt for the usual one. Crystal Data for $C_{32}H_{39}BiN_2$ (M =660.63 g/mol): monoclinic, space group P21/c (no. 14), a = 13.3245(3) Å, b = 8.7704(2) Å, c = 28.1768(7) Å, β = 95.6290(10)°, V = 3276.90(13) Å3, Z = 4, T = 115.00 K, μ(CuKα) = 10.687 mm-1, D_{calc}

= 1.339 g/cm^3, 23035 reflections measured (6.304° ≤ 2Θ ≤ 112.18°), 4201 unique (R_{int} = 0.0909, R_{sigma} = 0.0580) which were used in all calculations. The final R_1 was 0.0495 (I > 2σ(I)) and wR_2 was 0.1324 (all data). CCDC No. 2191158.

2.7.12 Reduction of azobenzene

Azobenzene (0.0091g, 0.050 mmol) and $BiCl_3$ (0.0158g, 0.050 mmol) were combined and dissolved in THF (0.5 mL). NMR spectroscopy of this solution revealed no reaction between azobenzene and $BiCl_3$. $Li_3CN_2Dipp_2$ (0.0238g, 0.050 mmol) was dissolved in THF (0.5 mL). Both solutions were cooled to -25°C, and the $BiCl_3$ and azobenzene solution was added dropwise to a stirred solution of the lithium salt. The reaction was allowed to stir 2 hours, and an NMR was taken again. No evidence of diphenylhydrazine formation could be found.

2.7.13 Synthesis of 1,3-Bis(1-chloro-1-methylethyl)benzene

HCl in Et_2O (2M, 8 mL) was added directly to 1,3-Bis(1-hydroxy-1-methylethyl)benzenediol (0.389g, 2 mmol). The reaction was allowed to stir for 2 hours, and the volatiles were removed under reduced pressure to yield the product in quantitative yield. ^{1}H NMR ($CDCl_3$, 300 MHz): δ = 7.96 (t, 1H, J = 2.0Hz), 7.60 (dd, 2H, J = 2.0, 7.7 Hz), 7.41 (t, 1H, J = 7.8 Hz), 2.10 (s, 12H).

2.7.13 Attempted synthesis of tetramethyl Dipp ligand

1,3-Bis(1-chloro-1-methylethyl)benzene (0.462g, 2 mmol), was dissolved in acetonitrile (10 mL). Trimethylsilyl triflate (0.889g, 4.00 mmol) was added, and the reaction was heated to 60C for 1 hour. Then 2,6-diisopropylaniline (0.75 mL, 4 mmol)

and triethylamine (0.55 mL, 4 mmol) were. The reaction was allowed to stir at room temperature overnight. No evidence of reaction was observed.

2.7.14 Synthesis of 1,3-Benzenedimethan-$\alpha^1,\alpha^1,\alpha^3,\alpha^3$-$d_4$-ol

This synthesis was adapted from a literature procedure.[43] Isophthaloyl chloride (1.55g, 7.65 mmol) and sodium borodeuteride (0.961g, 22.96 mmol) were dissolved in THF (50 mL). BF_3*Et_2O (1.23 mL, 9.95 mmol) was dissolved in THF (30 mL). The BF_3*Et_2O solution was added to the acyl chloride and sodium borodeuteride solution dropwise, then the reaction was refluxed overnight. Once finished, the reaction mixture was poured into a beaker, then 95% ethanol was added to quench excess $NaBD_4$ (caution! Beware of fizzing over!). All solvent was removed under reduced pressure (beware of bumping). It is important to remove as much THF as possible as it will make the next step much easier. After removal of solvent, distilled water (50 mL) was added, and the product was extracted with 3x20 mL of diethyl ether. The organic layer was dried over anhydrous $MgSO_4$, and volatiles were removed under reduced pressure. This gave an initial yield of 0.600g (55%). Further basification of the aqueous layer followed by 3 extractions using diethyl ether resulted in another 0.35g of product. The last traces of THF could be removed by sonicating the solid with pentane, followed by decanting off the pentane and vacuum drying. Total yield was 0.95 g (88%). ^{1}H NMR ($CDCl_3$, 300 MHz): δ = 7.42-7.24 (m, 4H), 1.88 (s, 2H).

2.7.15 Synthesis of 1,3-Bis(bromomethyl-d_2)benzene

This synthesis was adapted from a literature procedure.[44] 1,3-Benzenedimethan-$\alpha^1,\alpha^1,\alpha^3,\alpha^3$-$d_4$-ol was dissolved in HBr in acetic acid (8 mL). The reaction was stirred at

room temperature for 2 hours, and then it was poured *slowly* into a saturated sodium bicarbonate solution. Suction filtration afforded the crude product as a white solid. Recrystallization from hot hexanes resulted in the formation of colourless crystals (0.622g, 80%). ^{1}H NMR ($CDCl_3$, 300 MHz): δ = 7.42 (s, 1H), 7.37-7.30 (m, 3H).

2.7.16 Representative synthesis of amides

Isophthaloyl chloride (4.06g, 20 mmol) was dissolved in hexane (100 mL), and the reaction cooled to 0°C. Triethylamine (5.54 mL, 40 mmol) was added in one portion, followed by dropwise addition of 2,6-diisopropylaniline (7.54 mL, 40 mmol). This reaction made a lot of white precipitate very quickly and was allowed to stir overnight. The solid was filtered off and dissolved in dichloromethane (50 mL). Water (30 mL) was added, and the DCM layer was separated. Two more extractions with DCM (2x20 mL) followed, and the organic layer was dried over anhydrous $MgSO_4$. Rotary evaporation afforded the product as a white solid (7.19g, 74%). The solid was soluble in DCM, hot toluene, and hot ethyl acetate. ^{1}H NMR ($CDCl_3$, 500 MHz): δ = 8.55 (t, 1H, 1.5 Hz), 8.17m (dd, 2H, J = 1.8, 7.8 Hz), 7.69 (t, 1H, J = 7.8 Hz), 7.52 (s, 2H), 7.38 (t, 2H, J = 7.8 Hz), 7.28 (d, 4H, J = 5 Hz), 3.18 (sept, 4H, J = 6.9 Hz), 1.27 (d, 24H, J = 6.9 Hz).

2.7.17 Representative deprotonation of amides

This procedure is based on a literature preparation.[34] The diamide from the previous synthesis (4.84g, 10 mmol) was suspended in toluene (120 mL), and cooled to -35°C. Methyllithium (1.6M, 21.9 mL, 35 mmol) was added dropwise, and the reaction was subsequently heated to reflux for 45 minutes. The toluene was then removed under reduced pressure, and the orange solid washed with hexane. This solid was not possible

to characterize by NMR due to extremely poor solubility in C_6D_6, however, a small amount of product was quenched with D_2O, and 2 peaks were seen by deuterium NMR. ^2H NMR (CH_2Cl_2, 46 MHz): δ = 8.42 (br. s, 1D), 7.57 (br. s, 2D).

2.7.18 Activation of perfluoroaniline using $SOCl_2$

The use of metal Keck clamps in this setup is not recommended as they corrode, and ground glass joints should be sealed with Teflon tape to keep HCl from leaking.

This reaction was performed following a literature procedure.[45] Perfluoroaniline (3.00g, 16.4 mmol), was dissolved in toluene (30 mL). Thionyl chloride (5.95 mL, 82 mmol) was added, and the reaction was refluxed overnight. The reaction was allowed to cool to room temperature, and the toluene and thionyl chloride distilled off at 1 atm. When vacuum was applied, an orange liquid came over. A total of 3.36g of crude product were obtained, which was found to be 75% pure by NMR, resulting in an actual product yield of 2.52g (67%). Despite the impurity (likely consisting of unreacted aniline) the product was used without any further purification. ^{19}F NMR ($CDCl_3$, 282 MHz): δ = -139.3, -153.7, 161.2.

2.7.19 Reaction of activated perfluoroaniline with isophthalaldehyde

Isophthalaldehyde (0.724g, 5.4 mmol) was dissolved in toluene (10 mL) and placed in a dropping funnel. Separately, the impure activated perfluoroaniline (2.52g, 11 mmol) was dissolved in toluene (20 mL). The aldehyde solution was added dropwise to the activated aniline, and the reaction heated to reflux for 48 hours. The reaction, however, failed to proceed to completion, even when refluxed for an additional 48 hours.

2.7.20 Representative procedure for the synthesis of imines using $Ti(OEt)_4$

Isophthalaldehyde (0.67g, 5 mmol), was dissolved in toluene (30 mL). To this solution was added 3,5-bis(trifluoromethyl)aniline (1.56 mL, 10 mmol) and titanium ethoxide (2.09 mL, 10 mmol). The reaction was stirred over the weekend, then saturated aqueous NH_4Cl (20 mL) and ethyl acetate (20 mL) were added. The precipitate was removed by filtration. The aqueous layer was extracted 3 times with ethyl acetate, dried over $MgSO_4$, and volatiles removed under reduced pressure. This afforded 2.66g of solid of around 90% purity. ^1H NMR ($CDCl_3$, 300 MHz): δ = 8.60 (s, 2H), 8.53 (s, 1H), 8.13 (d, 2H, J = 7.4 Hz), 7.78 (br. s, 2H), 7.69 (t, 1H, J = 7.4 Hz), 7.67 (s, 4H). ^{19}F NMR ($CDCl_3$, 282 MHz): δ = -62.9.

2.7.21 Representative procedure for the reduction of imines

This reduction was based on a literature procedure.[46] The diimine from the previous reaction (2.41g, 4.33 mmol) was dissolved in absolute ethanol (15 mL). The solution was cooled down to 0°C, and sodium borohydride (0.360g, 9.53 mmol) was added. The reaction was warmed to room temperature and stirred for 3 hours. The mixture was then poured into 40 mL of distilled water, causing a white precipitate to form. The pH was adjusted to 8 using HCl and $NaHCO_3$, then the solution was cooled using an ice bath. Suction filtration isolated the product, which was redissolved in 20 mL of absolute ethanol, which was them pumped off to remove the water. The final yield was 2.00g (82%). ^1H NMR ($CDCl_3$, 500 MHz): δ = 7.43 (dd, 1H, J = 7.3, 8.0 Hz), 7.39 (br. s, 1H), 7.34 (dd, 2H, J = 1.1, 7.7 Hz), 7.20 (br. s, 2H), 7.00 (br. s, 4H), 4.52 (br. s, 2H), 4.43 (s, 4H). ^{13}C NMR ($CDCl_3$, 125 MHz): δ = 148.4, 138.5, 129.5, 126.9, 126.4, 112.0 (d, J = 2.48 Hz), 110.63 (quint, J = 3.79 Hz), 47.8. ^{19}F NMR ($CDCl_3$, 470 MHz): δ = -63.3.

2.7.22 Preparation of silylamines

m-xylylenediamine (1.98 mL, 15.00 mmol), was dissolved into dry THF (100 mL), and cooled using an ice bath. 2.5M n-butyllithium in hexanes (12 mL, 30.00 mmol) was added dropwise via cannula, forming a purple solution along with some precipitate. The solution was allowed to warm up to room temperature and left to stir for 1 hour. Subsequently, the solution was cooled back down to 0°C, and triethylchlorosilane (5.04 mL, 30.00 mmol) was added dropwise via cannula, causing the precipitate in the flask to gradually dissolve. This reaction was allowed to stir overnight. The THF was removed under reduced pressure, and 100 mL of dry pentane was added. After being allowed to stir for 30 minutes, the insoluble lithium chloride was filtered off, and pumping off the pentane yielded the product as a light orange oil (5.12g, 94%). The synthetic procedure for the bis(trimethylsilyl)amine was identical, except for the substitution of trimethylchlorosilane for triethylchlorosilane. These compounds could be used without further purification and spectral data are given for the as-obtained products. *CN_2TMS_2:* ^{1}H NMR (C_6D_6, 500 MHz): δ=7.32 (br. s, 1H, H_A), 7.24 (dd, 1H, J=6.9, 8.0 Hz, H_C), 7.14-7.18 (m, 2H, H_B), 3.85 (d, 4H, J=8.1Hz, C<u>H</u>$_2$), 0.49 (br. s, 2H, N<u>H</u>), 0.08 (s, 18H, Si(C<u>H</u>$_3$)$_3$). ^{13}C NMR (C_6D_6, 125 MHz): δ=144.7, 128.5, 126.1, 125.5, 46.4, 0.20. *CN_2TES_2:* ^{1}H NMR (C_6D_6, 300 MHz): δ=7.39 (br. s, 1H, H_A), 7.25 (dd, 1H, J=5.8, 8.8 Hz, H_C), 7.16-7.22 (m, 2H, H_B), 3.90 (d, 4H, J=8.0 Hz, C<u>H</u>$_2$), 0.99 (t, 18H, J=7.9 Hz, Si(CH$_2$C<u>H</u>$_3$)$_3$),0.56 (q, 12H, J=7.9 Hz, Si(C<u>H</u>$_2$CH$_3$)$_3$), 0.47 (br. s, 2H, N<u>H</u>). ^{13}C NMR (C_6D_6, 125 MHz): δ=144.4, 128.0, 127.9, 125.6, 125.0, 46.2, 7.1, 4.8.

2.7.23 Synthesis of the tetramethyl silylamine

The starting material was made from 1,3-Bis(1-isocyanato-1-methylethyl)benzene by following a literature procedure.[47] The unsilylated amine (1.00g, 5.20 mmol), along with triethylamine (1.45 mL, 10.40 mmol) was dissolved in pentane (30 mL). Trimethylchlorosilane (1.32 mL, 10.40 mmol) was added dropwise, making a fluffy powdery salt. The reaction was allowed to stir overnight, and the triethylamine hydrochloride was removed by filtration. All volatiles were removed under reduced pressure, affording the product as a colourless oil (1.16g, 66%). ^{1}H NMR (C_6D_6, 500MHz): δ = 7.91 (t, 1H, J=1.9 Hz), 7.33 (dd, 2H, J=1.9, 7.9 Hz), 7.22 (dd, 1H, J=7.5, 8.0 Hz), 1.50 (s, 12H), 0.09 (s, 18H).

2.7.24 Attempting to make the tetramethyl silylamine bismuth compound

The silylated amine (0.337g, 1 mmol) was dissolved in toluene (5 mL). The mixture was cooled to -80°C, and *sec*-butyllithium (1.4M, 2.21 mL, 3.10 mmol), was added dropwise, making a yellow solution. The reaction was allowed to warm to room temperature, then refluxed for 1 hour. No change in colour was observed. The reaction was then cooled down to 0°C, and bismuth (III) chloride (0.315g, 1mmol), dissolved in THF (5 mL) was added dropwise. The reaction turned brown-green. The reaction was allowed to stir at room temperature for 30 mins, then the solvent was removed under reduced pressure. The NMR spectrum looked like a difficult-to-interpret mess, however.

2.7.25 Representative procedure for double deprotonation of silylamines

CN_2TMS_2 from above (5.00g, 13.71 mmol) was dissolved into dry THF (100 mL) and cooled using an ice bath. 2.5M n-butyllithium in hexanes (10.9 mL, 27.41 mmol) was

added dropwise via cannula, forming a purple solution. The reaction was then allowed to warm up to room temperature and stirred for 30 minutes, after which the THF was removed under reduced pressure. 100 mL of dry pentane was subsequently added, and the mixture allowed to stir for 30 minutes. Filtration afforded the product as a white solid (4.22g, 62%), with each molecule of product being bound to 1.65 molecules of THF, as determined by ^{1}H NMR spectroscopy. *$Li_2CN_2TMS_2$:* ^{1}H NMR (C_6D_6, 500 MHz): δ=7.34 (t, 2H, J=6.7 Hz, H_B), 7.21 (t, 1H, J=6.7 Hz, H_C), 7.04 (s, 1H, H_A), 4.06 (s, 4H, $C\underline{H}_2$), 0.31 (s, 18H, $Si(C\underline{H}_3)_3$). THF peaks visible at 3.57 and 1.34 ppm. *$Li_2CN_2TES_2$:* ^{1}H NMR (C_6D_6, 300 MHz): δ=8.24 (s, 1H, H_A), 7.25 (dd, 1H, J=6.8, 8.1 Hz, H_C), 6.97 (br. d, 2H, J=7.5 Hz, H_B), 4.43 (s, 4H, $C\underline{H}_2$), 0.99 (t, 18H, J=7.9 Hz, $Si(CH_2C\underline{H}_3)_3$), 0.46 (q, 12H, $Si(C\underline{H}_2CH_3)_3$). THF peaks visible at 3.54 and 1.38 ppm.

2.7.26 Synthesis of $(BiCN_2TMS_2)_2$

$Li_2CN_2TMS_2$ (1.33g, 3.00 mmol) was dissolved in 40 mL of toluene and cooled to 0°C. 1.6M n-butyllithium in hexane (1.96 mL, 3.15 mmol) was added dropwise. Subsequently, the reaction was allowed to warm to room temperature, then refluxed for 30 minutes. Upon completion of reflux, the mixture was cooled to -78°C, and a solution of bismuth trichloride (0.946g, 3.00 mmol) dissolved in 15 mL THF was added dropwise. The reaction was allowed to warm to room temperature and stirred for 1 hour. All solvents were removed in vacuo, and 50 mL of hexanes was added. After stirring for 30 minutes, the mixture was filtered, concentrated to 3 mL, and cooled to -25°C to grow crystals. The product was isolated as a light orange powder (0.44g, 30%). Although the product is formed as the main species in this reaction (>90%), the isolated crystalline yield is low due to high solubility. It should be noted that this product tends to make oils

when pumped dry from pentane or hexane, but these can be solidified by adding a minimal amount of benzene and pumping dry. Slow evaporation of a benzene solution is also effective for growing X-ray quality crystals. Light orange solid. MP: 159-161°C. Elemental Analysis (calcd./expt.): C (34.56/35.63) H (5.18/4.94) N (5.76/5.10) ^{1}H NMR (C_6D_6, 500 MHz, see Supporting Information for detailed assignments): δ=7.30 (d, 2H, J=7.4 Hz), 7.05 (t, 2H, J=7.4 Hz), 6.42 (d, 2H, J=17.2 Hz), 6.41 (d, 2H, J=6.7 Hz), 5.44 (d, 2H, J=18.2 Hz), 5.23 (d, 2H, J=15.4 Hz), 5.22 (d, 2H, J=18.6 Hz), 0.38 (s, 18H), 0.24 (s, 18H). ^{13}C NMR (C_6D_6, 75 MHz): δ=179.3, 165.7, 167.7, 127.9, 123.4, 123.1, 62.2, 52.5, 2.3, 2.0. ^{29}Si NMR from ^{29}Si-^{1}H HMBC: (C_6D_6, 300 MHz): δ=8.3. FT-IR (transmission, drop-cast onto KBr plate): 674 (vw), 744 (vw), 764 (w), 782 (w), 833 (vs), 899 (vs), 961 (vw), 984 (vw), 1046 (m), 1076 (m), 1100 (m), 1163 (vw), 1246 (s), 1321 (w), 1437 (w), 1579 (w), 2815 (m), 2894 (vw), 2950 (w), 3037 (m). Crystal Data for $C_{28}H_{50}Bi_2N_4Si_4$ (M = 973.04 g/mol): monoclinic, space group C2/c (no. 15), a = 16.2365(7) Å, b = 16.1333(6) Å, c = 13.7602(7) Å, β = 96.415(2)°, V = 3581.9(3) Å3, Z = 4, T = 125.0 K, μ(MoKα) = 9.969 mm-1, D_{calc} = 1.804 g/cm^3, 50530 reflections measured (3.57° ≤ 2Θ ≤ 61.022°), 5487 unique (R_{int} = 0.0370, R_{sigma} = 0.0195) which were used in all calculations. The final R_1 was 0.0253 (I > 2σ(I)) and wR_2 was 0.0565 (all data).

2.7.27 Synthesis of $(BiCN_2TES_2)_2$

$Li_2CN_2TES_2$ (1.49g, 3.00 mmol) was dissolved in 40 mL of toluene and cooled to 0°C. 1.6M n-butyllithium in hexane (1.96 mL, 3.15 mmol) was added dropwise. Subsequently, the reaction was allowed to warm to room temperature, then refluxed for 30 minutes. Upon completion of reflux, the mixture was cooled to -78°C, and a solution

of bismuth trichloride (0.946g, 3.00 mmol) dissolved in 15 mL THF was added dropwise. The reaction was allowed to warm to room temperature and stirred for 1 hour. All solvents were removed in vacuo, and 50 mL of hexanes was added. After stirring for 30 minutes, the mixture was filtered, concentrated to 3 mL, and cooled to -25°C to grow crystals. The product was isolated as large orange crystals (0.23g, 14%). Although the product is formed as the main species in this reaction (>90%), the isolated crystalline yield is low due to high solubility. It should be noted that this product tends to make oils when pumped dry from pentane or hexane, but these can be solidified by adding a minimal amount of benzene and pumping dry. Slow evaporation of a benzene solution is also effective for growing X-ray quality crystals. Orange solid. MP: 114-117°C (dec.). Elemental Analysis (calcd./expt.): C (42.09/42.17) H (6.54/6.49) N (4.91/4.83). ^{1}H NMR (C_6D_6, 500 MHz, see Supporting Information for detailed assignments): δ=7.33 (d, 2H, J=7.4 Hz), 7.05 (t, 2H, J=7.4 Hz), 6.42 (d, 2H, J=16.8 Hz), 6.37 (d, 2H, J=7.5 Hz), 5.66 (d, 2H, J=18.3 Hz), 5.32 (d, 2H, J=16.8 Hz), 5.26 (d, 2H, J=18.4 Hz), 1.03 (t, 18H, J=7.9 Hz), 0.94 (td, 18H, J=7.8, 2.4 Hz), 0.77-1.03 (m, 24H). ^{13}C NMR (C_6D_6, 75 MHz): δ=180.2, 166.0, 157.8, 127.8, 123.2, 122.9, 62.5, 53.6, 9.0, 8.4, 8.2, 6.9. ^{29}Si NMR from ^{29}Si-^{1}H HMBC: (C_6D_6, 300 MHz): δ=12.1. FT-IR (transmission, drop-cast onto KBr plate): 731 (s), 763 (m), 874 (m), 920 (m), 974 (w), 1008 (m), 1064 (m), 1101 (w), 1163 (vw), 1235 (m), 1319 (vw), 1376 (vw), 1414 (w), 1457 (w), 1579 (w), 2805 (vw), 2874 (vs), 2907 (s), 2951 (vs), 3038 (w). Crystal Data for $C_{40}H_{74}Bi_2N_4Si_4$ (M =1141.35 g/mol): triclinic, space group P-1 (no. 2), a = 9.295(3) Å, b = 9.945(3) Å, c = 13.279(4) Å, α = 79.956(16)°, β = 72.925(7)°, γ = 84.135(8)°, V = 1153.6(6) Å3, Z = 1, T = 125.0 K, μ(MoKα) = 7.752 mm-1, D_{calc} = 1.643 g/cm^3, 44727 reflections measured (4.166° ≤ 2Θ ≤

52°), 4529 unique (R_{int} = 0.0426, R_{sigma} = 0.0208) which were used in all calculations. The final R_1 was 0.0255 ($I > 2\sigma(I)$) and wR_2 was 0.0572 (all data). CCDC No. 2191303.

2.7.28 Thermal stability experiment

The bismuth dimer of interest (0.02 mmol) was dissolved in C_6D_6 (0.6 mL) and heated to 80°C using a J. Young NMR tube. NMR spectra were initially taken after 30 mins, then every hour, followed by every three hours. When most of the starting material had been decomposed (and Bi metal deposited), NMR spectra were taken once a day. In the case of the $BiCN_2TMS_2$, the reaction was heated to 110°C overnight after 5 days heating to 80°C, to complete decomposition of the starting material.

2.7.29 Scrambling experiment

Compounds **$(BiCN_2TES)_2$** (0.023g, 0.02 mmol) and **$(BiCN_2TMS)_2$** (0.020g, 0.02 mmol) were dissolved in 0.7 mL of C_6D_6 using a conventional NMR tube sealed first with Parafilm and then with Teflon. They were initially left to stand for 1 hour at room temperature before an NMR was taken, after which they were heated to 50°C for 1 hour and another NMR was taken. Subsequently, the compounds were heated to 80°C and NMR spectra were taken every hour initially, then every 6 hours, and finally every 24 hours. The reaction was stopped when full decomposition (deposition of Bi metal) of starting material was observed. No evidence of a heteroleptic complex was detected.

2.7.30 Reaction of triethylphosphine oxide with the TMS dimer

$(BiCN_2TMS_2)_2$ (0.024g, 0.05 mmol) was dissolved in C_6D_6 (0.7 mL). Triethylphosphine oxide (0.013g, 0.10 mmol) was added to the TMS dimer solution. No

change in the ^{31}P shift of triethylphosphine oxide was observed, but some autoreduction was observed by ^{1}H NMR.

2.7.31 Reaction of the TMS dimer with pyridine N-oxide

$(BiCN_2TMS_2)_2$ (0.024g, 0.05 mmol) was dissolved in chloroform-D (0.7 mL). Pyridine N-oxide (0.0095g, 0.10 mmol) was added to the TMS dimer solution. No reaction was observed, even upon heating to 80°C.

Chapter 3: Reuse of a Waste Product

3.1 Contributions

Dr. Karlee Bamford is thanked for performing XRD on tris(Ph_3PNTMS)Bi, and Dr. Saurabh Chitnis is thanked for solving the crystal structure. Maxwell Lohoar is thanked for performing the synthesis of the PNP cations and for performing NMR characterization on them. Nicholas Murphy is thanked for the synthesis of Ph_3PNCl, Ph_3PNI, Ph_3PNOTf, and for performing the reactions of Ph_3PNCl with the P_2N_6 cages, as well as for providing their NMR spectra.

3.2 Converting Ph_3PNTMS into a Ligand

3.2.1 Attempted Synthesis of an NCN Ligand

Most amines are good nucleophiles, owing to the relatively high basicity of the lone pair on nitrogen. While imines (such as pyridine) are generally weaker bases than amines, however, the silyl group on Ph_3PNTMS is very electron-donating, which should increase the nucleophilicity of that nitrogen. The literature offers numerous examples where Ph_3PNTMS reacts with electrophiles, such as halophosphines,[48, 49] halosilanes,[50] and sulfonyl chlorides.[51] All of these reactions proceed via the loss of a TMS halide. Therefore, the first attempt at converting Ph_3PNTMS into a more valuable product involved performing an S_N2 reaction with *m*-xylylene dibromide, where it was hoped that TMSBr would spontaneously be lost to make the 1,3-disubstituted compound (Figure 59). Unfortunately, this reaction was unsuccessful, as no evidence of reaction could be found by ^{31}P NMR, even after several days of reflux. This reaction was also tried with the lithium salt, following a literature procedure, but was not much more successful.[52, 53]

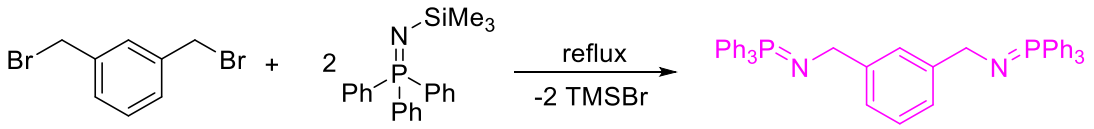

Figure 59. Attempted reaction of Ph_3PNTMS with m-xylylene dibromide.

3.2.2 Synthesis and Structure of tris(Ph_3PNTMS)Bi

After realizing that the previous attempt was unsuccessful, we decided on a new way to use Ph_3PNTMS as a ligand. Instead of trying to remove the TMS group, we instead, following literature procedure,[54] proceeded to *ortho*-lithiate the Ph_3PNTMS, which resulted in the formation of a dimeric salt bound to ether (Figure 60). This lithium salt was subsequently reacted with bismuth chloride. Extraction into hot toluene and concentration under vacuum yielded the compound as a colourless solid. Single diamond-shaped crystals for XRD were grown from hot benzene and revealed that the bismuth had bonded to three equivalents of Ph_3PNTMS in a pyramidal geometry (Figure 61).

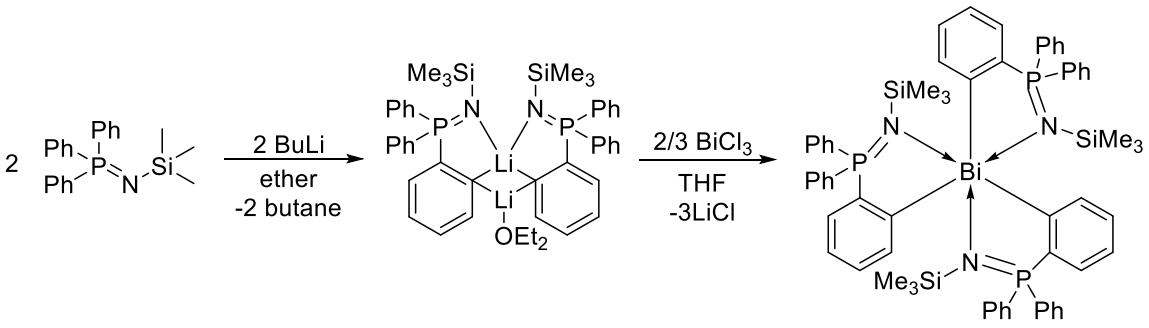

Figure 60. Ortho-lithiation of Ph_3PNTMS, and subsequent reaction with $BiCl_3$.

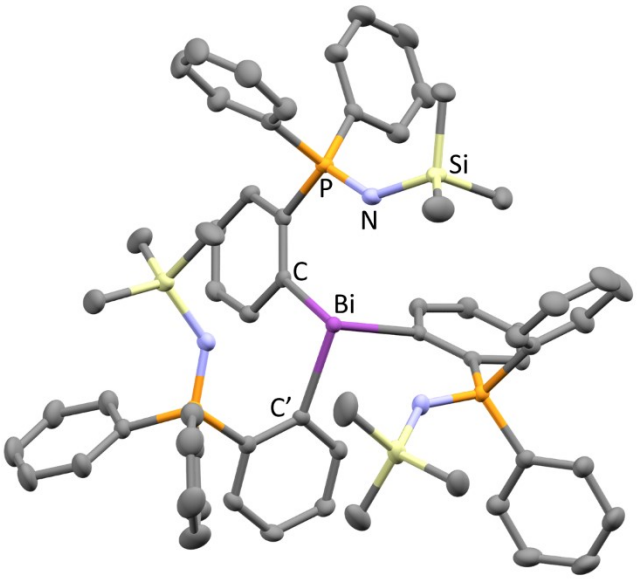

Figure 61. XRD structure of tris(Ph_3PNTMS)Bi, with key atoms labelled. Hydrogen atoms omitted for clarity.

Examining the XRD structure of this compound revealed that the Bi-C connectivity was similar to that observed in triphenylbismuth, however, the longer Bi-C bonds [2.335Å in of tris(Ph_3PNTMS)Bi vs 2.257(2) Å in $BiPh_3$], together with the more acute C-Bi-C' angle [91.11° in of tris(Ph_3PNTMS)Bi vs 95.28(8)° in $BiPh_3$], are indicative of increased steric crowding around the Bi centre induced by the TMS groups. This steric crowding is also apparent on the phosphine imine side: the N-Si bond is longer [1.705(1)Å in tris(Ph_3PNTMS)Bi vs 1.686(2)Å in free $Ph_3PNSiMe_3$], and the P-N-Si angle is more acute [134.4(1)° in of tris(Ph_3PNTMS)Bi vs 140.2(2)° in free $Ph_3PNSiMe_3$] than in the free ligand. Most interestingly, however, the P-N bond is slightly longer in tris(Ph_3PNTMS)Bi (1.549(2)Å) than in free $Ph_3PNSiMe_3$ (1.542(2)Å). Given that the P-N bond is length is not in a location where it would be overly affected by sterics, this suggests slightly lower electron density in the P-N bond, which could be indicative of dative bonding between N and Bi. The Bi-N distance was found to be

3.028Å, which is well within the sum of the van der Waals radii of Bi and N (4.2Å). Finally, the Wiberg bond index between Bi and N was found to be 0.0787, consistent with values observed in dative bonding. Taken together, these results suggest that there is indeed dative bonding occurring between Bi and N in this compound. This resulted in increased electron density around Bi, with the HOMO of tris(Ph_3PNTMS)Bi being 1.18 eV higher in energy than that of $BiPh_3$.[25]

3.2.3 Reactivity of tris(Ph_3PNTMS)Bi

The most unusual feature of this bismuth compound was its extreme stability. It could be left on the bench top for a week with no signs of degradation, was stable for an hour in refluxing 95% ethanol, and could be washed free of lithium chloride using distilled water. This compound's unusual stability probably arose from two features. It had extremely poor solubility in solvents other than benzene and toluene, and even in those solvents, heating was required to initially break up the crystal lattice. Benzene and toluene are both quite hydrophobic, which would have made it harder for water molecules to react with the compound. Probably more importantly, however, was that the hydrolytically sensitive bismuth-carbon and nitrogen-phosphorus bonds were very well shielded by three phenyl rings (Figure 61), making it sterically difficult for the water molecule to get close enough to induce hydrolysis.

A recent publication showed that two related compounds, made by Marschak et al, (Figure 62), were able to be reversibly excited by UV light, and showed some potential for photocatalysis.[55] Given that our compound was structurally similar to theirs, and was more electron-rich, we proposed that it might make a good photocatalyst.

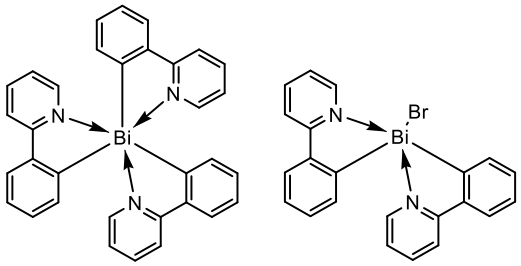

Figure 62. The two bismuth compounds made by Marschak et al. These compounds are structurally similar to the $Bi(Ph_3PNTMS)_3$ compound we prepared.

Unfortunately, despite being fairly electron rich around Bi, with a DFT-calculated HOMO energy of -5.44 eV (the HOMO of $BiPh_3$ is -6.62 eV), the compound we synthesized showed no absorbance or fluorescence in the UV-Vis spectrum (Figure 63), making it unsuitable for any photocatalytic applications. This is not entirely unexpected, given that the LUMO lies at -0.80 eV, giving the compound a HOMO-LUMO gap of 4.64 eV. This equates to a λ_{max} of 267 nm, in the UV-C range and well beyond what our UV-Vis spectrometer was capable of measuring.

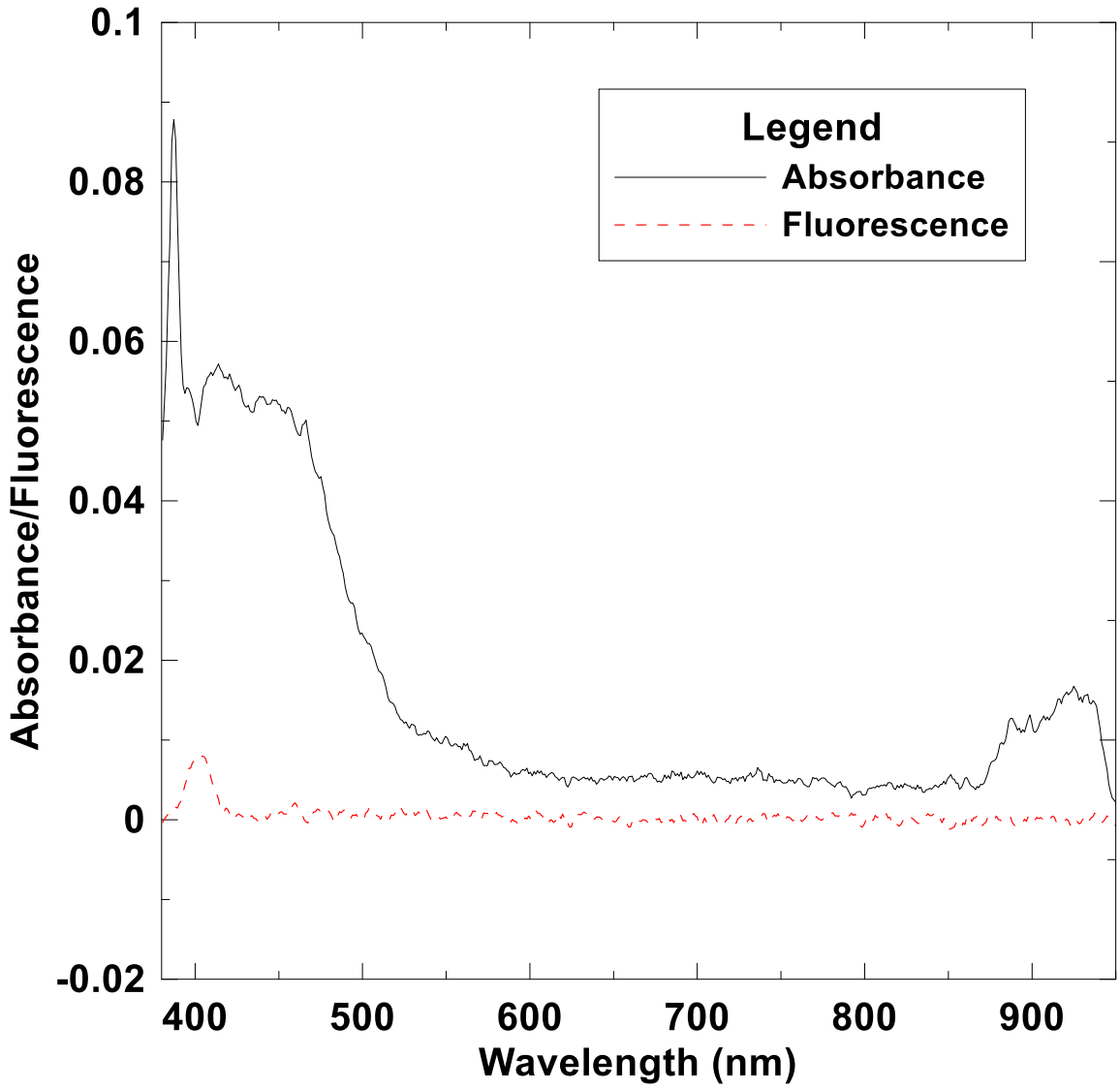

Figure 63. Absorbance (solid line) and fluorescence (dashed line) spectra of tris(Ph_3PNTMS)Bi in toluene.

Seeing as our bismuth compound had no photocatalytic potential, we decided to try and investigate the compound's reactivity. Attempted reaction with iodomethane and methyl triflate resulted in the formation of insoluble salts, which we attribute to the nitrogen being methylated, but the TMS group not being eliminated (Figure 64). Reactions with sodium *tert*-butoxide was also tried and HCl in ether were also attempted, but neither was particularly successful. This was possibly due to poor solubility of the

sodium *tert*-butoxide in the mesitylene, while the HCl reaction likely protonated the imine, resulting in a poorly soluble solid. A final reaction was attempted, where we tried to oxidize the bismuth with sulfur, but that showed no sign of reaction.

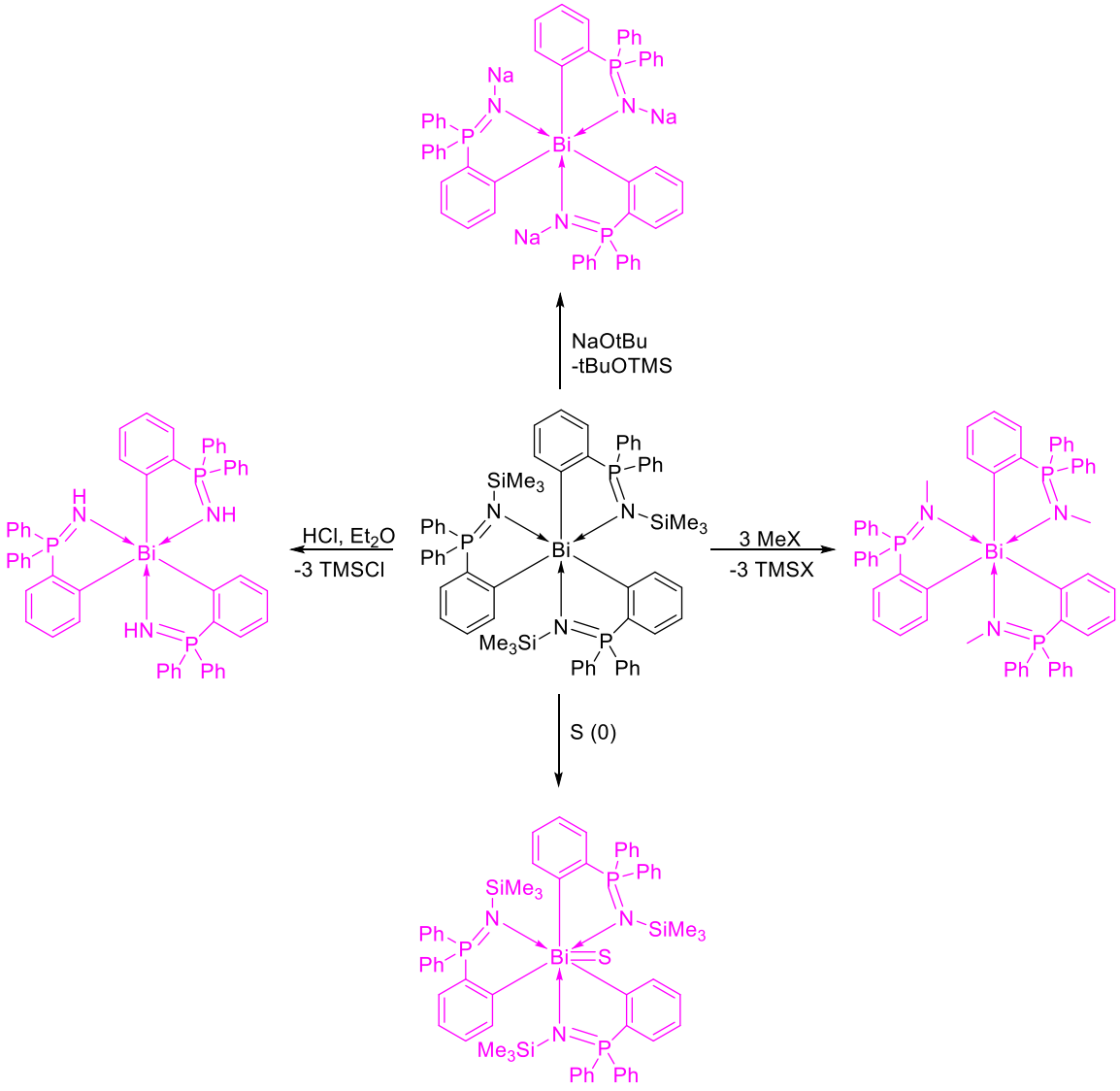

Figure 64. Attempted reactions of tris(Ph_3PNTMS)Bi with HCl, NaO^tBu, MeI, MeOTf, and sulfur.

3.2.4 Attempted Synthesis of bis(Ph_3PNTMS)BiCl

We also tried placing two equivalents of Ph_3PNTMS onto bismuth, instead of three. This would leave a chloride present on the metal, which could then be replaced

with a hydride, potentially enabling hydrobismuthination. Our group has successfully used silylated naphthalenediamine ligands for hydrostibination.[56] Hydrobismuthination had also been attempted with these ligands, however all attempts to replace the chloride on the Bi with a hydride resulted in the formation of dimers, due to the massive size mismatch between Bi and H and the subsequent weak bond. However, we felt that this phosphine imine ligand would be relatively similar structurally to the naphthalenediamine ligands, albeit more electron-rich, giving it a chance of stabilizing the bismuth hydride. When the synthesis was attempted (Figure 65), the NMR unexpectedly showed that one of the TMS groups had been lost (Figure 66, 67), and there were two distinct phosphorus environments (Figure 68). We think that this occurred because of TMSCl elimination from the bismuth centre, which turned one of the Ph_3PNTMS groups into a Ph_3PN group, which resulted in it becoming an X_2 donor instead of an LX donor. We thought of preventing this by replacing the TMS groups on the Ph_3PNTMS with *t*-Bu groups, making Ph_3PN*t*-Bu, however, this was not done out of the interest of time.

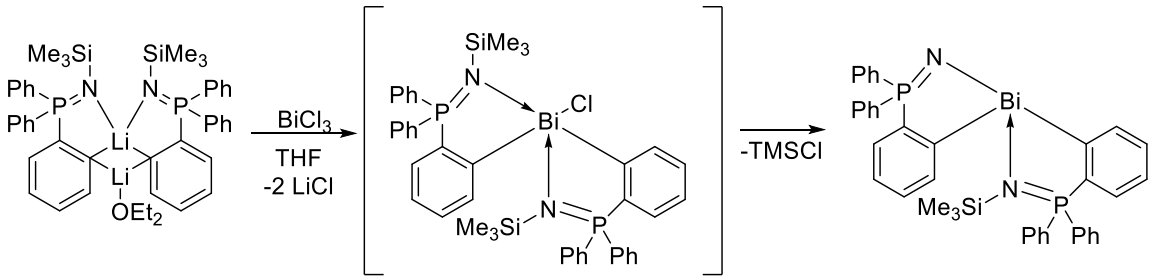

Figure 65. Reaction of 2 equivalents of ortho-lithiated Ph_3PNTMS with $BiCl_3$.

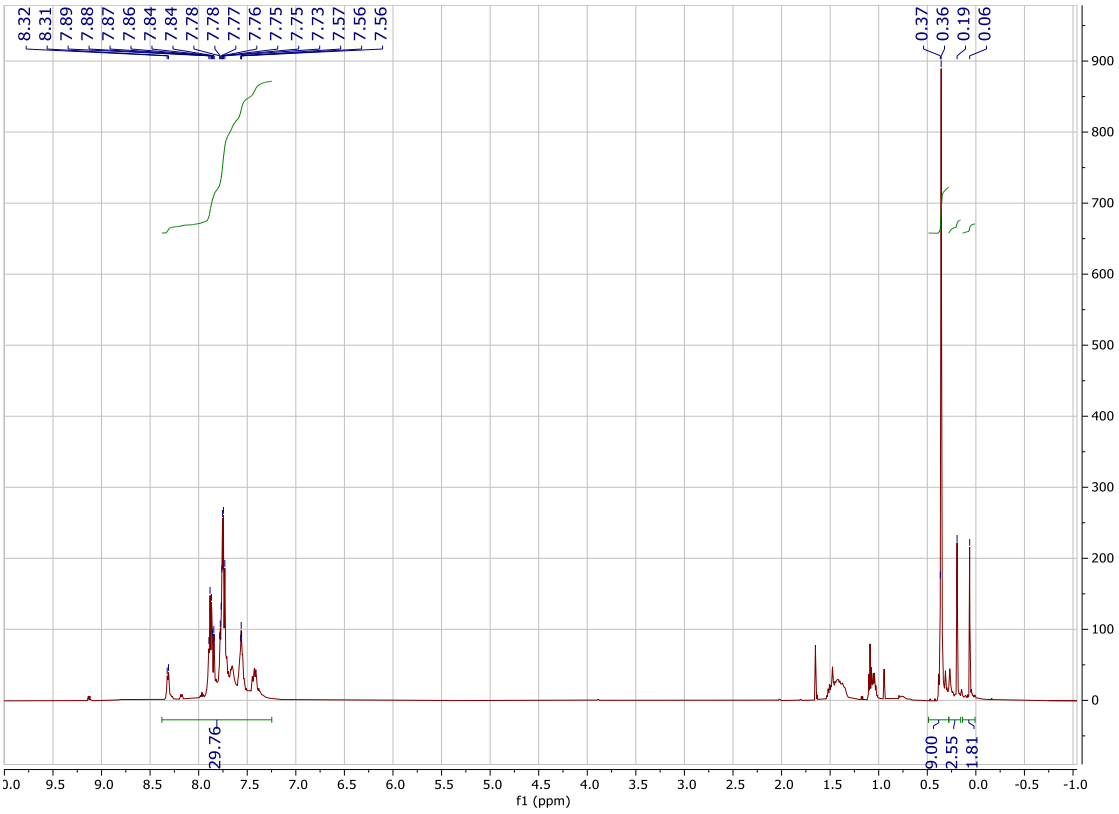

Figure 66. The ^{1}H NMR (DCM, 500 MHz) of the reaction product of 2 equivalents of $Ph_3PNTMSLi$ with $BiCl_3$, following a DCM extraction and wash with pentane. Note the unusually low amount of TMS protons.

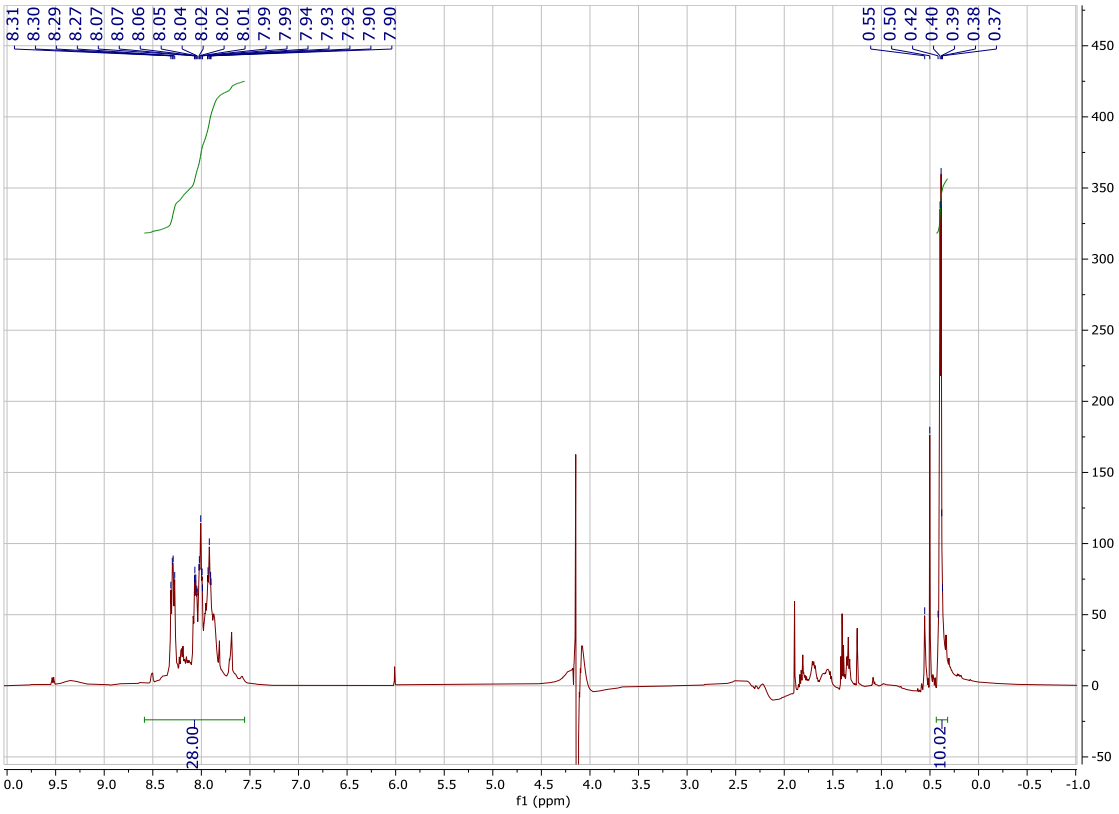

Figure 67. The ^{1}H NMR (THF) of the reaction product of 2 equivalents of $Ph_3PNTMSLi$ with $BiCl_3$, following a DCM extraction and wash with pentane. Note the unusually low amount of TMS protons.

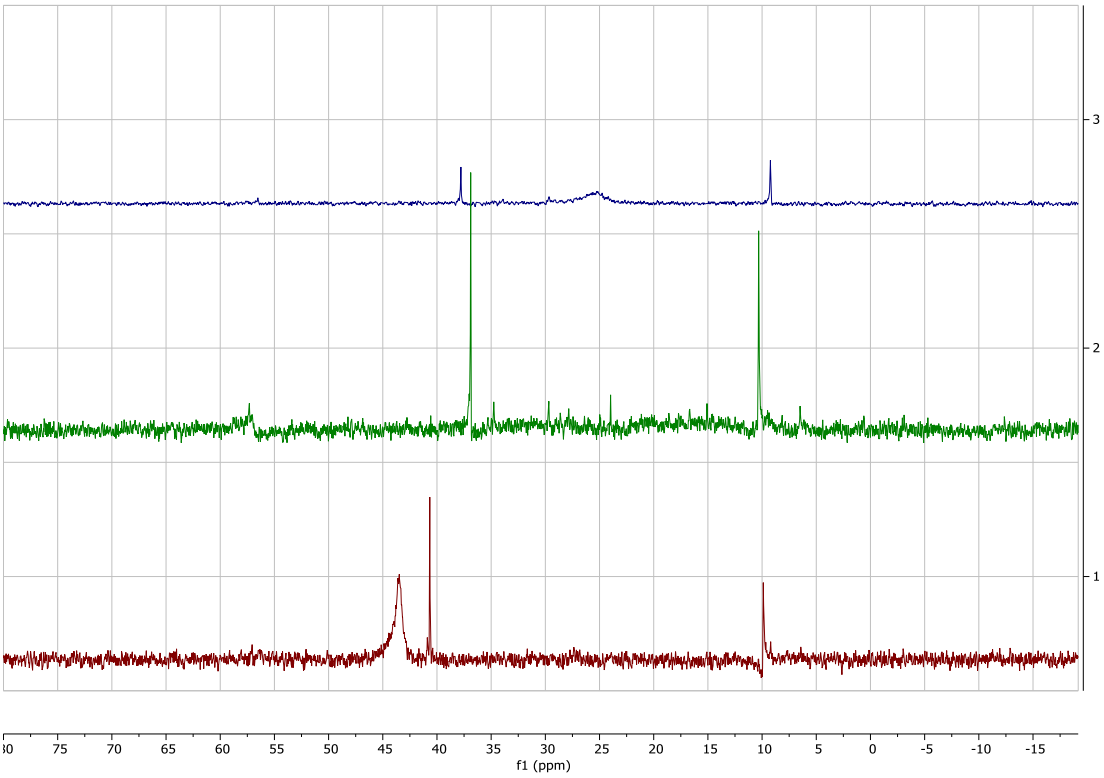

Figure 68. ^{31}P NMR spectra of the reaction product of 2 equivalents of $Ph_3PNTMSLi$ with $BiCl_3$, following a DCM extraction and wash with pentane. NMR solvents (top to bottom): 1,2-difluorobenzene, THF, DCM.

3.3 Reactions of Ph_3PNTMS with trialkyl/triaryl phosphine dihalides

Despite our lack of success with eliminating TMSBr from an alkyl halide, we decided that Ph_3PNTMS might yet eliminate TMSBr or TMSCl from a more ionic source of bromide or chloride, namely a trialkyl/aryl phosphine dihalide. This reaction would make a compound with the general formula $[R_3PNPR'_3]^+[X]^-$, also known as a PNP cation. These salts are useful as the PNP cation is relatively weakly coordinating, enabling them to be used as a soluble source of halide. These cations are most often made by reacting the tertiary phosphine with PCl_5 and hydroxylamine hydrochloride.[57] Unfortunately, this process lacks atom economy. Alternatively, these cations can be made by replacing the TMS group on the nitrogen with a halogen, turning the nitrogen from a

nucleophile into an electrophile. Then, the R_3PNX reacts with R_3P to make the desired compound.[58] However, the synthesis of R_3PNX (described later), is often not trivial. On the other hand, trialkyl/aryl phosphine dihalides are easy to make from direct reaction of the phosphine with the halogen, and R_3PNTMS can be easily made from a Staudinger reaction of TMS-N_3 with the appropriate phosphine (Figure 69) Our route to synthesis involved simply combining Ph_3PNTMS with a phosphine dihalide in acetonitrile and heating to 80°C for 1 hour. This afforded the $[R_3PNPR'_3]^+[X]^-$ compound in nearly quantitative yield (Figure 69). The reaction worked with triarylphosphine dihalides and small trialkyl phosphine dihalides but did not work well with tricyclohexylphosphine dibromide or dichloride, likely due to that phosphine's large size. This can be understood by comparing the Tolman cone angle of the three phosphines, which is a measure of the steric bulk. PMe_3 and PPh_3 have small and moderate Tolman cone angles of 118±2° and 145±2°, respectively, while PCy3 has a much larger Tolman cone angle of 170±2°, consistent with that phosphine's increased bulk.[59]

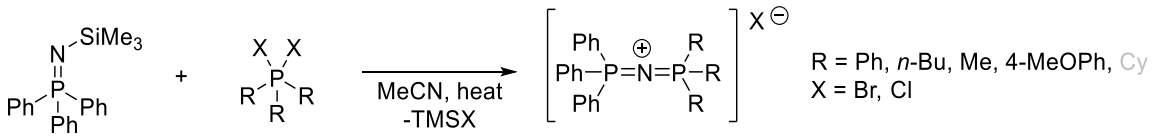

Figure 69. Reaction of Ph_3PNTMS with tertiary phosphine dihalides, making a PNP cation via loss of TMSX.

3.4 Reactions of Ph_3PNTMS to make Ph_3PNX (X=halogen)

3.4.1 Reaction of Ph_3PNTMS with $PhICl_2$

A significant challenge faced our research group is making a source of electrophilic nitrogen. While electrophilic phosphorus is well known (i.e., PCl_3),

electrophilic nitrogen is much rarer, with the most common sources being salts such as nitronium tetrafluoroborate. Nonetheless, we felt that this was a goal worth pursuing, as it would enable us to make C-N bonds by reacting a source of electrophilic nitrogen with a lithium salt, eliminating the need for catalytic C-N cross-couplings, which have proven troublesome in our research group.

Our initial plain involved following a literature procedure where we combined Ph_3PNTMS with $PhICl_2$, which acted as a solid source of Cl_2. This reaction proceeded via the elimination of TMSCl and iodobenzene, making Ph_3PNCl (Figure 70).

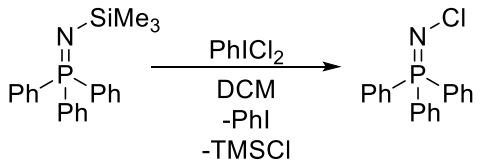

Figure 70. One possible synthesis of Ph_3PNCl, involving $PhICl_2$ as a source of Cl_2, and driven by TMSCl elimination.

$PhICl_2$ could be made via two different literature methods: either by reacting iodosobenzene with two equivalents of TMSCl, eliminating TMSOTMS, or by reacting iodobenzene itself with concentrated aqueous HCl in the presence of hydrogen peroxide, which, over time, would cause $PhICl_2$ to precipitate out (Figure 71). Both methods were successful: the iodosobenzene method was simpler to set up and work up and gave a higher yield, but the iodobenzene route's starting materials were much cheaper. As a result, we ended up using mainly the iodobenzene route for making our $PhICl_2$.

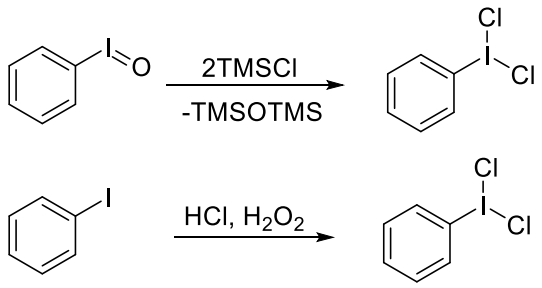

Figure 71. Two different methods of making $PhICl_2$. One involves reaction iodosobenzene with TMSCl, the other iodobenzene with HCl in the presence of H_2O_2.

3.4.2 Development of a More Atom-Economical Route

Though this reaction was successful, it had a major weakness: using $PhICl_2$ meant that the reaction had very poor atom economy, which threatened to undermine its intended purpose as a green reaction to reduce waste from the cage synthesis. Additionally, $PhICl_2$ is not especially stable, tending to break down into Cl_2 and PhI unless it is kept in a cold, dark place. As a result, we sought other methods to install the halogen onto the Ph_3PNTMS. One promising route involved the reaction of I_2O_5 with Ph_3PNTMS, making Ph_3PNIO_2 (Figure 72).[60] While this reaction was simple to perform, we were not able to find a way to selectively remove the oxygen atoms. Magnesium and zinc were excessively strong reducing agents, making an ionic salt, while copper did not appear to perform any reaction, probably because it was not a sufficiently strong reducing agent.

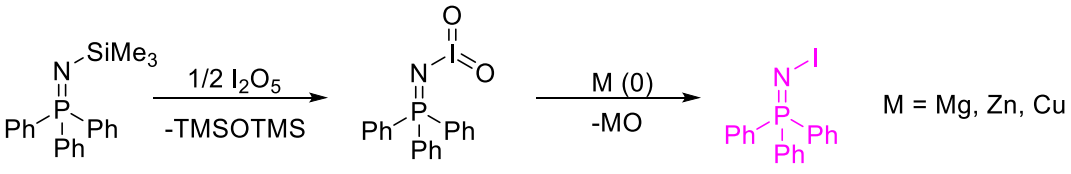

Figure 72. Converting Ph_3PNTMS to Ph_3PNIO_2 using I_2O_5 and attempting to remove the oxygen atoms using a metal reducing agent.

We also tried reacting Ph_3PNTMS with Br_2 and I_2. These reactions both ended up making the $Ph_3PNTMS*Br_2$ and $Ph_3PNTMS*I_2$ adducts, respectively, which would not eliminate TMSX even upon heating (Figure 73).

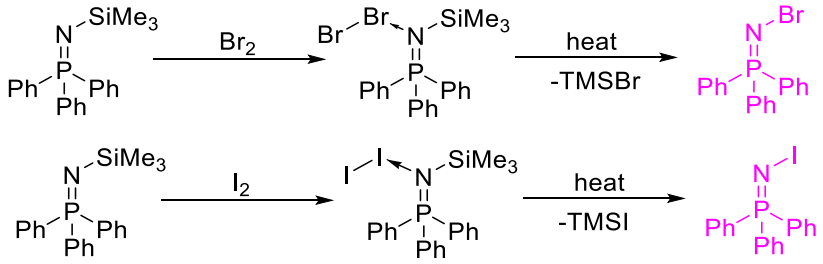

Figure 73. Reactions of Ph_3PNTMS with bromine and iodine, and subsequent attempts to remove the TMS group.

Next, we tried following a literature procedure to remove the TMS from the $Ph_3PNTMS*ICl$ adduct to form Ph_3PNI (Figure 74). This compound should be more reactive than Ph_3PNCl, due to the greater size mismatch between N and I compared to N and Cl, making the iodide a better leaving group than the chloride.[4] Due to availability, we initially substituted NaF for KF due to availability (Figure 74), but this reaction ultimately made Ph_3PF_2 instead of the desired Ph_3PNCl (Figure 74). Interestingly, however, the reaction did make the desired product when KF was used; we are not sure why the choice of counterion in the fluoride salt matters. It is possible that the difference in reaction pathways is due to the difference in lattice energies between KF and NaF, or between KCl and NaCl, which would in turn be related to the ionic sizes. In the binary alkali metal halides, ionic compounds with the best size match between cation and anion tend to have the highest lattice energies. The sizes of Na^+ (1.19Å) and F^- (1.16Å), which might make NaF a poorer source of F^- than KF, where the larger size of the K^+ ion (1.52Å) leads to weaker interactions between it and F^-. Similar conclusions can be

concluded when comparing KCl and NaCl: Cl^- is closer in size (1.67Å) to K^+ than Na^+, which may make the formation of KCl a stronger driving force than the formation of NaCl, resulting in the formation of fewer byproducts.[4]

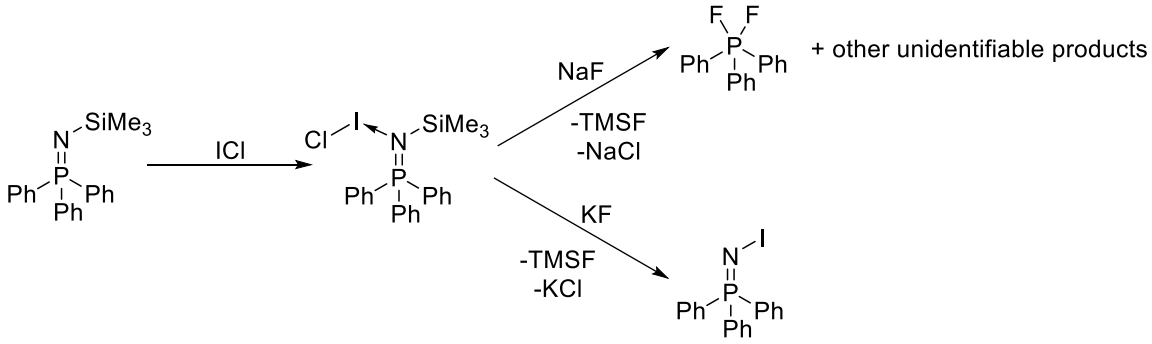

Figure 74. Two different schemes for making Ph_3PNI via Ph_3PNTMS^*ICl, one involving NaF (unsuccessful) and one involving KF (successful).

The iodide could then be further functionalized by reacting it with AgOTf in DCM, making Ph_3PNOTf, which, due to triflate being an excellent leaving group, is expected to be an excellent source of electrophilic nitrogen. Examining the ^{31}P NMR spectra of the various Ph_3PNX species (Figure 75), showed a clear trend, with the ^{31}P nucleus of Ph_3PNOTf being the most deshielded, while that of Ph_3PNCl was the most shielded. In this case, it is reasonable to assume that more deshielded ^{31}P nucleus means a lower electron density in the P=N bond, as is the case for adducts of triethylphosphine oxide with Lewis acids.[61] A more weakly coordinating anion should increase the partial positive charge on N and lower electron density in the P=N bond, which is consistent with the observed trends.

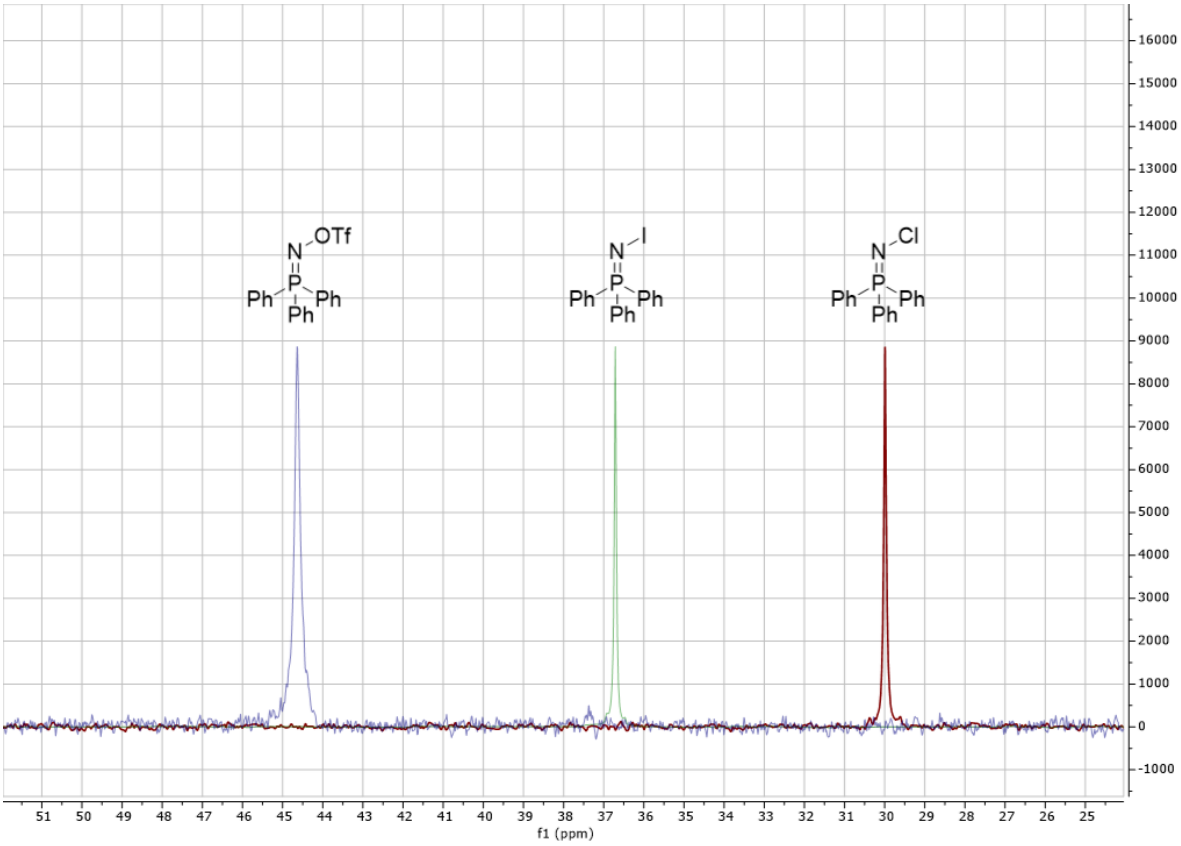

Figure 75. Comparison of the ^{31}P NMR spectra of Ph_3PNOTf (left), Ph_3PNI (centre), and Ph_3PNCl (right).

Our final attempt involved removing the TMS group from Ph_3PNTMS prior to reacting it with the halogens. This route would avoid working with ICl, which is highly corrosive towards metals. We first tried using alcohols to remove the TMS group, but the alcohols were hard to dry, and the resulting Ph_3PNH tended to hydrolyse. So, we settled on using 2 equivalents of HCl in ether, which made the hydrochloride salt. Two equivalents of BuLi in THF removed all the protons and made the lithium salt Ph_3PNLi (Figure 76). This lithium salt did indeed react with Br_2 and I_2, but the products were not particularly clean: we do not know why this is the case (Figure 76, 77). One possibility is that given that Ph_3PNX, once formed, is a nitrogen-centered electrophile, and a solution of halogen was added dropwise to a solution of lithium salt, the Ph_3PNLi may have

quickly reacted with the Ph_3PNX product even at -78°C. This would result in the of $[Ph_3PNPPh_3]^+$ and a low yield of desired product. It is possible that the reaction could have been made more successful by adding a solution of Ph_3PNLi to a solution of I_2 or Br_2, and this is a reaction that our research group would like to re-investigate in the future.

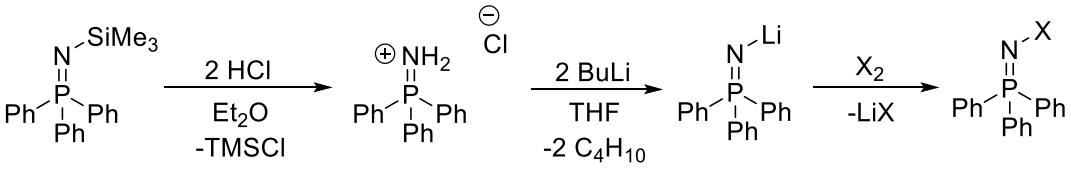

Figure 76. Converting Ph_3PNTMS to Ph_3PNLi by initially removing the TMS group with HCl. The lithium salt was then reacted with the halogen.

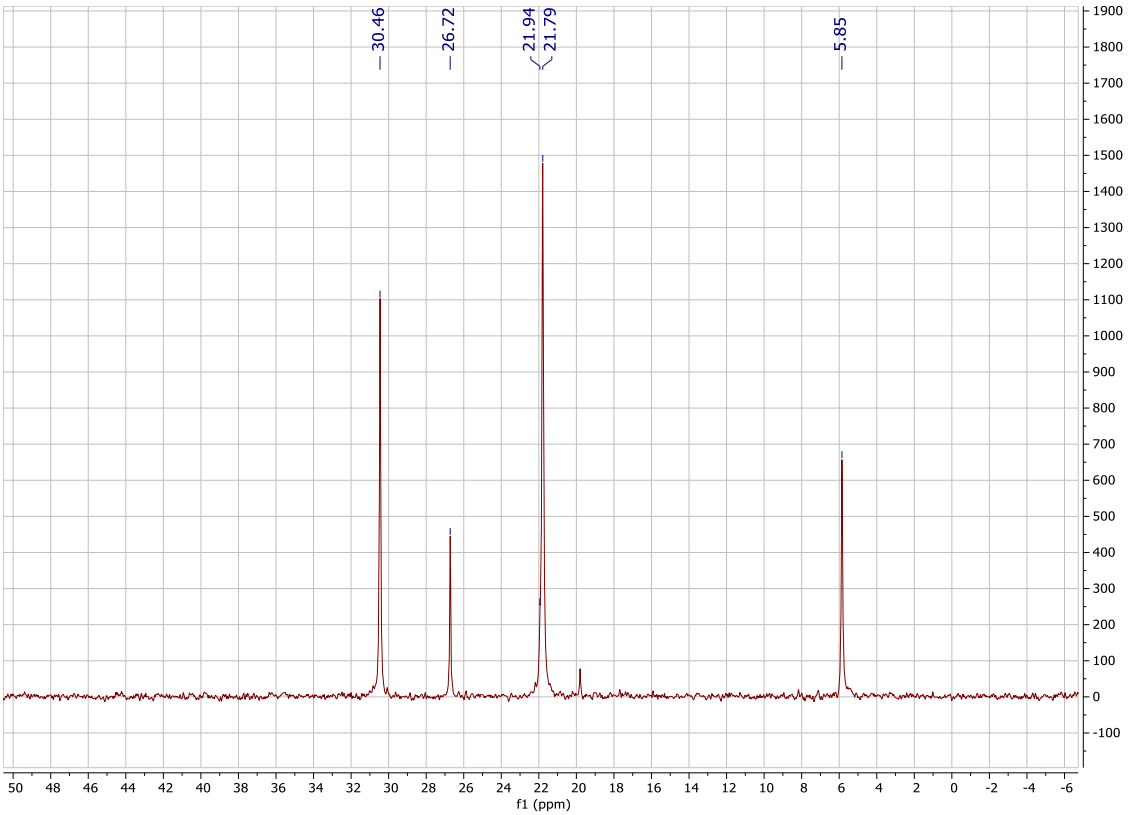

Figure 77. Attempted synthesis of Ph_3PNBr from Ph_3PNLi and Br_2. The peak at 30.5 ppm is assigned to product, while that at 21.8 ppm is assigned to be $[Ph_3PNPPh_3]^+$. The identities of the peaks at 26.7 and 5.9 ppm are unknown.

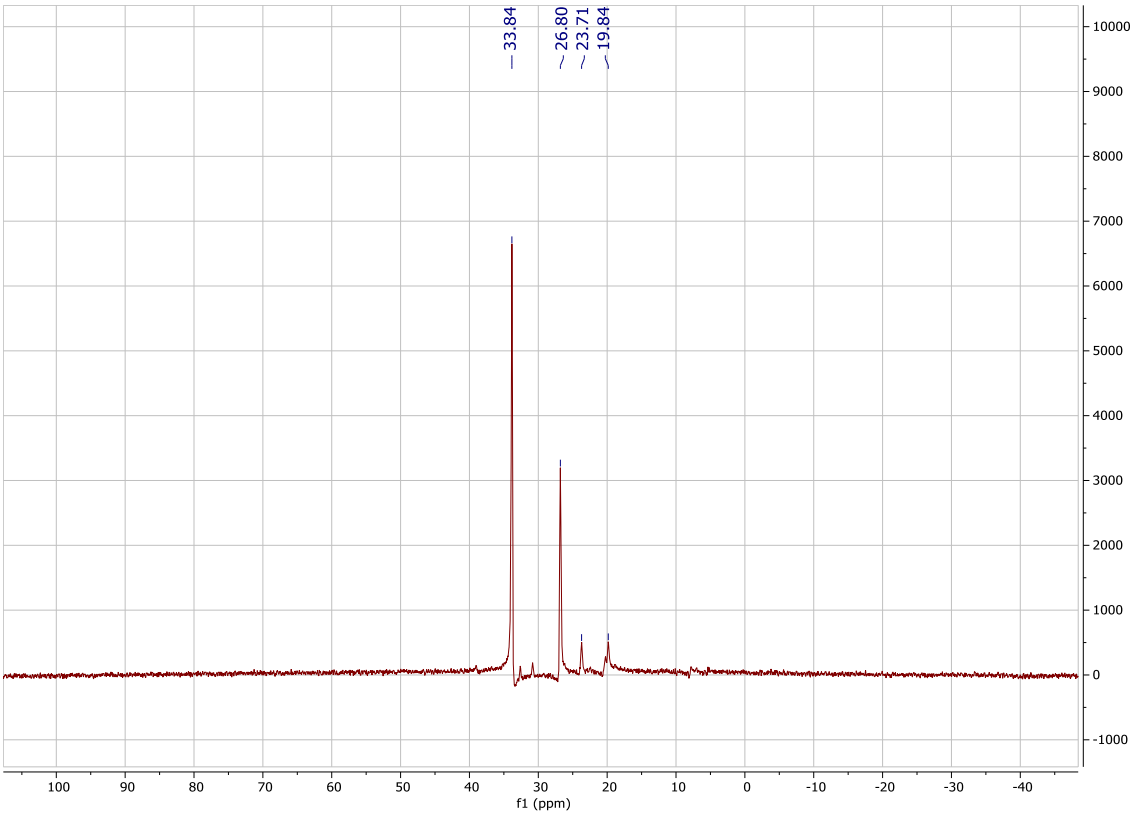

Figure 78. Attempted synthesis of Ph_3PNI from Ph_3PNLi and I_2. The peak at 33.8 ppm is assigned to product. The identity of the other peaks is unknown.

3.4.3 Reactions of Ph_3PNCl with P_2N_6 Cage

With a source of electrophilic nitrogen in hand, a logical next step was to react this compound with a nucleophile. Since the P_2N_6 cages have nucleophilic phosphorus atoms, we decided to try and react these with Ph_3PNCl. Thankfully, the reaction with the P_2N_6 cage proceeded smoothly (Figure 79), yielding the expected three peaks in the ^{31}P NMR within 10 mins. The dication could be synthesized by adding 1 equivalent of Ph_3PNCl to the monocation, or by adding 2 equivalents of Ph_3PNCl to the P_2N_6 cage, which yielded an NMR spectrum with only two peaks.

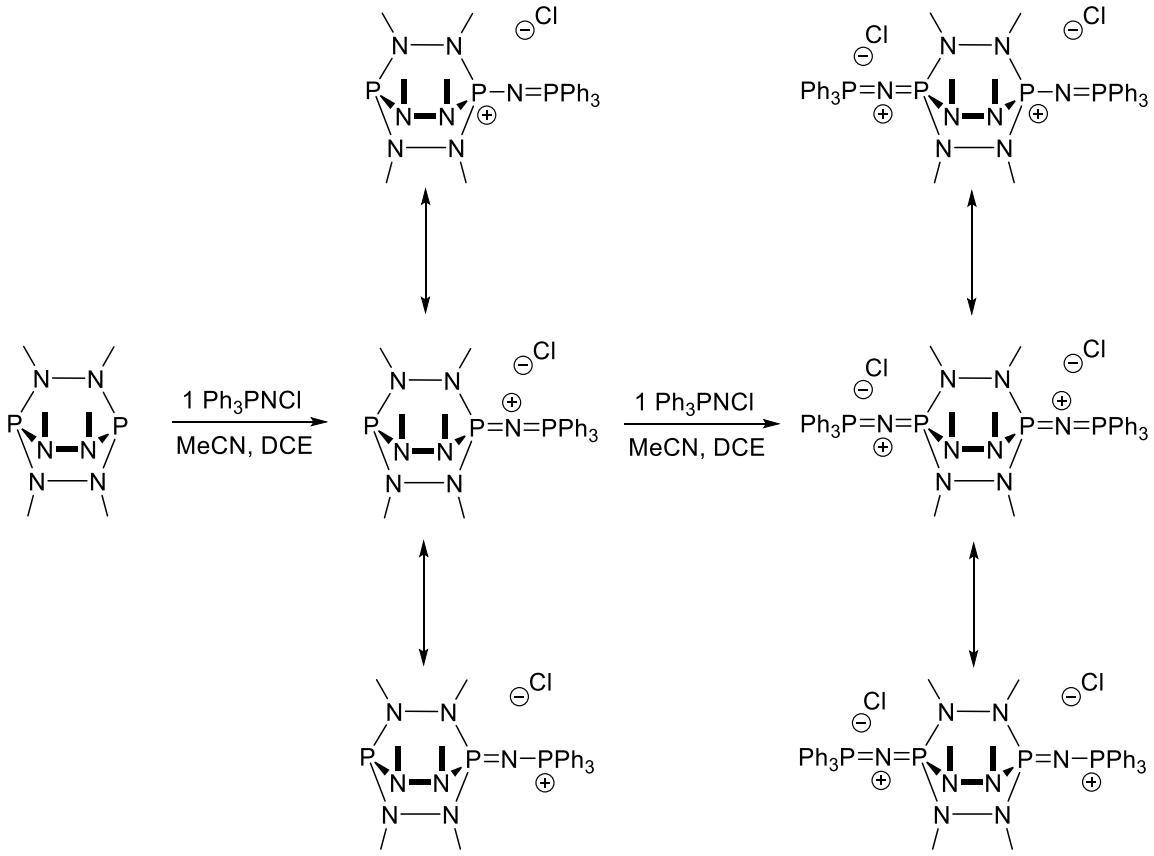

Figure 79. The reactions performed between the P_2N_6 cage and Ph_3PNCl, making the mono and dications. Also shown are the resonance structures of the products.

By examining the ^{31}P NMR spectra (Figure 77), we were able to assign the major signals. The peak at 107.9 ppm corresponds to the starting material, while the doublet of doublets at 6.4 ppm corresponds to the middle P (V), which is split twice by two different phosphorus environments. The doublet at 99.3 ppm corresponds to the P (III) remaining in the monocation, while the PPh_3 group in the monocation comes in at 18.9 ppm as a doublet, which is consistent with the ^{31}P shift observed in $[Ph_3PNPPh_3]Cl$ of 21.1 ppm. It is a bit unusual that the ^3J P-N-N-P coupling is stronger (91.4 Hz) than the ^2J P=N=P coupling (37.9 Hz). However, these results are consistent with the weak coupling constants observed in our other asymmetric PNP cations: no coupling was observed in $[Ph_3PNPBu_3)Br$, and the ^2J P=N=P coupling constant of $[(4\text{-}MeOPh)_3PNPPh_3]Br$ was

small (6.9 Hz). We attibute this to the highly fluxional nature of the P=N bonds, which have multiple resonance structures (Figure 79). In the dication, the in-cage phosphorus atoms appear at -7.2 ppm, and the PPh_3 groups appear at 32.1 ppm. Again, no ^2J P=N=P coupling is observed, as with $[Ph_3PNPBu_3]Br$.

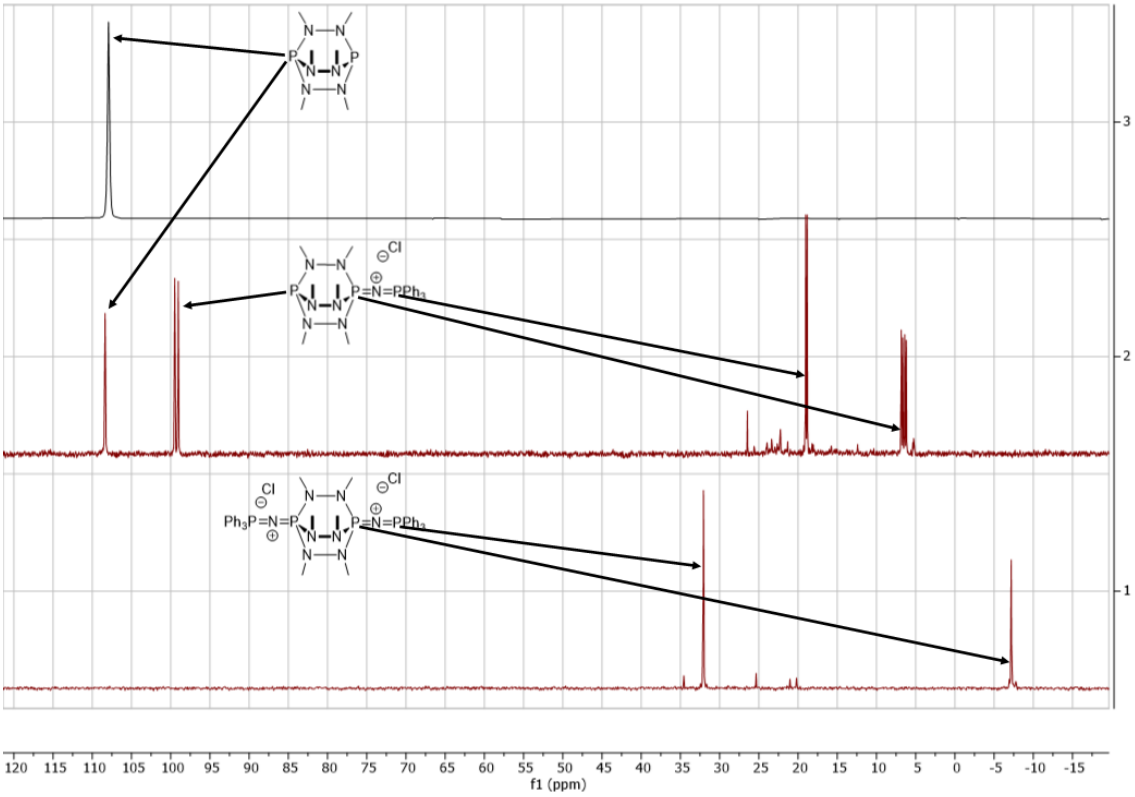

Figure 80. NMR spectra of the starting cage (top), monocation (middle) and dication (bottom).

3.5 Experimental

3.5.1 Synthetic Procedures

All manipulations were performed using standard Schlenk and glovebox techniques under an atmosphere of dry nitrogen. Solvents were dried over Na/benzophenone (tetrahydrofuran, pentanes, hexanes, diethyl ether, toluene, benzene-

d6) or over calcium hydride (dichloromethane, acetonitrile, 1,2-difluorobenzene, dichloromethane-d2, acetonitrile-d3, chloroform-d) and distilled prior to use. Reaction glassware was baked in a 130°C oven for at least 1 h prior to use and assembled under nitrogen while hot. Melting points were obtained for samples sealed in glass capillaries and are uncorrected.

3.5.2 Nuclear Magnetic Resonance

NMR spectra are referenced to tetramethylsilane (^{1}H, ^{13}C), 85% H_3PO_4 (^{31}P) on a Bruker AV-300 spectrometer or a Bruker AV-500 spectrometer with residual solvent used for chemical shift calibration. Samples for NMR spectroscopy were prepared and sealed inside the glovebox with Parafilm before removal into ambient atmosphere.

3.5.3 Vibrational Spectroscopy

Infrared spectra were obtained on a Bruker instrument between KBr plates with the sample dropcast as a thin film.

3.5.4 UV-Vis spectroscopy

UV-VIS spectra were obtained on a cordless SpectroVis Plus spectrometer using a glass cuvette.

3.5.5 Single-crystal XRD

Single crystals diffraction experiments were performed on a Bruker APEX-II CCD diffractometer or D8 Venture diffractometer. Reflections were integrated using the APEX 3 software[35] and solved using SHELXT[36] and refined using SHLEXL[37] with the Olex2 software GUI.

3.5.6 Mass spectrometry

Electro-Spray Ionization (ESI) and Atmospheric Pressure Chemical Ionization (APCI) spectra were obtained on a Bruker micrOTOF instrument.

3.5.7 Elemental Analysis

Elemental analyses were preformed using samples packaged inside a glovebox. Combustion analysis was performed using an Elementar Unicube instrument in CHN/S mode. Note that the journal requirements of ±0.40% accuracy for all elements have recently been critically re-evaluated.[38]

3.5.8 Reagents

Bismuth(III) chloride was purchased from Oakwood Chemicals and purified by vacuum sublimation (10-2 mbar, 200°C) prior to use. Iodobenzene was purchased from Millipore Sigma and used as received. ^{n}BuLi was purchased from Millipore Sigma and used as received. HCl in ether was purchased from Sigma Aldrich and used as received. Ph_3P was purchased from Sigma Aldrich and used as received.

3.5.9 Synthesis of tris(Ph_3PNTMS)Bi

Lithiation of Ph_3PNTMS using ^{n}BuLi was performed following a literature procedure.[54] However, the reaction was determined to be complete after 2 hours, via ^{31}P NMR.

o-lithio Ph_3PNTMS (5.05 g, 6.43 mmol) was dissolved into THF (25 mL). $BiCl_3$ (1.35g, 4.29 mmol) dissolved in THF (25 mL), and cooled to -78°C. The $BiCl_3$ solution was added dropwise to the Li salt, and the cooling bath was removed after 15 mins. After

stirring for another 2 hours, the reaction mixture made a dark orange solution. All THF was removed under reduced pressure, and 100 mL of distilled water was added to the solid. This mixture was sonicated for 10 mins, and then suction filtered. The dark grey solid was extracted with 140 mL of boiling toluene. The solution was filtered off, and the toluene was pumped off under reduced pressure. Ether (100 mL) was added to the residue, followed by a 5-minute sonication. Suction filtration offered the product as a white powder (3.60g, 67%). Single crystals, suitable for XRD, were grown by recrystallization from hot benzene, layered with pentane. ^{1}H NMR (C_6D_6, 500 MHz): 8.19 (dt, 3H, J = 1.4, 7.6 Hz), 7.92 (dd, 3H, J = 1.6, 11.7 Hz), 7.90 (dt, 3H, J = 1.4, 11.7 Hz), 7.57 (dt, 3H, J = 1.2, 11.7 Hz), 7.55 (dd, 3H, 1.5, 11.6 Hz), 7.52 (ddd, 3H, J= 1.1, 7.8, 12.6 Hz), 7.22-7.18 (m, 6H), 7.18-7.15 (m, 6H), 7.05 (tq, 3H, J = 1.51, 7.3 Hz), 7.02-6.93 (m, 9H), 6.63 (tt, 3H, J = 1.7, 7.4 Hz), 0.12 (s, 27H). ^{13}C NMR (C_6D_6, 125 MHz): 187.4 (d, J = 16.3 Hz), 144.6 (d, J = 17.2 Hz), 139.3 (d, J = 126.7 Hz), 137.4 (d, J= 21.9 Hz), 136.7 (d, J = 22.0 Hz), 134.4 (d, J = 19.5 Hz), 132.9 (d, J = 10.1 Hz), 132.6 (s), 132.5 (d, J = 9.7 Hz), 130.6 (d, J= 2.0 Hz), 129.9 (d, J = 2.0 Hz), 128.2 (s), 128.0 (d, J = 11.2 Hz), 127.6 (d, J = 11.7 Hz), 124.9 (d, 13.8 Hz), 4.6 (d, 3.5 Hz). ^{31}P NMR (C_6D_6, 202 MHz): δ = 12.3 (q, J = 11.4 Hz). ^{29}Si-^{1}H HMBC: (C_6D_6, 500 MHz): δ = -7.4. Melting/decomposition point > 260°C. FT-IR (transmission, drop-cast onto KBr plate): 676 (m), 694 (s), 720 (s), 750 (s), 830 (s), 857 (s), 999 (w), 1028 (vw), 1104 (s), 1185 (w), 1234 (vs), 1436 (s), 1481 (m), 1567 (w), 1818 (w), 1859 (w), 2892 (w), 2946 (m), 3040 (m).

3.5.10 Methylation of tris(Ph_3PNTMS)Bi

On the first attempt, tris(Ph_3PNTMS)Bi (0.062g, 0.05 mmol) was dissolved in THF (0.6 mL) in a vial, and iodomethane (0.0093 mL, 0.15 mmol) was added to the vial in one portion. The suspension was put into an NMR tube, and no evidence of reaction was found. Heating to 60°C failed to result in reactivity.

On a second attempt, tris(Ph_3PNTMS)Bi (0.062g, 0.05 mmol) was dissolved in 1,2-dichloroethane (0.6 mL) in a vial, and methyl triflate (0.017 mL, 0.15 mmol) was added to the vial in one portion. The suspension was put into an NMR tube, and no evidence of reaction was found. The reaction was heated to 80°C, which resulted in all the components going into solution, however, the ^{31}P NMR showed an unintelligible mass of peaks.

3.5.11 Reaction of tris(Ph_3PNTMS)Bi with NaO^{t}Bu

Tris(Ph_3PNTMS)Bi (0.125g, 0.10 mmol) was added to mesitylene (0.7 mL), and NaO^{t}Bu (0.0096g, 0.10 mmol) and 18-crown-6 (0.0264g, 0.10 mmol) were added. The suspension was transferred from a vial to an NMR tube and heated to 80°C. Multiple peaks were observed in the ^{31}P NMR, but the products were not identifiable.

3.5.12 Reaction of tris(Ph_3PNTMS)Bi with HCl

Tris(Ph_3PNTMS)Bi (0.454g, 0.36 mmol) was dissolved in THF (8 mL), and HCl (4M in dioxane, 0.27 mL, 1.09 mmol) was added. While additional precipitate did form, it was insoluble in anything other than DMSO. The ^{31}P NMR taken in DMSO showed three peaks.

3.5.13 Reaction of tris(Ph_3PNTMS)Bi with sulfur

Tris(Ph_3PNTMS)Bi (0.062g, 0.05 mmol) was dissolved in benzene (0.6 mL) in a vial, and sulfur (0.0016 g, 0.05 mmol) was added to the vial in one portion. The suspension was put into an NMR tube, and no evidence of reaction was found, even if heated to 80°C overnight.

3.5.14 Attempt to make bis(Ph_3PNTMS)BiCl

o-lithio Ph_3PNTMS (3.37 g, 4.29 mmol) was dissolved in THF (25 mL). $BiCl_3$ (1.35g, 4.29 mmol) was dissolved in THF (25 mL) and the solution cooled to -78°C. The solution of lithium salt was added dropwise. After 15 minutes, the cooling was removed, and the reaction allowed to stir for 2 hours, making a dark orange solution. The THF was removed under reduced pressure, and the product extracted using DCM (60 mL). The DCM extract was filtered, and the solvent removed under reduced pressure. Washing the solid residue yielded a white solid, which was determined to primarily consist of Bi(Ph_3PNTMS)(Ph_3PN). Attempts to perform the reaction in toluene and oDFB were not successful.

3.5.15 Synthesis of $PhICl_2$

This synthesis was adapted from a literature procedure.[62] Iodobenzene (10.00 ml, 89.2 mmol) was placed in a 500 mL round-bottom flask. The flask was placed into an ice-water bath, and 10M HCl in H_2O was added dropwise, followed by hydrogen peroxide (30% in H_2O, 3 mL). A large lumpy mass of product started to form. After 1 hour, the solid was isolated by suction filtration. Another 3 mL of H_2O_2 was added to the filtrate, which was put back into the round-bottom flask, and the reaction allowed to

proceed for another hour, producing another large lumpy mass of product. This was also isolated by suction filtration. Both batches of solid were washed with distilled water, dissolved a minimal amount of DCM, and dried over anhydrous $MgSO_4$. This solution was concentrated using rotary evaporation at 400mbar and 35°C until product just started to crystallize, at which point the flask was put in the freezer. After product isolation, further concentration and recrystallizations produced more product. The final yield was 10.26g (42%) after three rounds of concentration and crystallization. 1H NMR (CH_2Cl_2, 300MHz): δ = 7.62 (d, 2H, J = 8.7 Hz), 7.05 (t, 1H, J = 7.4 Hz), 6.91 (t, 2H, J = 7.9 Hz).

3.5.16 Reduction of Ph_3PNIO_2 with metals

The reaction of Ph_3PNTMS with I_2O_5 followed a literature procedure.[60] However, it was important to ensure the I_2O_5 was well ground, as the reaction produced poor yields when the poorly soluble I_2O_5 was lumpy.

For each metal reduction, Ph_3PNIO_2 (0.0435g, 0.10 mmol) was dissolved in THF (0.7 mL) and placed in an NMR tube. For each attempted reduction, 0.20 mmol of Zn, Mg, or Cu was added to the NMR tube. The reaction was heated overnight to 80°C. These reactions were severely hampered, however, by the poor solubility of the starting material in THF, and very limited conversion was observed.

3.5.17 Synthesis of Ph_3PNLi

This reaction was adapted from a literature procedure.[52] Ph_3PNTMS (5.24g, 15 mmol) was dissolved in Et_2O (75 mL), and the reaction mixture cooled to 0°C. HCl in dioxane (4M, 7.5 mL, 30 mmol) was added dropwise, forming a lot of white precipitate. The reaction was allowed to stir for 30 mins, and the solvent removed via filter cannula.

The flask was subsequently vacuum dried for 1 hour to remove all traces of HCl and TMSCl. THF (75 mL) was then added to the solid, and the suspension was cooled to 0°C. ^{n}BuLi (2.5M in hexanes, 12 mL, 30 mmol) was added dropwise, and the reaction allowed to warm to room temperature and stirred for 30 minutes. The solvent was removed under reduced pressure, and toluene (75 mL) was added to extract the product. After stirring overnight, the LiCl was filtered off, and the toluene was removed under reduced pressure. The light-yellow solid was then washed with pentane and dried *in vacuo*. Total yield was 3.20 g (75%). ^{1}H NMR (C_6H_6, 300 MHz): 6.98-6.26 (m, 7H), 6.13-5.58 (m, 8H). ^{31}P NMR (C_6H_6, 121 MHz): δ = 5.7.

3.5.18 Reaction of Ph_3PNLi with Br_2

Ph_3PNLi (0.283g, 1 mmol) was dissolved in THF (4 mL) in a 25 mL Schlenk flask. Br_2 (0.051 mL, 1 mmol) was dissolved in THF (4 mL) in a 25 mL Schlenk bomb. The lithium salt solution was cooled to -78°C, and the Br_2 was slowly added to the Li salt. The red-brown colour of the Br_2 almost completely disappeared within 3 minutes, and the Li salt (of limited solubility) went into solution after that time as well. The reaction was then warmed to room temperature, causing a white precipitate to form, and an aliquot was examined using ^{31}P NMR, revealing multiple products. The reaction was retried in toluene using the exact same quantities of solvents and reagents and the same conditions, apart from adding the Br_2 directly to the pre-cooled toluene to prevent the formation of *p*-bromotoluene. This also failed to provide a single clean product.

3.5.19 Reaction of Ph_3PNLi with I_2

Ph_3PNLi (0.0283g, 0.1 mmol) was dissolved in THF (0.4 mL). I_2 (0.0254g, 0.1 mmol) was dissolved in THF (0.4 mL). Both solutions were cooled to -20°C in a glove box freezer, and the I_2 solution was slowly added to the solution of Li salt. The mixture was warmed to room temperature and added to an NMR tube. ^{31}P NMR showed two major peaks at 33.8 and 25.6 ppm.

3.5.20 Synthesis of Ph_3PNCl

$PhICl_2$ (1.25g, 4.54 mmol) was dissolved in DCM (16 mL) in a foil-covered round bottom flask. This solution was cooled to -20°C, then slowly added to solid Ph_3PNTMS (1.59g, 4.54 mmol), also in a foil-covered round bottom flask equipped with a magnetic stirbar. The reaction was allowed to warm to room temperature, stirred for 2 hours, then checked by NMR. All volatiles were removed under reduced pressure, and hexane (25 mL) was added. The hexane solution was filtered, and the residue was extracted with toluene (2x25 mL). Evaporation of the toluene afforded the product as a white solid (0.78g, 68%). ^{31}P $\{^1H\}$ NMR (toluene, 202 MHz): $\delta = 20.9$.

3.5.21 Synthesis of mono-capped P_2N_6 cage

The P_2N_6 cage (0.0779g, 0.25 mmol) was placed in a sample vial, to which 1.2 mL of acetonitrile was added initially, followed by 1.2 mL of DCE. In a separate vial equipped with a stirbar, the Ph_3PNCl (0.0590g, 0.25 mmol) was added. The solution of P_2N_6 cage was slowly added to the Ph_3PNCl with stirring, and the reaction was allowed to proceed for 10 minutes before an NMR was taken, which showed ~25% unreacted cage (appearing as a singlet at 107.9 ppm) and ~75% the desired product. All Ph_3PNCl

was consumed. Product ^{31}P {^{1}H} NMR (50:50 DCE:MeCN, 202 MHz): δ = 99.2 (d, J = 91.4 Hz), 18.9 (d, J = 38.5 Hz), 6.5 (dd, J = 38.5, 91.4 Hz).

3.5.22 Synthesis of di-capped P_2N_6 cage

The P_2N_6 cage (0.0779g, 0.25 mmol) was placed in a sample vial, to which 1.2 mL of acetonitrile was added initially, followed by 1.2 mL of DCE. In a separate vial equipped with a stirbar, the Ph_3PNCl (0.118g, 0.50 mmol) was added. The solution of P_2N_6 cage was slowly added to the Ph3PNCl with stirring, and the reaction was allowed to proceed for 10 minutes All Ph_3PNCl was consumed. ^{1}H NMR (50:50 DCE:MeCN, 300 MHz): δ = 7.74-7.65 (m, 12H), 7.60 (tq, 6H, J = 1.6, 7.2 Hz). 7.54-7.45 (m, 12H). The CH_3 groups on the cage are not visible due to the use of non-deuterated solvent. ^{31}P {^{1}H} NMR (50:50 DCE:MeCN, 202 MHz): δ = 32.0, -7.2.

3.5.23 Synthesis of Ph_3PNTMS*ICl

This synthesis was performed via a slightly modified literature procedure.[63] Iodine monochloride (1.65g, 10.2 mmol) was dissolved in DCM (8 mL). A solution of Ph_3PNTMS (3.56g, 10.2 mmol) was dissolved in DCM (12 mL) and added dropwise via cannula to the ICl solution. The reaction rapidly turned orange and formed a precipitate within 5 minutes. The ^{31}P[48] NMR spectrum showed complete product consumption after 1 hour. Removing the DCM resulted in the formation a very sticky, foamy orange tar. To make the product easier to handle, it was sonicated with ether (20 mL) for 1 hour and then stirred. Suction filtration afforded the product as a yellow solid (3.49g, 68%). ^{1}H NMR (DCM, 500 MHz): δ = 7.67-7.55 (m, 9H). 7.53-7.44 (m, 6H), -0.07 (s, 9H). ^{31}P {^{1}H} NMR (DCM, 202 MHz): δ = 30.1 (br. s.)

3.5.24 Synthesis of Ph_3PNI

The synthesis of Ph_3PNI was based on a literature procedure.[63] $Ph_3PNTMS*ICl$ (1.27g, 2.48 mmol) was dissolved in MeCN (20mL), and KF (2.87g, 49.4 mmol) was added. The reaction was refluxed for 30 mins, then filtered while hot. The filtrate was allowed to very slowly cooled to room temperature, then placed in the freezer. Cubic orange crystals formed in the solution, which were isolated via suction filtration (0.74g, 74%). ^{31}P $\{^1H\}$ NMR (DCM, 202 MHz): $\delta = 36.7$.

3.5.25 Synthesis of Ph_3PNOTf

AgOTf (0.0128g, 0.05 mmol) was dissolved in DCM (0.75 mL), and added dropwise to a stirring solution of Ph_3PNI (0.0201g, 0.05 mmol) dissolved in DCM (0.75 mL), which immediately resulted in the formation of a precipitate of AgI. The reaction was allowed to run at room temperature for 10 minutes before an NMR was taken. ^1H NMR (DCM, 500 MHz): $\delta = 7.70$ (tq, 3H, J = 1.5, 7.6 Hz), 7.64 (dd, 6H, J = 7.8, 11.2 Hz), 7.55 (td, 6H, J = 3.2, 7.6 Hz). ^{31}P $\{^1H\}$ NMR (DCM, 202 MHz): $\delta = 44.6$.

3.5.26 Representative Synthesis of PNP Cations

Ph_3PNTMS (0.1 mmol, 0.035g) was dissolved in MeCN (0.35 mL) and a suspension of R_3PBr_2 (0.1 mmol) in MeCN (0.35 mL) was added. The reaction was heated to 80°C for 1 hour. The solvent was then removed under reduced pressure before the designated NMR solvent was added.

3.5.26.1 [Ph_3PNPPh_3]Br

^1H NMR (DCM, 500 MHz): $\delta = 7.75$-7.67 (m, 6H), 7.57-7.49 (m, 24H). $^{31}P\{^1H\}$ NMR (DCM, 202 MHz): $\delta = 21.1$.

3.5.21.2 [$Ph_3PNP(4\text{-}MeOPh)_3$]Br

^{1}H NMR ($CDCl_3$, 300 MHz): δ = 7.70-7.58 (m, 5H), 7.53-7.40 (m, 15H), 7.33 (dd, 6H, J = 8.7, 12.6), 6.94 (dd. 6H, J = 2.6, 8.8 Hz), 3.87 (s, 9H). $^{31}P\{^1H\}$ NMR ($CDCl_3$, 121 MHz): δ = 20.6 (d, J = 7.0 Hz), 19.6 (d, J = 7.0 Hz).

3.5.21.3 [Ph_3PNPBu_3]Br

^{1}H NMR ($CDCl_3$, 300 MHz): δ = 7.73-7.56 (m, 15H), 2.08-1.95 (m, 6H), 1.46-1.23 (m, 12H), 0.79 (t. 9H, J = 7.1 Hz). ^{13}C NMR ($CDCl_3$, 75 MHz): δ = 133.7 (d, J = 2.6 Hz), 131.9 (d, J = 10.9 Hz), 129.6 (d, J = 13.6 Hz), 27.0 (d, J = 64.2 Hz), 23.8, 23.7 (d, J = 9.4 Hz), 13.6. $^{31}P\{^1H\}$ NMR ($CDCl_3$, 121 MHz): δ = 40.5, 15.7.

3.5.27 Representative Synthesis of R_3PBr_2

Ph_3P (10.0g, 38.1 mmol) was dissolved in toluene (100 mL). Br_2 (1.95 mL, 38.1 mmol) was added dropwise. The reaction was allowed to stir overnight, and then the supernatant decanted off. The solid was subsequently washed with pentane and filtered, offering the product as a white solid (15.2g, 94%). ^{31}P NMR ($CDCl_3$, 202 MHz): δ = 54.5.

Chapter 4: Conclusions

This thesis reports two studies: how minor geometric changes to a ligand can have a major effect on the structure and stability of a bismuth complex, and potential ways to reuse a waste product from another chemical synthesis.

4.1 Mesomeric Tuning at Bi Centres

In summary, we managed to make two different Bi (III) compounds based on CN_2 ligands, both of them based on silylated m-xylylenediamine. They were both dimers at room temperature, which we attribute to the small size of the silanes employed. Employing bulkier groups, such as large silanes or 2,6-diisopropylphenyl, in an attempt to prevent dimerization, resulted in the spontaneous reduction of the Bi (III) centre to a Bi (I) centre, as indicated by NMR and XRD. Similar results were observed when this ligand was used with Sb, while P and As were too small to effectively coordinate to this pincer ligand and ended up making oligomers. A deuterated CN_2Dipp_2 compound was synthesized in an attempt to get a kinetic isotope effect and determine the mechanism of this reduction, but the formation of multiple products made determining a KIE impossible. Nonetheless, we came up with two possible mechanisms for how this autoreduction might occur, both of which involving the bismuth centre. Removing the benzylic hydrogens and replacing them with methyl groups or oxygen in order to prevent autoreduction resulted in issues with solubility in both cases, possibly due to the Li salt being unable to dimerize. Employing a chelating aniline to prevent autoreduction resulted in issues deprotonating the central carbon on the xylene backbone, possibly due to the methoxy groups directing lithiation to the anisole rings instead.

In the future, we hope to re-investigate the tetramethyl NCN ligand, as this ligand's inability to lose H_2 from the benzylic positions will make reduction from Bi (III) to Bi (I) less likely. Furthermore, the increased steric bulk at the benzyl positions should make dimerization much less favourable. Instead of trying to triply deprotonate the ligand, we suggest making the more soluble dilithium salt and reacting that with a transition metal halide such as $TiCl_4$ or $ScCl_3$.Then, a metathesis reaction with $BiCl_3$ should yield the desired Bi (III) compound, with $TiCl_4$ or $ScCl_3$ being the by-product (Figure 81).

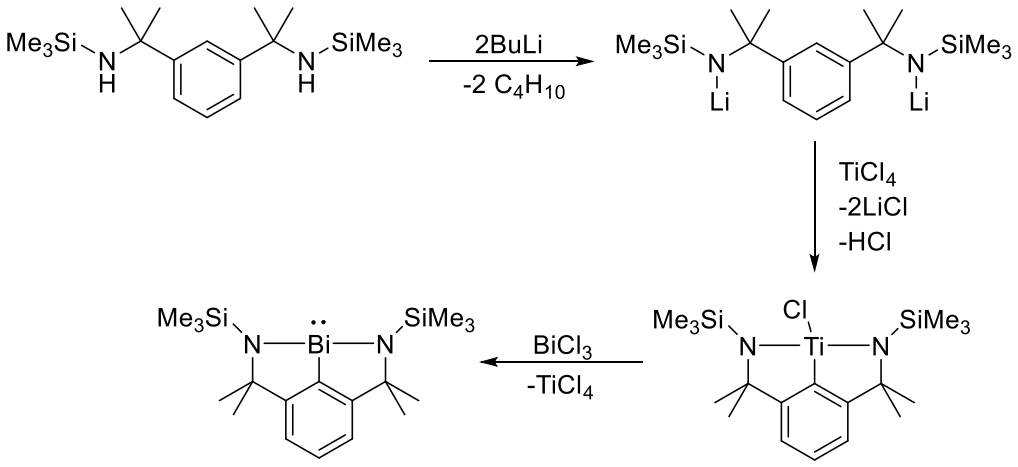

Figure 81. Future synthetic scheme to make the tetramethyl NCN Bi compound, via transition metal metathesis. The $TiCl_4$ could be substituted for $ScCl_3$ if required.

4.2 Reuse of a Synthetic Waste Product

In conclusion, we have managed to find a use for Ph_3NTMS. *Ortho*-lithiation made it a decent ligand for bismuth, although the compound it made had no interesting properties that we were able to determine, aside from exceptional stability. The reactions of Ph_3PNTMS with R_3PX_2 were facile and proceeded in high yield, providing a new synthetic method for making these weakly coordinating cations. The literature synthesis of Ph_3PNCl was successful, and it was indeed a useful source of electrophilic nitrogen,

enabling the synthesis of mono- and dications from the P_2N_6 cage. Unfortunately, the literature route suffered from poor atom economy due to the use of $PhICl_2$, which made it much less green that we would have initially hoped. Attempts were made to develop a more atom-economical route, and it was found that direct reaction of Ph_3PNTMS with ICl was most effective, making $Ph_3PNTMS*ICl$. Reaction with KF then removed the TMS group, making Ph_3PNI. This compound could then be reacted with AgOTf to make Ph_3PNOTf, which is expected to be a much more powerful source of Ph_3PN^+ than the chloride or iodide.

In future, we hope to make the compound $[Ph_3PN]^+[BArF]^-$, which will be an exceptionally strong (and soluble) source of Ph_3PN^+, and react this with a P_4N_5 cage (Figure 82), making a tetracation of high Lewis acidity. Unlike common Lewis acids, the LUMO for this tetracation inside the cage, making it inaccessible and preventing its quenching – effectively, this compound would be a "frustrated Lewis acid" (Figure 82). We are also hoping to react Ph_3PNCl and Ph_3PNI with lithium salts in syntheses of future ligands. The resulting phosphine imines could either be used as is, or converted into free amines (Figure 83), which could then be further functionalized.

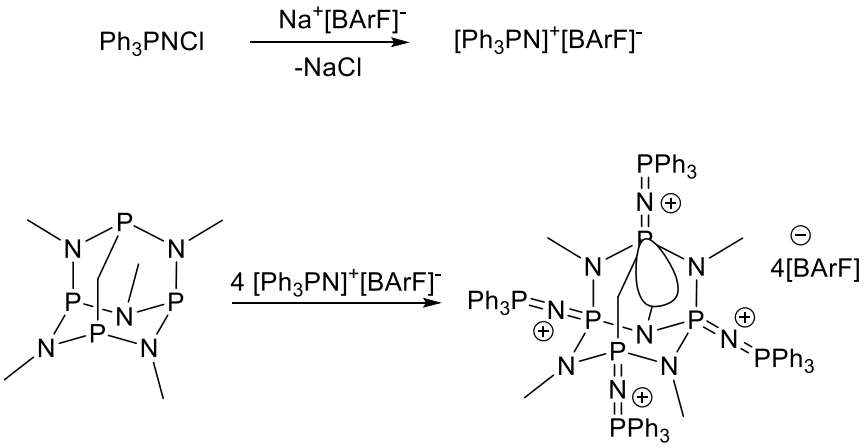

Figure 82. Converting Ph_3PNCl into $[Ph_3PN]^+[BArF]^-$, and the subsequent reaction between the P4 cage and $[Ph_3PN]^+[BArF]^-$, making a tetracation. The indicated orbital is the LUMO and is located inside the cage.

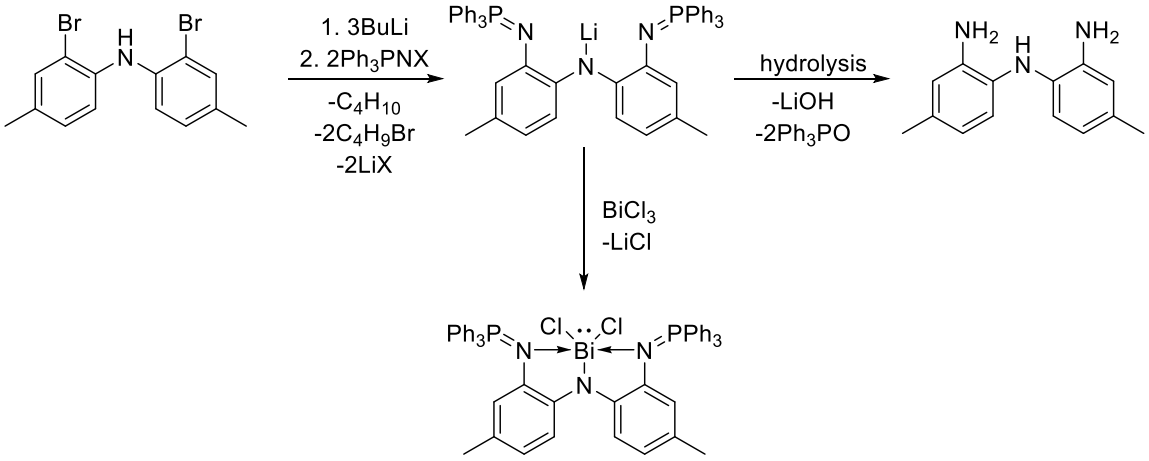

Figure 83. Some example reactions of Ph_3PNX with lithium salts, and how these could be used to make future ligands. X = Cl, I

References

(1) George W. Parshall, S. D. I. *Homogeneous Catalysis: The Applications and Chemistry of Catalysis by Soluble Transition Metal Complexes*; Wiley, 1992.

(2) Kotha, S.; Lahiri, K.; Kashinath, D. Recent Applications of the Suzuki—Miyaura Cross-Coupling Reaction in Organic Synthesis. *ChemInform* **2003**, *34* (9). DOI: https://doi.org/10.1002/chin.200309228. Miyaura, N.; Yamada, K.; Suzuki, A. A new stereospecific cross-coupling by the palladium-catalyzed reaction of 1-alkenylboranes with 1-alkenyl or 1-alkynyl halides. *Tetrahedron Letters* **1979**, *20* (36), 3437-3440. DOI: https://doi.org/10.1016/S0040-4039(01)95429-2.

(3) Dorel, R.; Grugel, C. P.; Haydl, A. M. The Buchwald–Hartwig Amination After 25 Years. *Angewandte Chemie International Edition* **2019**, *58* (48), 17118-17129. DOI: https://doi.org/10.1002/anie.201904795. Hartwig, J. F. Transition Metal Catalyzed Synthesis of Arylamines and Aryl Ethers from Aryl Halides and Triflates: Scope and Mechanism. *Angewandte Chemie International Edition* **1998**, *37* (15), 2046-2067. DOI: https://doi.org/10.1002/(SICI)1521-3773(19980817)37:15<2046::AID-ANIE2046>3.0.CO;2-L.

(4) Gary L. Meissler, P. J. F., Donald A. Tarr. *Inorganic Chemistry*; Pearson, 1991.

(5) Amatayakul, W.; Ramnäs, O. Life cycle assessment of a catalytic converter for passenger cars. *Journal of Cleaner Production* **2001**, *9* (5), 395-403. DOI: https://doi.org/10.1016/S0959-6526(00)00082-2.

(6) Yaroshevsky, A. A. Abundances of chemical elements in the Earth's crust. *Geochemistry International* **2006**, *44* (1), 48-55. DOI: 10.1134/S001670290601006X.

(7) Cinti, D.; Angelone, M.; Masi, U.; Cremisini, C. Platinum levels in natural and urban soils from Rome and Latium (Italy): significance for pollution by automobile catalytic converter. *Science of The Total Environment* **2002**, *293* (1), 47-57. DOI: https://doi.org/10.1016/S0048-9697(01)01137-8. Stohs, S. J.; Bagchi, D. Oxidative mechanisms in the toxicity of metal ions. *Free Radical Biology and Medicine* **1995**, *18* (2), 321-336. DOI: https://doi.org/10.1016/0891-5849(94)00159-H.

(8) Tasker, S. Z.; Standley, E. A.; Jamison, T. F. Recent advances in homogeneous nickel catalysis. *Nature* **2014**, *509* (7500), 299-309. DOI: 10.1038/nature13274.

(9) Ranjit, S.; Lee, R.; Heryadi, D.; Shen, C.; Wu, J. E.; Zhang, P.; Huang, K.-W.; Liu, X. Copper-Mediated C–H Activation/C–S Cross-Coupling of Heterocycles with Thiols. *The Journal of Organic Chemistry* **2011**, *76* (21), 8999-9007. DOI: 10.1021/jo2017444.

(10) Humphreys, J.; Lan, R.; Tao, S. Development and Recent Progress on Ammonia Synthesis Catalysts for Haber–Bosch Process. *Advanced Energy and Sustainability Research* **2021**, *2* (1), 2000043. DOI: https://doi.org/10.1002/aesr.202000043.

(11) Ogawa, T.; Ruddy, A. J.; Sydora, O. L.; Stradiotto, M.; Turculet, L. Cobalt- and Iron-Catalyzed Isomerization–Hydroboration of Branched Alkenes: Terminal Hydroboration with Pinacolborane and 1,3,2-Diazaborolanes. *Organometallics* **2017**, *36*, 417-423. Ruddy, A. J.; Kelly, C. M.; Crawford, S. M.; Wheaton, C. A.; Sydora, O. L.; Small, B. L.; Stradiotto, M.; Turculet, L. (N-Phosphinoamidinate)Iron Pre-Catalysts for the Room Temperature Hydrosilylation of Carbonyl Compounds with Broad Substrate Scope at Low Loadings. *Organometallics* **2013**, *32*, 5581-5588. Webster, R. L. β-Diketiminate complexes of the first row transition metals: applications in catalysis. *Dalton Transactions* **2017**, *46* (14), 4483-4498, 10.1039/C7DT00319F. DOI: 10.1039/C7DT00319F.

(12) Davey, S. G. Allene reduction: Selectively stopping halfway. *Nature Reviews Chemistry* **2017**, *1* (11), 0093. DOI: 10.1038/s41570-017-0093. Cahiez, G.; Moyeux, A. Cobalt-Catalyzed Cross-Coupling Reactions. *Chemical Reviews* **2010**, *110* (3), 1435-1462. DOI: 10.1021/cr9000786.

(13) Collman, J. P. Patterns of organometallic reactions related to homogeneous catalysis. *Accounts of Chemical Research* **1968**, *1* (5), 136-143. DOI: 10.1021/ar50005a002. Niu, S.; Hall, M. B. Theoretical studies on reactions of transition-metal complexes. *Chem Rev* **2000**, *100* (2), 353-406. DOI: 10.1021/cr980404y From NLM.

(14) Power, P. P. Main-group elements as transition metals. *Nature* **2010**, *463* (7278), 171-177. DOI: 10.1038/nature08634.

(15) Gillespie, R. J. The VSEPR model revisited. *Chemical Society Reviews* **1992**, *21* (1), 59-69, 10.1039/CS9922100059. DOI: 10.1039/CS9922100059.

(16) Abbenseth, J.; Goicoechea, J. M. Recent developments in the chemistry of non-trigonal pnictogen pincer compounds: from bonding to catalysis. *Chemical Science* **2020**, *11* (36), 9728-9740, 10.1039/D0SC03819A. DOI: 10.1039/D0SC03819A.

(17) Kundu, S. Pincer-Type Ligand-Assisted Catalysis and Small-Molecule Activation by non-VSEPR Main-Group Compounds. *Chem Asian J* **2020**, *15* (20), 3209-3224. DOI: 10.1002/asia.202000800 From NLM.

(18) Peris, E.; Crabtree, R. H. Key factors in pincer ligand design. *Chem Soc Rev* **2018**, *47* (6), 1959-1968. DOI: 10.1039/c7cs00693d From NLM.

(19) Bradley, B.; Singleton, M.; Po, A. L. W. BISMUTH TOXICITY—A REASSESSMENT*. *Journal of Clinical Pharmacy and Therapeutics* **1989**, *14* (6), 423-441. DOI: https://doi.org/10.1111/j.1365-2710.1989.tb00268.x.

(20) Chu, T.; Nikonov, G. I. Oxidative Addition and Reductive Elimination at Main-Group Element Centers. *Chemical Reviews* **2018**, *118* (7), 3608-3680. DOI: 10.1021/acs.chemrev.7b00572. Kundu, S.; Li, B.; Kretsch, J.; Herbst-Irmer, R.; Andrada, D. M.; Frenking, G.; Stalke, D.; Roesky, H. W. An Electrophilic Carbene-Anchored Silylene-Phosphinidene. *Angew Chem Int Ed Engl* **2017**, *56* (15), 4219-4223. DOI: 10.1002/anie.201700420 From NLM. Hofmann, A.; Pranckevicius, C.; Tröster, T.; Braunschweig, H. Aluminum(I)/Boron(III) Redox Reactions. *Angew Chem Int Ed Engl* **2019**, *58* (11), 3625-3629. DOI: 10.1002/anie.201813619 From NLM. Anker, M. D.; Coles, M. P. Isoelectronic Aluminium Analogues of Carbonyl and Dioxirane Moieties. *Angew Chem Int Ed Engl* **2019**, *58* (38), 13452-13455. DOI: 10.1002/anie.201907884 From NLM. Brand, A.; Uhl, W. Sterically Constrained Bicyclic Phosphines: A Class of Fascinating Compounds Suitable for Application in Small Molecule Activation and Coordination Chemistry. *Chemistry – A European Journal* **2019**, *25* (6), 1391-1404. DOI: https://doi.org/10.1002/chem.201803331. Akiba, K.-y. *Chemistry of Hypervalent Compounds*; Wiley-VCH, 1998.

(21) Baccolini, G.; Mezzina, E.; Todesco, P. E.; Foresti, E. Facile synthesis of fused benzo-1,2,3-thiadiphospholes, a new heterocyclic system. *Journal of the Chemical Society, Chemical Communications* **1988**, (4), 304-305, 10.1039/C39880000304. DOI: 10.1039/C39880000304.

(22) Cui, J.; Li, Y.; Ganguly, R.; Inthirarajah, A.; Hirao, H.; Kinjo, R. Metal-Free σ-Bond Metathesis in Ammonia Activation by a Diazadiphosphapentalene. *Journal of the American Chemical Society* **2014**, *136* (48), 16764-16767. DOI: 10.1021/ja509963m.

(23) Hentschel, A.; Brand, A.; Wegener, P.; Uhl, W. A Sterically Constrained Tricyclic PC3 Phosphine: Coordination Behavior and Insertion of Chalcogen Atoms into P−C Bonds. *Angewandte Chemie International Edition* **2018**, *57* (3), 832-835. DOI: https://doi.org/10.1002/anie.201711373.

(24) Mondal, M. K.; Zhang, L.; Feng, Z.; Tang, S.; Feng, R.; Zhao, Y.; Tan, G.; Ruan, H.; Wang, X. Tricoordinate Nontrigonal Pnictogen-Centered Radical Anions: Isolation, Characterization, and Reactivity. *Angewandte Chemie International Edition* **2019**, *58* (44), 15829-15833. DOI: https://doi.org/10.1002/anie.201910139.

(25) Pyykkö, P.; Atsumi, M. Molecular Single-Bond Covalent Radii for Elements 1–118. *Chemistry – A European Journal* **2009**, *15* (1), 186-197. DOI: https://doi.org/10.1002/chem.200800987.

(26) Marczenko, K. M.; Zurakowski, J. A.; Kindervater, M. B.; Jee, S.; Hynes, T.; Roberts, N.; Park, S.; Werner-Zwanziger, U.; Lumsden, M.; Langelaan, D. N.; et al. Periodicity in Structure, Bonding, and Reactivity for p-Block Complexes of a Geometry Constraining Triamide Ligand. *Chemistry – A European Journal* **2019**, *25* (71), 16414-16424. DOI: https://doi.org/10.1002/chem.201904361.

(27) Wang, F.; Planas, O.; Cornella, J. Bi(I)-Catalyzed Transfer-Hydrogenation with Ammonia-Borane. *Journal of the American Chemical Society* **2019**, *141* (10), 4235-4240. DOI: 10.1021/jacs.9b00594.

(28) Planas, O.; Peciukenas, V.; Cornella, J. Bismuth-Catalyzed Oxidative Coupling of Arylboronic Acids with Triflate and Nonaflate Salts. *Journal of the American Chemical Society* **2020**, *142* (26), 11382-11387. DOI: 10.1021/jacs.0c05343. Planas, O.; Wang, F.; Leutzsch, M.; Cornella, J. Fluorination of arylboronic esters enabled by bismuth redox catalysis. *Science* **2020**, *367* (6475), 313-317. DOI: doi:10.1126/science.aaz2258.

(29) Morrison, R. T. B., Robert Nielson. *Organic Chemistry*; Allyn and Bacon, Inc., 1959.

(30) Kindervater, M. B.; Marczenko, K. M.; Werner-Zwanziger, U.; Chitnis, S. S. A Redox-Confused Bismuth(I/III) Triamide with a T-Shaped Planar Ground State. *Angewandte Chemie International Edition* **2019**, *58* (23), 7850-7855. DOI: https://doi.org/10.1002/anie.201903354.

(31) Kindervater, M. B.; Hynes, T.; Marczenko, K. M.; Chitnis, S. S. Squeezing Bi: PNP and P2N3 pincer complexes of bismuth. *Dalton Transactions* **2020**, *49* (45), 16072-16076, 10.1039/D0DT01413C. DOI: 10.1039/D0DT01413C.

(32) Anita Ivanković, A. D., Anita Martinović Bevanda, Stanislava Talić. Review of 12 Principles of Green Chemistry in Practice. *International Journal of Sustainable and Green Energy* **2017**, *6* (3), 39-48. DOI: doi: 10.11648/j.ijrse.20170603.12.

(33) Bedard, J.; Roberts, N. J.; Shayan, M.; Bamford, K. L.; Werner-Zwanziger, U.; Marczenko, K. M.; Chitnis, S. S. (PNSiMe3)4(NMe)6: A Robust Tetravalent Phosphaza-adamantane Scaffold for Molecular and Macromolecular Construction**. *Angewandte Chemie International Edition* **2022**, *61* (25), e202204851. DOI: https://doi.org/10.1002/anie.202204851.

(34) Koller, J.; Sarkar, S.; Abboud, K. A.; Veige, A. S. Synthesis and Characterization of (2,6-iPrNCN)HfCl2- and (3,5-MeNCN)2Hf2- (where NCN = 2,6-bis[phenylazanidyl]methylphenyl): New Trianionic Pincer Ligands. *Organometallics* **2007**, *26* (22), 5438-5441. DOI: 10.1021/om700597u.

(35) Bruker. *APEX3, SAINT*; Bruker AXS Inc., Madison, Wisconsin, USA., 2018.

(36) Sheldrick, G. SHELXT - Integrated space-group and crystal-structure determination. *Acta Crystallographica Section A* **2015**, *71* (1), 3-8. DOI: doi:10.1107/S2053273314026370.

(37) Sheldrick, G. M. Crystal structure refinement with *SHELXL*. *Acta Crystallographica Section C* **2015**, *71* (1), 3--8. DOI: 10.1107/S2053229614024218.

(38) Kuveke, R. E. H.; Barwise, L.; van Ingen, Y.; Vashisth, K.; Roberts, N.; Chitnis, S. S.; Dutton, J. L.; Martin, C. D.; Melen, R. L. An International Study Evaluating Elemental Analysis. *ACS Central Science* **2022**, *8* (7), 855-863. DOI: 10.1021/acscentsci.2c00325.

(39) *Gaussian 16 Rev. C.01*; Wallingford, CT, 2016. (accessed.

(40) Weigend, F.; Ahlrichs, R. Balanced basis sets of split valence, triple zeta valence and quadruple zeta valence quality for H to Rn: Design and assessment of accuracy. *Phys. Chem. Chem. Phys.* **2005**, *7* (18), 3297-3305, 10.1039/B508541A. DOI: 10.1039/B508541A. Metz, B.; Stoll, H.; Dolg, M. Small-core multiconfiguration-Dirac–Hartree–Fock-adjusted pseudopotentials for post-d main group elements: Application to PbH and PbO. *J. Chem. Phys.* **2000**, *113* (7), 2563-2569. DOI: 10.1063/1.1305880. Johnson, E. R.; Becke, A. D. A post-Hartree-Fock model of intermolecular interactions: Inclusion of higher-order corrections. *The Journal of Chemical Physics* **2006**, *124* (17), 174104. DOI: 10.1063/1.2190220.

(41) Johnson, E. R.; Clarkin, O. J.; DiLabio, G. A. Density Functional Theory Based Model Calculations for Accurate Bond Dissociation Enthalpies. 3. A Single Approach for X−H, X−X, and X−Y (X, Y = C, N, O, S, Halogen) Bonds. *The Journal of Physical Chemistry A* **2003**, *107* (46), 9953-9963. DOI: 10.1021/jp035315q.

(42) Amijs, C. H. M.; van Klink, G. P. M.; van Koten, G. Carbon tetrachloride free benzylic brominations of methyl aryl halides. *Green Chemistry* **2003**, *5* (4), 470-474, 10.1039/B304673G. DOI: 10.1039/B304673G.

(43) 조수동; 박용대; Kim, J.-J.; Yoon, Y.-J. Facile Reduction of Carboxylic Acids, Esters, Acid Chlorides, Amides and Nitriles to Alcohols or Amines Using NaBH₄/BF₃·Et₂O. *Bulletin of the Korean Chemical Society* **2004**, *25* (3), 407-409. DOI: 10.5012/BKCS.2004.25.3.407.

(44) Tran, V. M.; Nguyen, T. K. N.; Sorna, V.; Loganathan, D.; Kuberan, B. Synthesis and Assessment of Glycosaminoglycan Priming Activity of Cluster-xylosides for Potential Use as Proteoglycan Mimetics. *ACS Chemical Biology* **2013**, *8* (5), 949-957. DOI: 10.1021/cb300665u.

(45) Belov, D. S.; Tejeda, G.; Tsay, C.; Bukhryakov, K. V. Ring-Closing Olefin Metathesis Catalyzed by Well-Defined Vanadium Alkylidene Complexes. *Chemistry – A European Journal* **2021**, *27* (14), 4578-4582. DOI: https://doi.org/10.1002/chem.202005438.

(46) Lee, I.-Y.; Gruber, T. D.; Samuels, A.; Yun, M.; Nam, B.; Kang, M.; Crowley, K.; Winterroth, B.; Boshoff, H. I.; Barry, C. E. Structure–activity relationships of antitubercular salicylanilides consistent with disruption of the proton gradient via proton shuttling. *Bioorganic & Medicinal Chemistry* **2013**, *21* (1), 114-126. DOI: https://doi.org/10.1016/j.bmc.2012.10.056.

(47) Sato, K.; Honma, T.; Sugai, S. Synthesis and Herbicidal Activities of 1,2-Benzisoxazole-3-acetamide Derivatives. *Agricultural and Biological Chemistry* **1985**, *49* (12), 3563-3567. DOI: 10.1080/00021369.1985.10867279 (acccessed 10/6/2022).

(48) Eckart, A.; Lux, K.; Karaghiosoff, K. Iminophosphoranyl Dichlorophosphines R3PNPCl2. *Zeitschrift für anorganische und allgemeine Chemie* **2014**, *640* (5), 962-967. DOI: https://doi.org/10.1002/zaac.201300518.

(49) Suárez Suárez, S.; Presa Soto, D.; Carriedo, G. A.; Presa Soto, A.; Staubitz, A. Experimental and Theoretical Study of the Living Polymerization of N-Silylphosphoranimines. Synthesis of New Block Copolyphosphazenes. *Organometallics* **2012**, *31* (7), 2571-2581. DOI: 10.1021/om201012g. Caminade, A.-M.; Roques, C.; Dufour, N.; Colombo, D.; Gonce, F.; Majoral, J.-P. Phosphorus dienic like systems. *Tetrahedron Letters* **1989**, *30* (49), 6869-6872. DOI: https://doi.org/10.1016/S0040-4039(01)93375-1.

(50) Saurwein, A.; Nobis, M.; Inoue, S.; Rieger, B. Synthesis of a Triphenylphosphinimide-Substituted Silirane as a “Masked” Acyclic Silylene. *Inorganic Chemistry* **2022**, *61* (26), 9983-9989. DOI: 10.1021/acs.inorgchem.2c00790.

(51) Morgan, P. E.; McCague, R.; Whiting, A. Asymmetric α-substitution versus aza Diels–Alder reaction of electron deficient N-sulfonyl imines. *Journal of the Chemical Society, Perkin Transactions 1* **2000**, (4), 515-525, 10.1039/A909116E. DOI: 10.1039/A909116E.

(52) Rahier, N. J.; Volle, J.-N.; Lacour, M. A.; Taillefer, M. Reactivity of Ph3PNLi towards PIII and PV electrophiles. *Tetrahedron* **2008**, *64* (28), 6645-6650. DOI: https://doi.org/10.1016/j.tet.2008.05.019.

(53) Sgro, M. J.; Stephan, D. W. Non-innocent reactivity of bis-phosphinimine pincer ligands in palladium complexes. *Dalton Transactions* **2011**, *40* (11), 2419-2421, 10.1039/C0DT01623C. DOI: 10.1039/C0DT01623C. Cristau, H. J.; Chiche, L.; Kadoura,

J.; Torreilles, E. L'aza-ylure N-lithie (C6H5)3P・NLi, reactif d'amination. *Tetrahedron Letters* **1988**, *29* (32), 3931-3934. DOI: https://doi.org/10.1016/S0040-4039(00)80385-8.

(54) Steiner, A.; Stalke, D. Substituent-Controlled Reactions of Iminophosphoranes with Methyllithium. *Angewandte Chemie International Edition in English* **1995**, *34* (16), 1752-1755. DOI: https://doi.org/10.1002/anie.199517521.

(55) Maurer, L. A.; Pearce, O. M.; Maharaj, F. D. R.; Brown, N. L.; Amador, C. K.; Damrauer, N. H.; Marshak, M. P. Open for Bismuth: Main Group Metal-to-Ligand Charge Transfer. *Inorganic Chemistry* **2021**, *60* (14), 10137-10146. DOI: 10.1021/acs.inorgchem.0c03818.

(56) Marczenko, K. M.; Zurakowski, J. A.; Bamford, K. L.; MacMillan, J. W. M.; Chitnis, S. S. Hydrostibination. *Angew Chem Int Ed Engl* **2019**, *58* (50), 18096-18101. DOI: 10.1002/anie.201911842 From NLM.

(57) Yu. Kukushkin, V.; Moiseev, A. I. Convenient synthesis of μ-nitridobis(triphenylphosphonium) chloride ([PPN]Cl) with contribution of PCl5 as chlorinating (PCl5+PPh3) or deoxygenating (PCl5+OPPh3) reagent. *Inorganica Chimica Acta* **1990**, *176* (1), 79-81. DOI: https://doi.org/10.1016/S0020-1693(00)85095-1.

(58) Grebe, J.; Schlecht, S.; Weller, F.; Harms, K.; Geiseler, G.; Dehnicke, K. N-Chlortriphenylphosphanimin und seine Anwendung als Edukt zur Synthese asymmetrischer PNP-Kationen. Kristallstrukturen von Ph3PNCl und [Ph3PNPEt3]Cl. *Zeitschrift für anorganische und allgemeine Chemie* **1999**, *625* (4), 633-636. DOI: https://doi.org/10.1002/(SICI)1521-3749(199904)625:4<633::AID-ZAAC633>3.0.CO;2-2.

(59) Müller, T. E.; Mingos, D. M. P. Determination of the Tolman cone angle from crystallographic parameters and a statistical analysis using the crystallographic data base. *Transition Metal Chemistry* **1995**, *20* (6), 533-539. DOI: 10.1007/BF00136415.

(60) Nußhär, D.; Weller, F.; Dehnicke, K. Phosphaniminato-Komplexe des Iods. Synthese und Kristallstrukturen von Ph3PNIO2 und Ph3PNSiMe3 · I2. *Zeitschrift für anorganische und allgemeine Chemie* **1994**, *620* (2), 329-333. DOI: https://doi.org/10.1002/zaac.19946200221.

(61) Erdmann, P.; Greb, L. What Distinguishes the Strength and the Effect of a Lewis Acid: Analysis of the Gutmann–Beckett Method. *Angewandte Chemie International Edition* **2022**, *61* (4), e202114550. DOI: https://doi.org/10.1002/anie.202114550.

(62) Poynder, T. B.; Chamorro Orué, A. I.; Tania; Sharp-Bucknall, L.; Flynn, M. T.; Wilson, D. J. D.; Athukorala Arachchige, K. S.; Clegg, J. K.; Dutton, J. L. On the

activation of PhICl2 with pyridine. *Chemical Communications* **2021**, *57* (40), 4970-4973, 10.1039/D1CC01567B. DOI: 10.1039/D1CC01567B.

(63) Jutta Grebe, F. W., Kurt Dehnicke. N-Iod-triphenylphosphanimin. Synthese und Kristallstrukturen von [Me3SiNPPh3 ICl] und Ph3PNI. *Zeitschrift für Naturforschung B* **1996**, *51b*, 1739-1743.

Appendix A: Spectra for Chapter 2

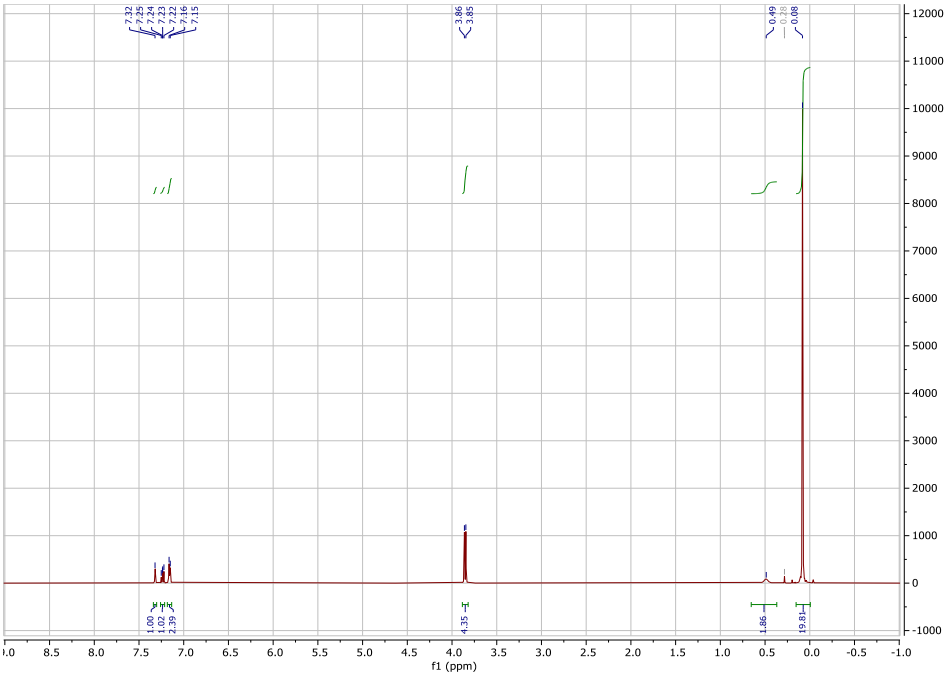

Figure A 1. Full ^{1}H NMR (500 MHz, C_6D_6) of **1H$_3$**. The multiplet at 7.16 ppm has some overlap with the residual solvent peak.

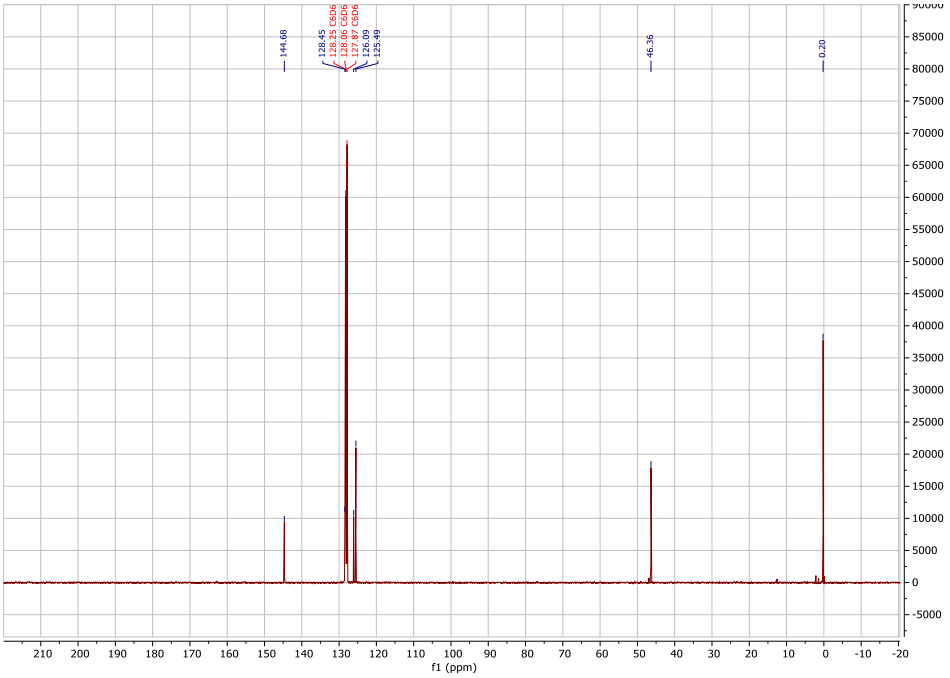

Figure A 2. Full ^{13}C NMR (C_6D_6, 125 MHz) of **1H$_3$**.

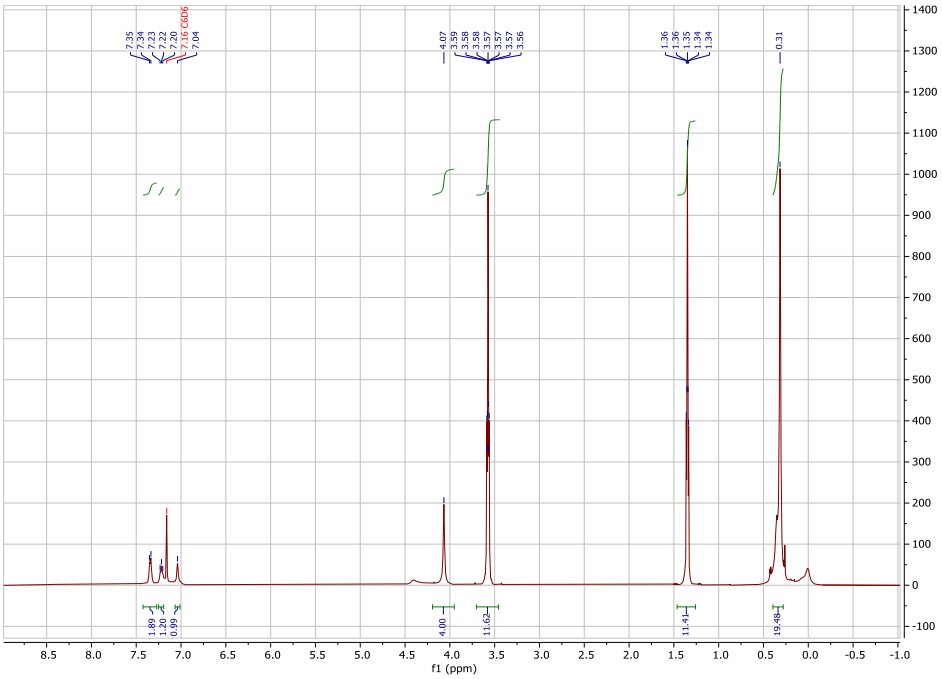

Figure A 3. Full ^{1}H NMR spectrum (500 MHz, C_6D_6) of **1HLi$_2$**. Peaks at 3.57 and 1.35 ppm are assigned to THF.

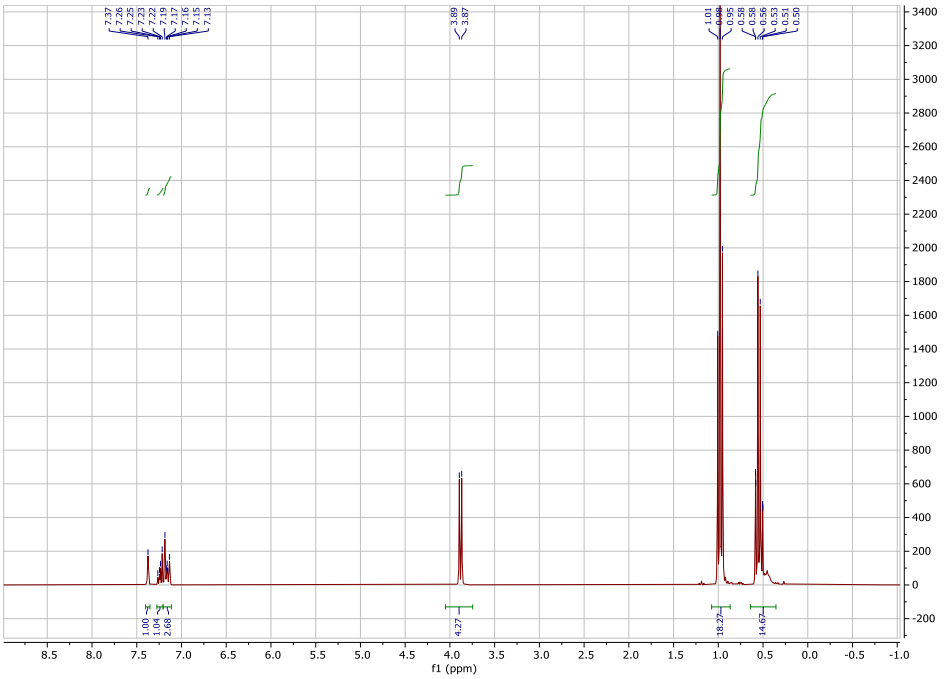

Figure A 4. Full 1H NMR spectrum (300 MHz, C_6D_6) of **2H$_3$**. The multiplet at 7.16 ppm has overlap with the solvent residual peak.

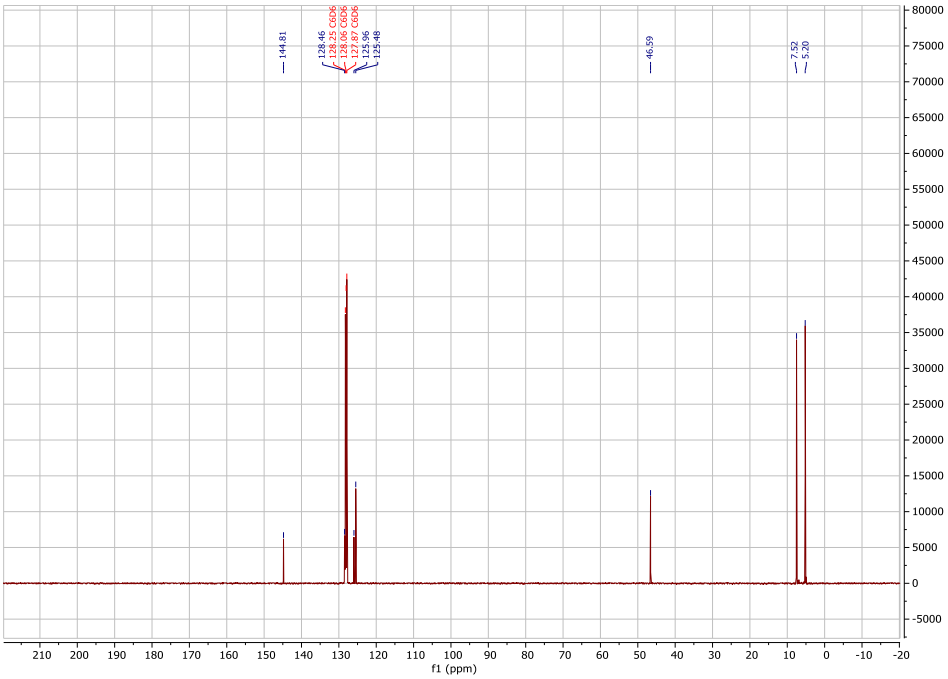

Figure A 5. Full ^{13}C NMR spectrum (125 MHz, C_6D_6) of **2H$_3$**.

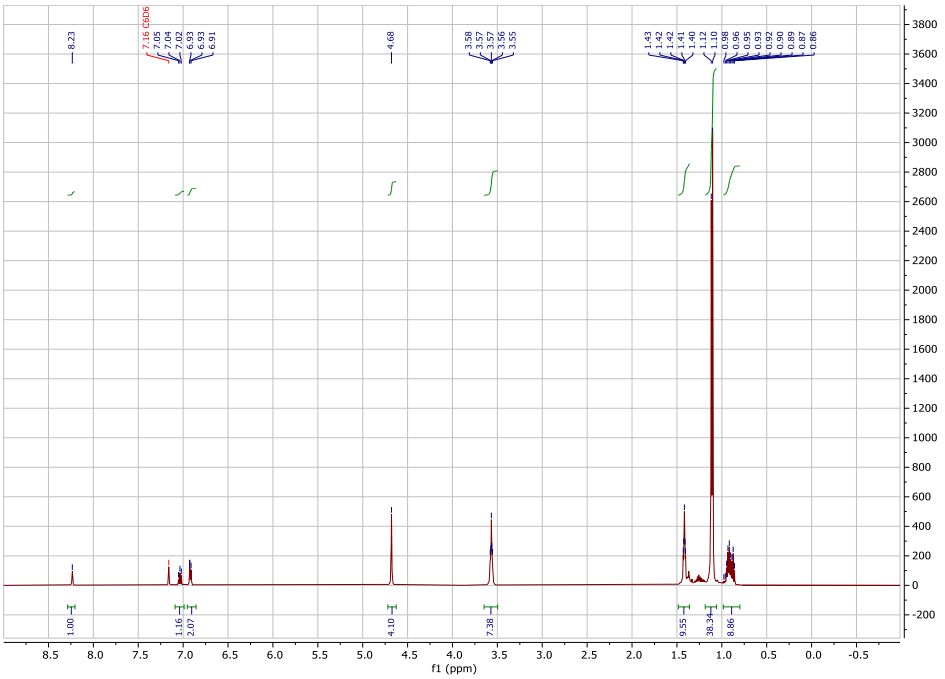

Figure A 6. Full ^{1}H NMR (300 MHz, C_6D_6) of **2HLi$_2$** compound. Peaks at 3.53 and 1.39 ppm are assigned to THF.

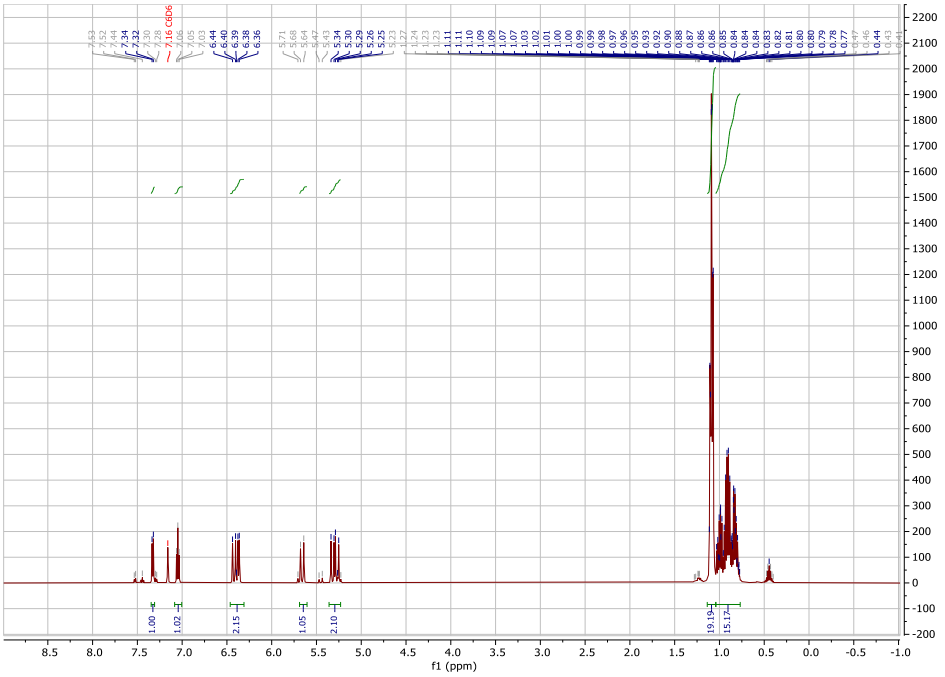

Figure A 7. Full 1H NMR (500 MHz, C_6D_6) of **(BiCN$_2$TES)$_2$**.

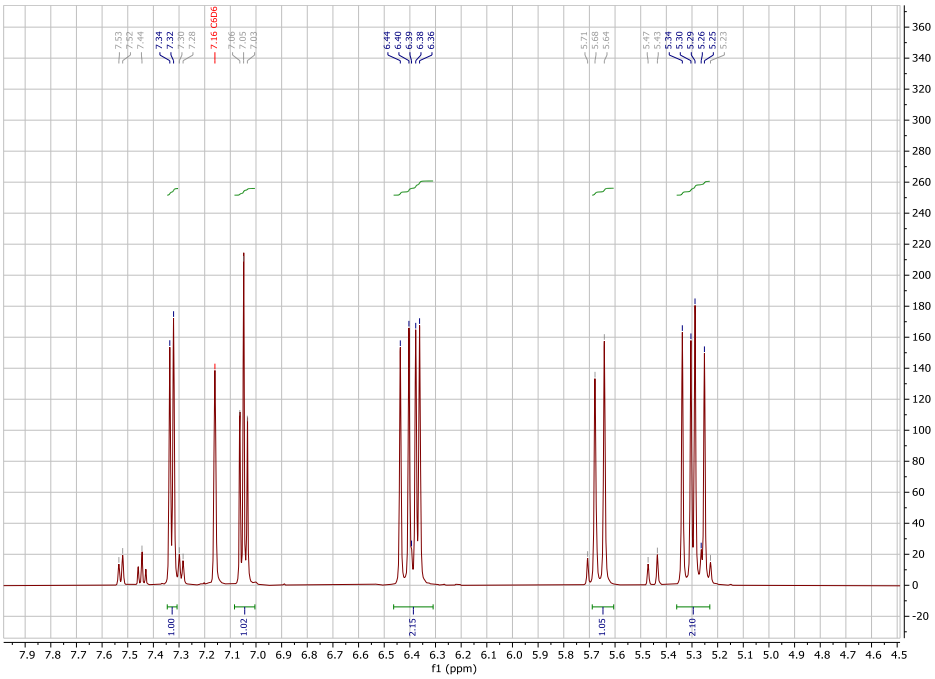

Figure A 8. Expanded view from 4.5 to 8.0 ppm of the ^{1}H NMR spectrum (500 MHz, C_6D_6) of **(BiCN$_2$TES)$_2$**.

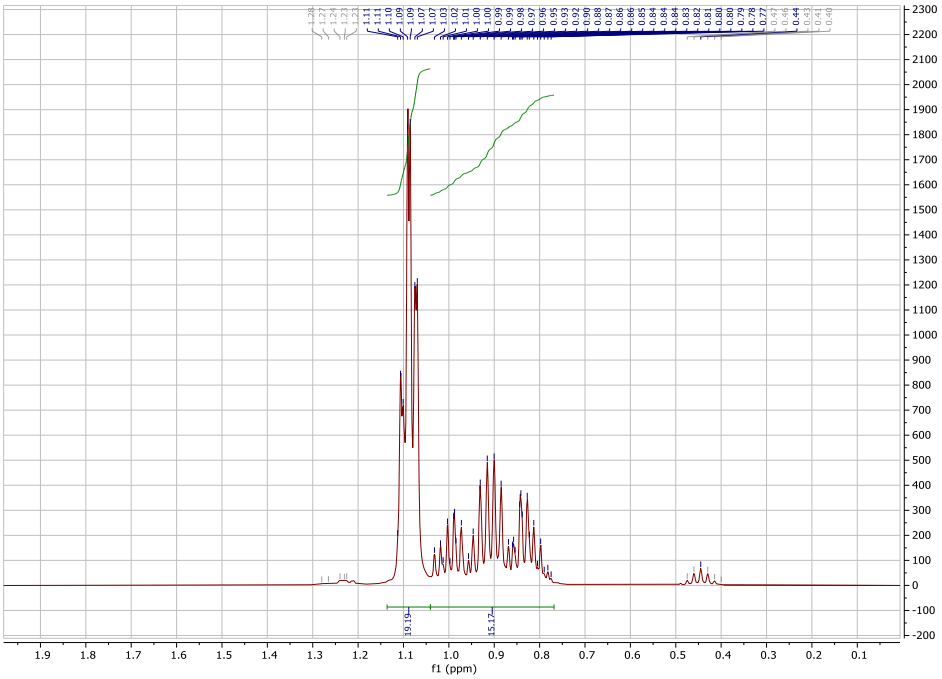

Figure A 9. Expanded view from -1.0 to 2.0 ppm of the ^{1}H NMR spectrum (500 MHz, C_6D_6) of **(BiCN$_2$TES)$_2$**.

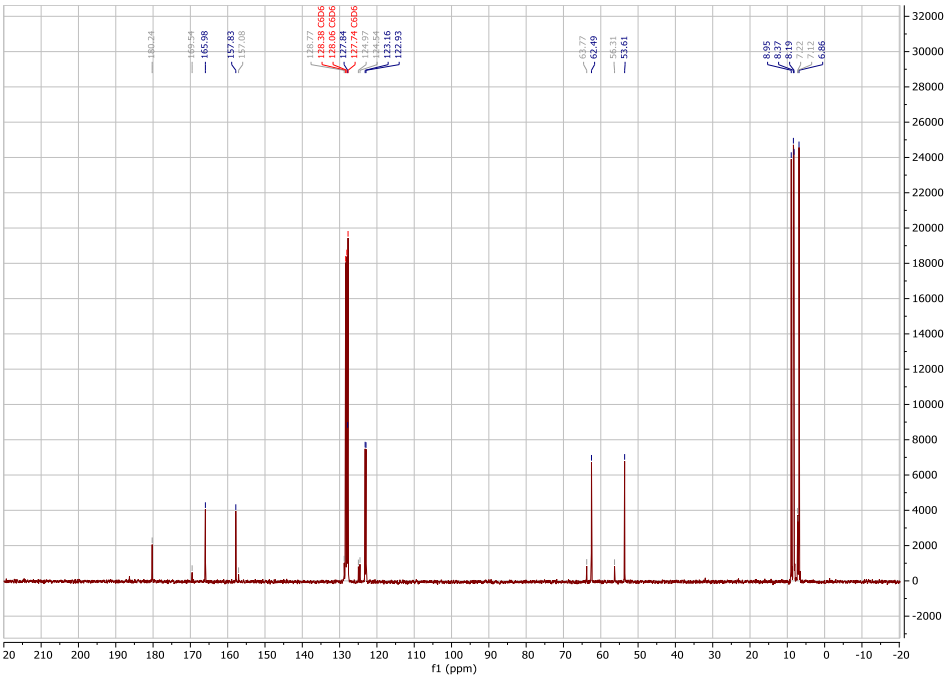

Figure A 10. Full ^{13}C NMR (75 MHz, C_6D_6) of **(BiCN$_2$TES)$_2$**.

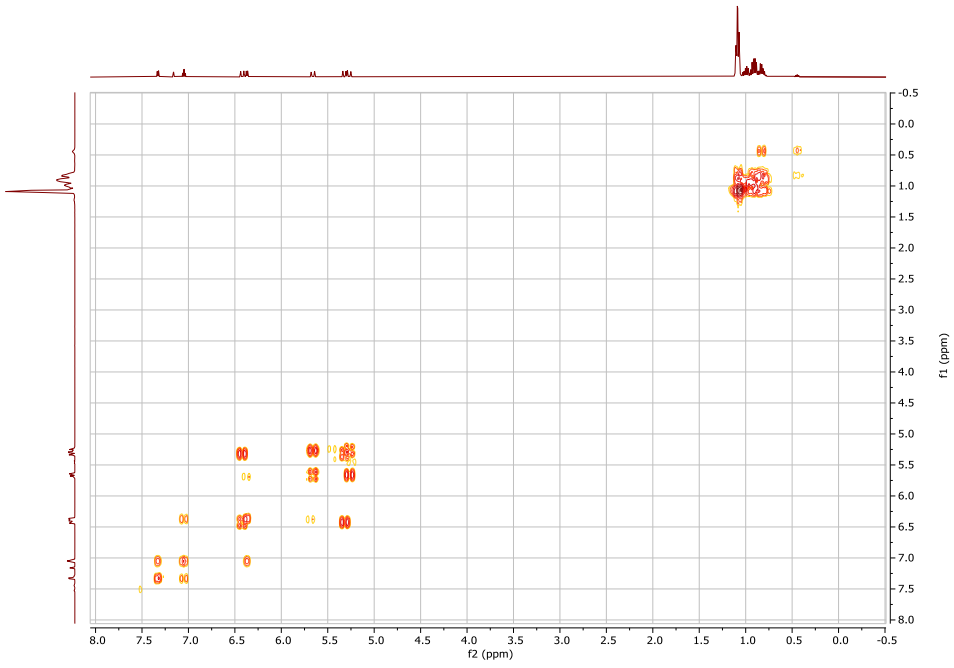

Figure A 11. Full ^{1}H COSY (300 MHz, C_6D_6) of **(BiCN$_2$TES)$_2$**.

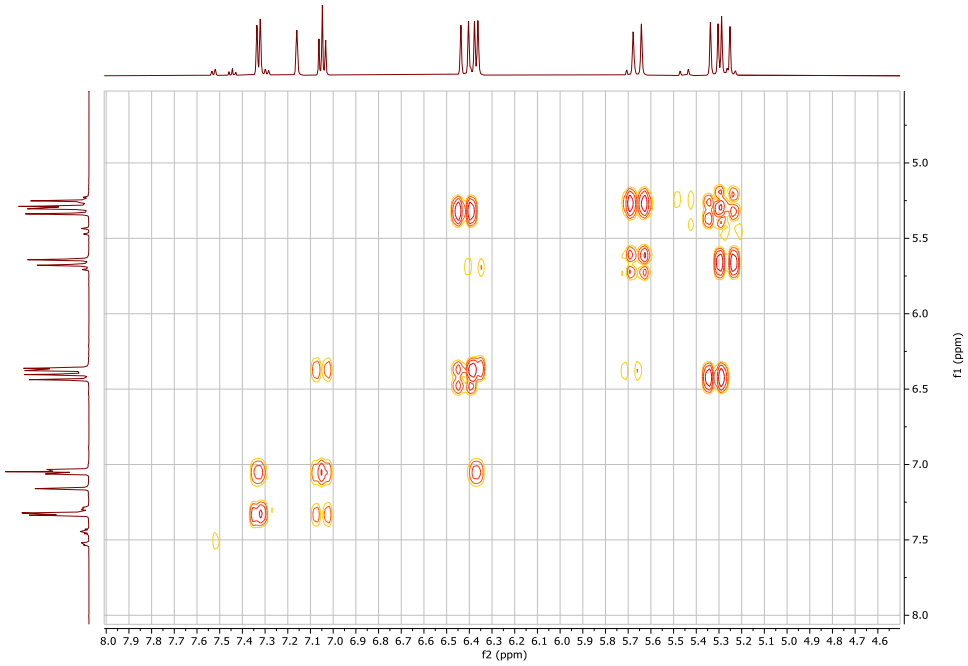

Figure A 12. Expanded view from 4.5 to 8.0 ppm of the ^{1}H COSY (300 MHz, C_6D_6) of **(BiCN$_2$TES)$_2$**.

Figure A 13. Full ^{1}H-^{13}C HSQC (300 MHz, 75 MHz, C_6D_6), of **(BiCN$_2$TES)$_2$**.

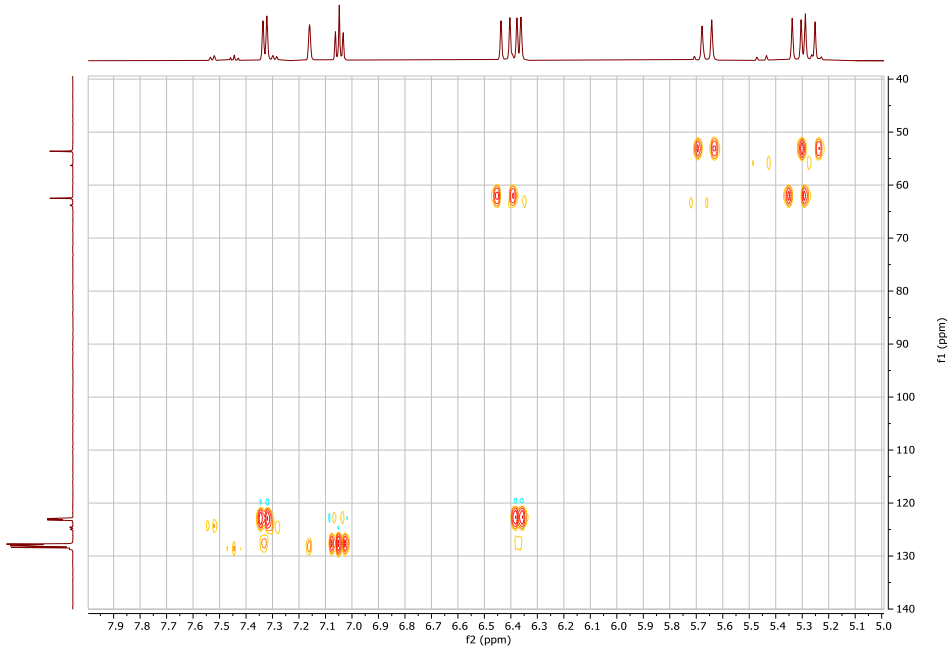

Figure A 14. Expanded view from 5.0 to 8.0 ppm (in the ^{1}H region) of the ^{1}H-^{13}C HSQC (300 MHz, 75 MHz, C_6D_6), of **(BiCN$_2$TES)$_2$**.

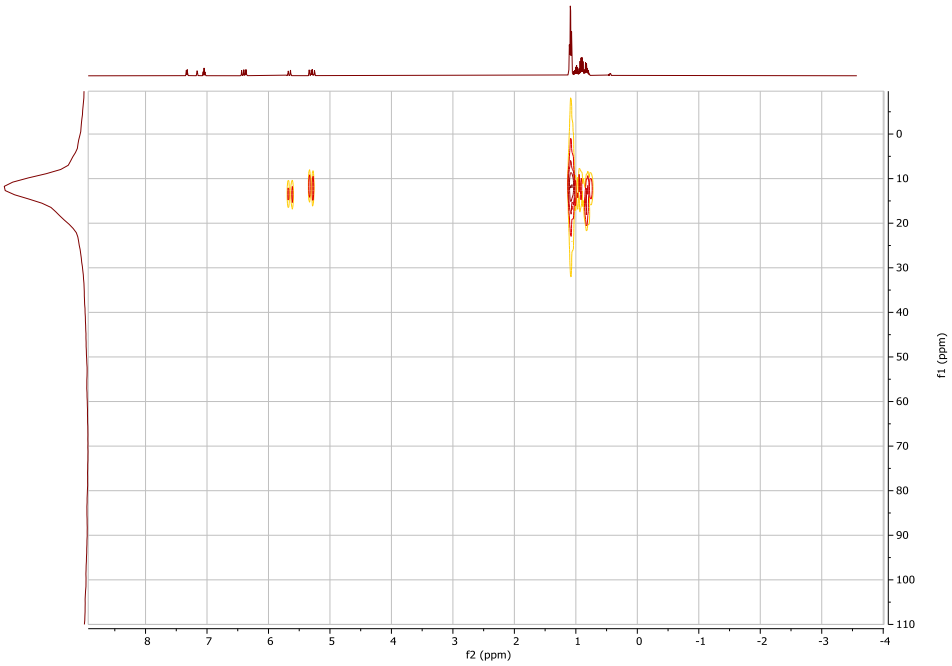

Figure A 15. Full ^{1}H-^{29}Si HMBC (300 MHz, 60 MHz, C_6D_6) for **(BiCN$_2$TES)$_2$**.

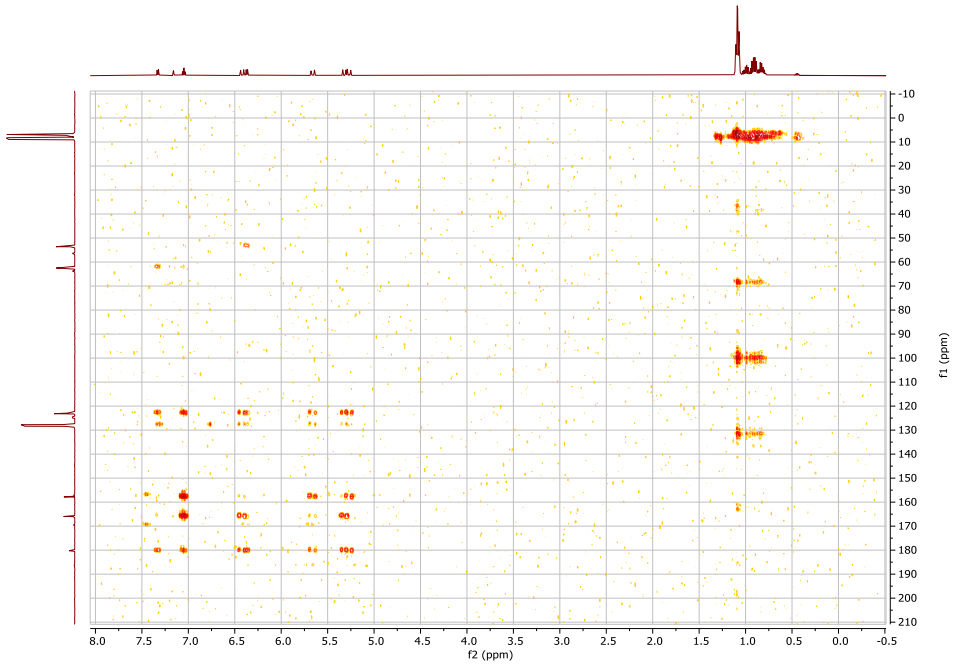

Figure A 16. Full ^{1}H-^{13}C HMBC (300 MHz, 75 MHz, C_6D_6), of **(BiCN$_2$TES)$_2$**.

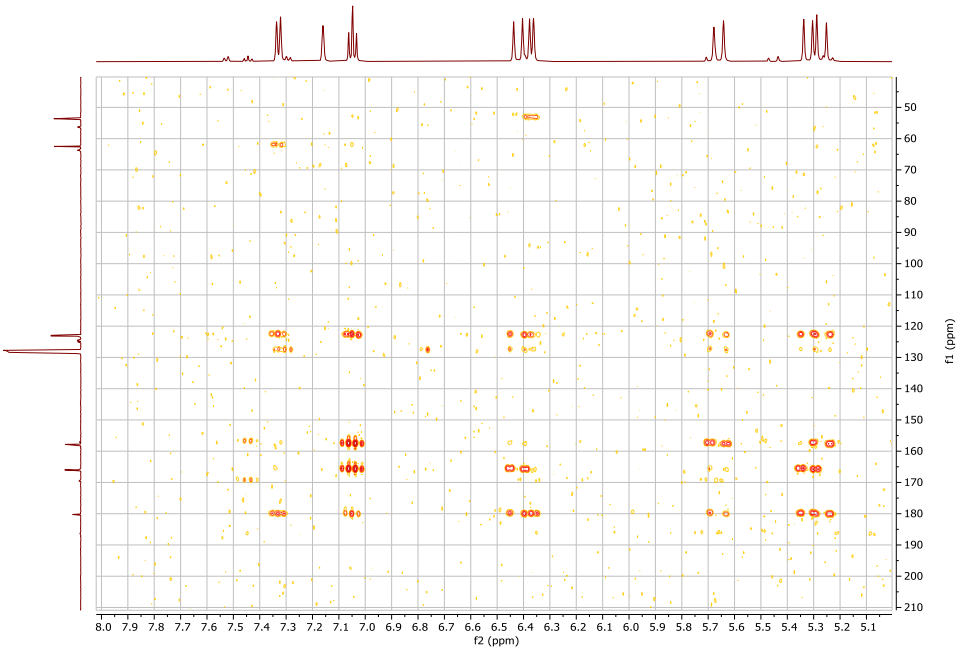

Figure A 17. Expanded view from 5.0 to 8.0 ppm (in the ^{1}H region) of the ^{1}H-^{13}C HMBC (300 MHz, 75 MHz, C_6D_6), of **(BiCN$_2$TES)$_2$**.

Figure A 18. Full ^{1}H NOESY (300 MHz, C_6D_6) for **(BiCN$_2$TES)$_2$**.

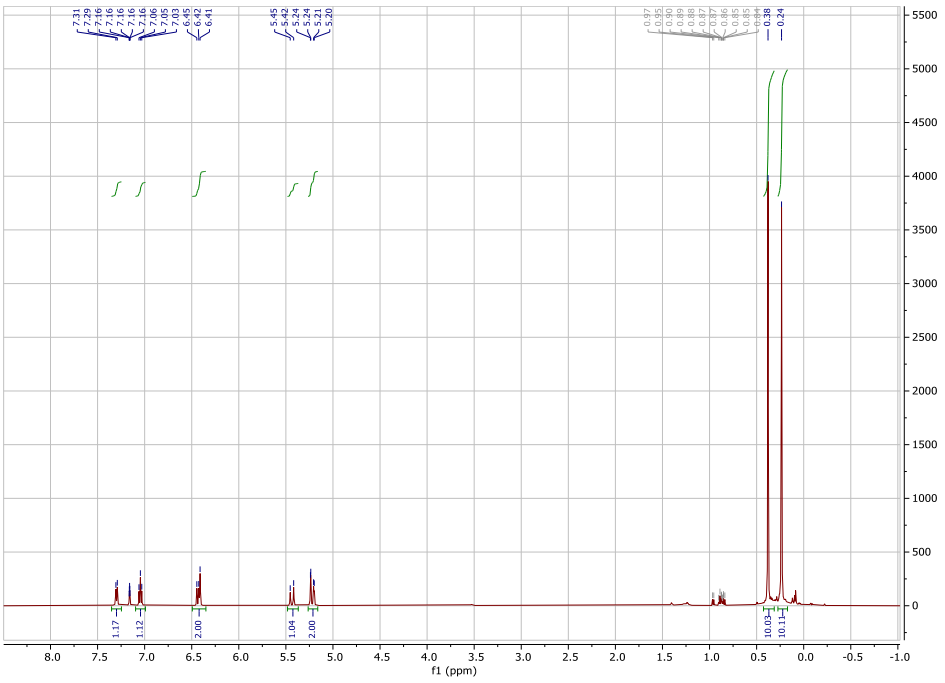

Figure A 19. Full 1H NMR (500 MHz, C_6D_6) of **(BiCN$_2$TMS)$_2$**.

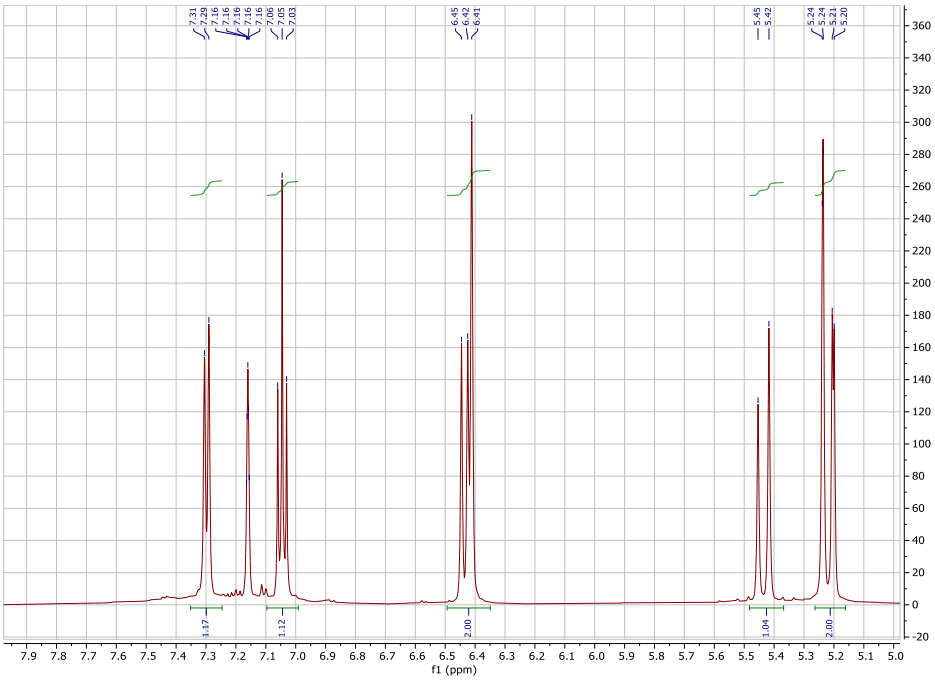

Figure A 20. Expanded view from 4.5 to 8.0 ppm of the ^{1}H NMR spectrum (500 MHz, C_6D_6) of **(BiCN$_2$TMS)$_2$**.

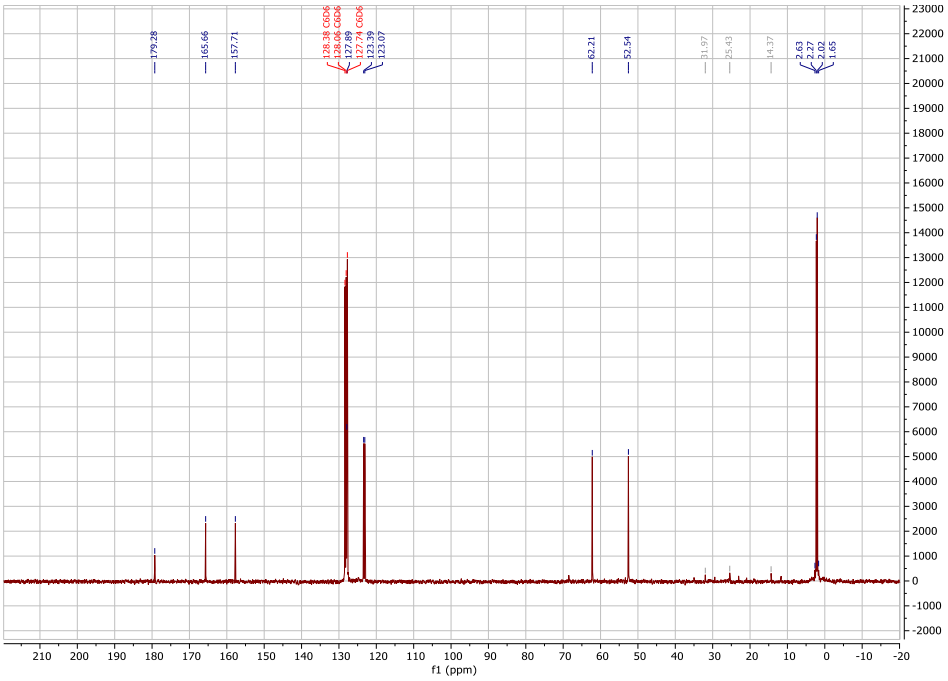

Figure A 21. Full ^{13}C NMR (75 MHz, C_6D_6) of **(BiCN$_2$TMS)$_2$**.

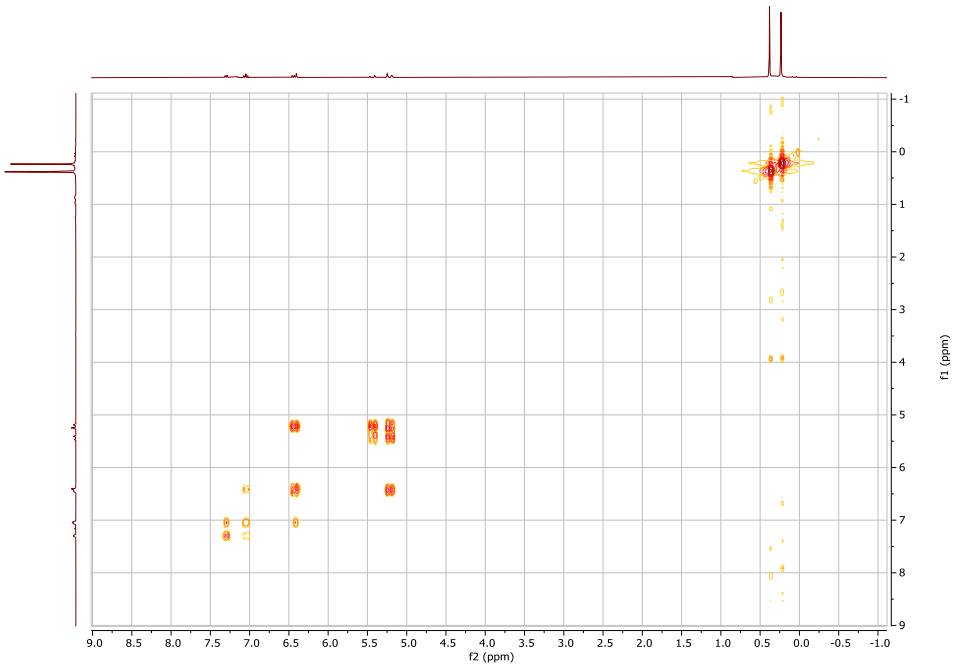

Figure A 22. Full ^{1}H COSY (300 MHz, C_6D_6) of **(BiCN$_2$TMS)$_2$**.

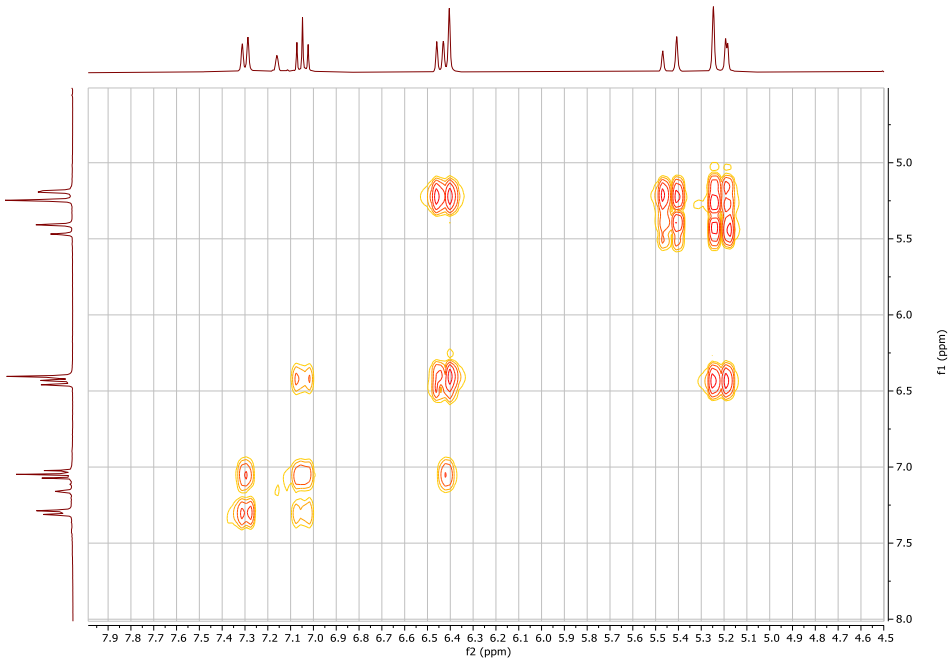

Figure A 23. Expanded view from 4.5 to 8.0 ppm of the ^{1}H COSY (300 MHz, C_6D_6) of **(BiCN$_2$TMS)$_2$**.

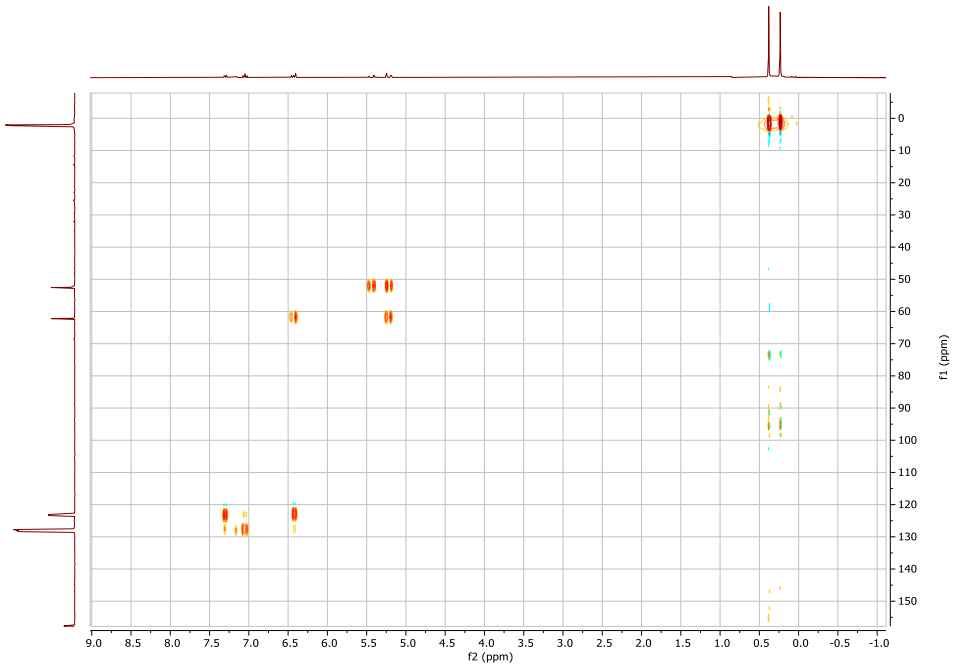

Figure A 24. Full ^{1}H-^{13}C HSQC (300 MHz, 75 MHz, C_6D_6), of **(BiCN$_2$TMS)$_2$**.

Figure A 25. Expanded view from 5.0 to 8.0 ppm (in the ^{1}H region) of the ^{1}H-^{13}C HSQC (300 MHz, 75 MHz, C_6D_6), of **(BiCN$_2$TMS)$_2$**.

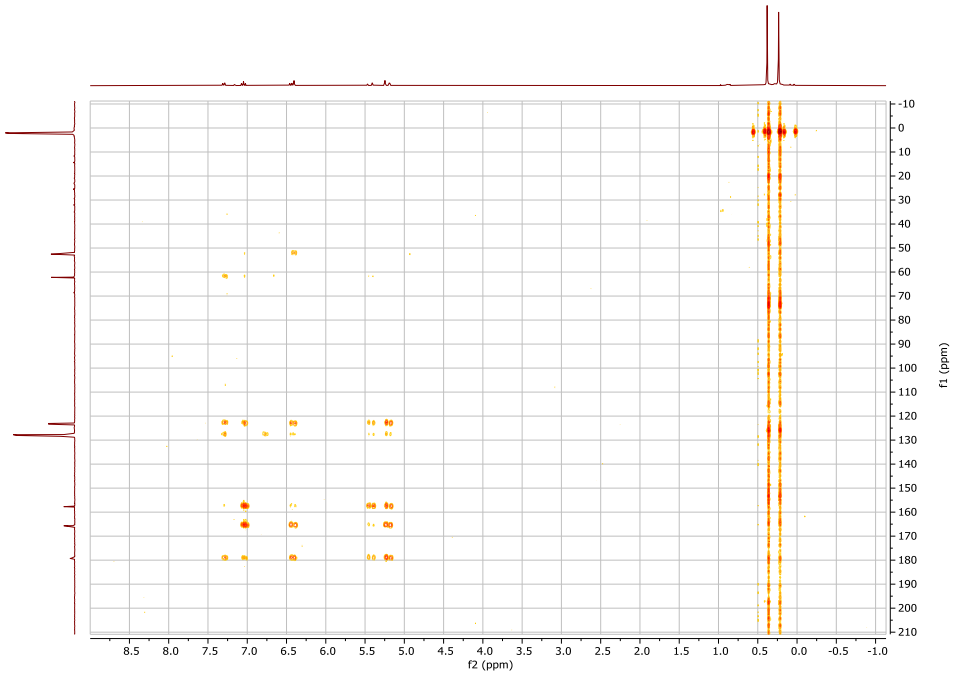

Figure A 26. Full ^{1}H-^{13}C HMBC (300 MHz, 75 MHz, C_6D_6), of **(BiCN$_2$TMS)$_2$**.

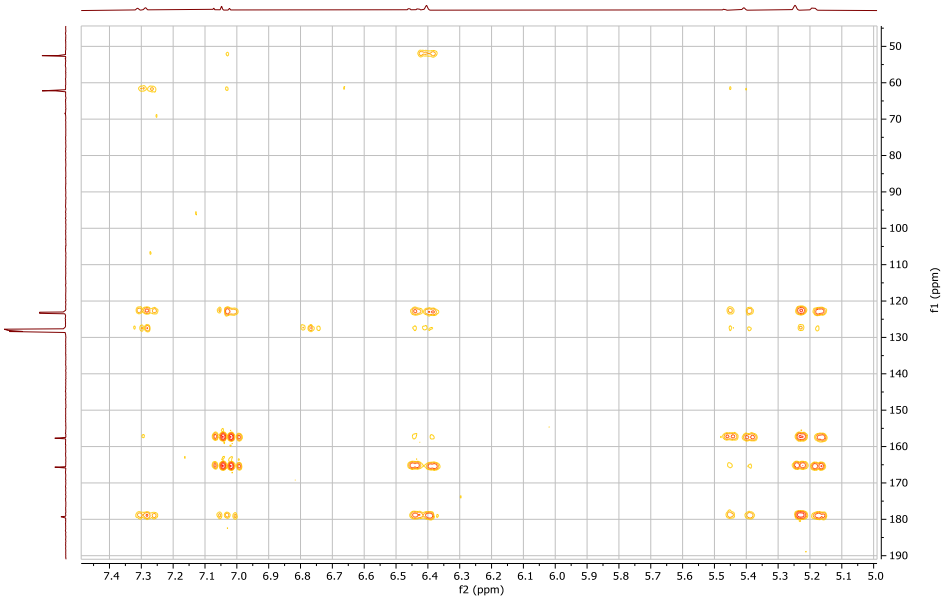

Figure A 27. Expanded view from 5.0 to 8.0 ppm (in the ^{1}H region) of the ^{1}H-^{13}C HMBC (300 MHz, 75 MHz, C_6D_6), of **(BiCN$_2$TMS)$_2$**.

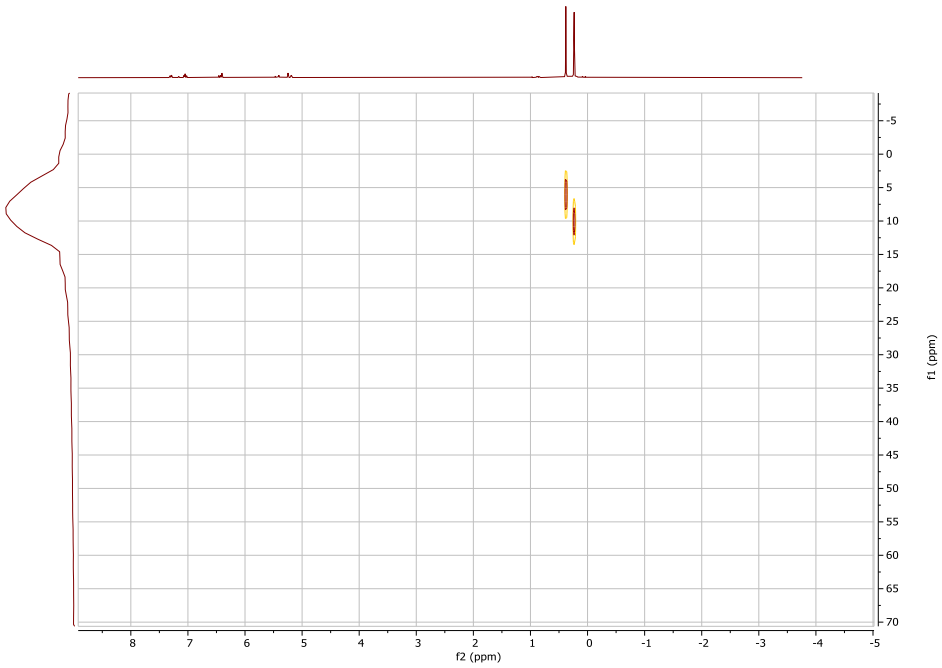

Figure A 28. Full ^{1}H-^{29}Si HMBC (300 MHz, 60 MHz, C_6D_6) for **(BiCN$_2$TMS)$_2$**.

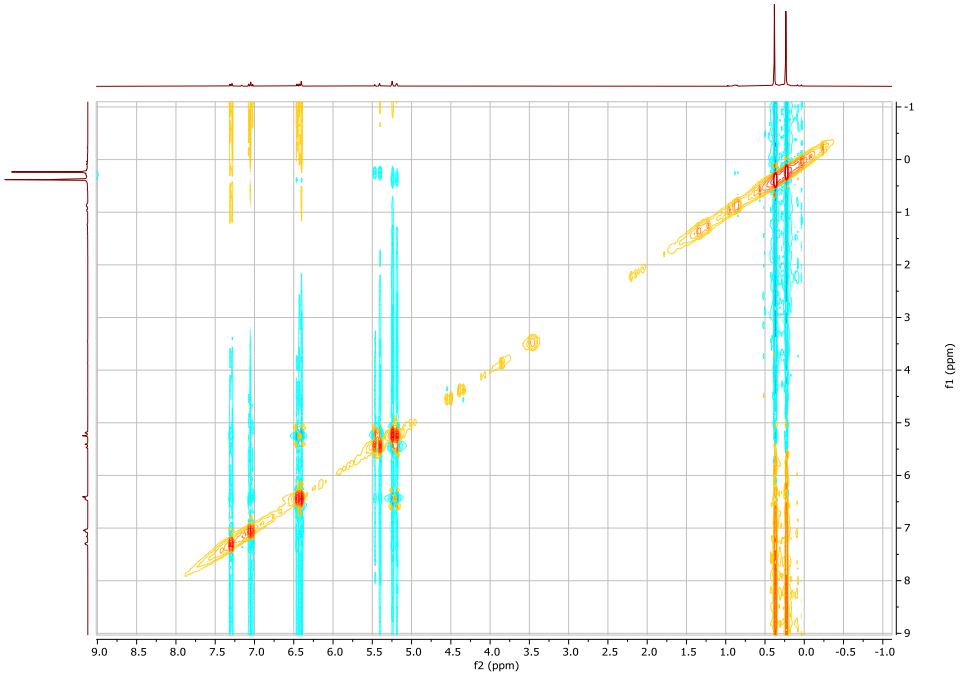

Figure A 29. Full ^{1}H NOESY (300 MHz, C_6D_6) for **(BiCN$_2$TMS)$_2$**.

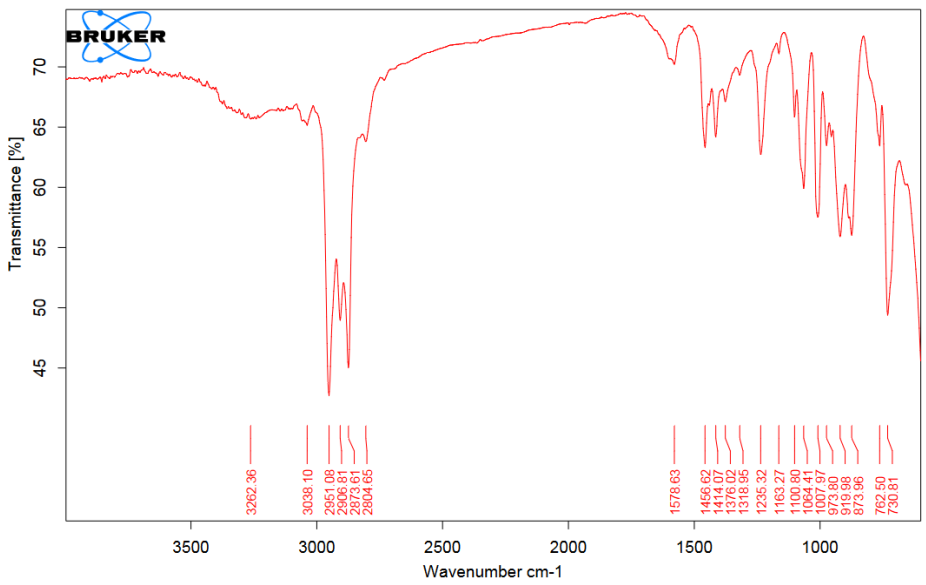

Figure A 30. IR spectrum (KBr plates, drop-cast) of **(BiCN$_2$TES)$_2$**, with major peaks annotated.

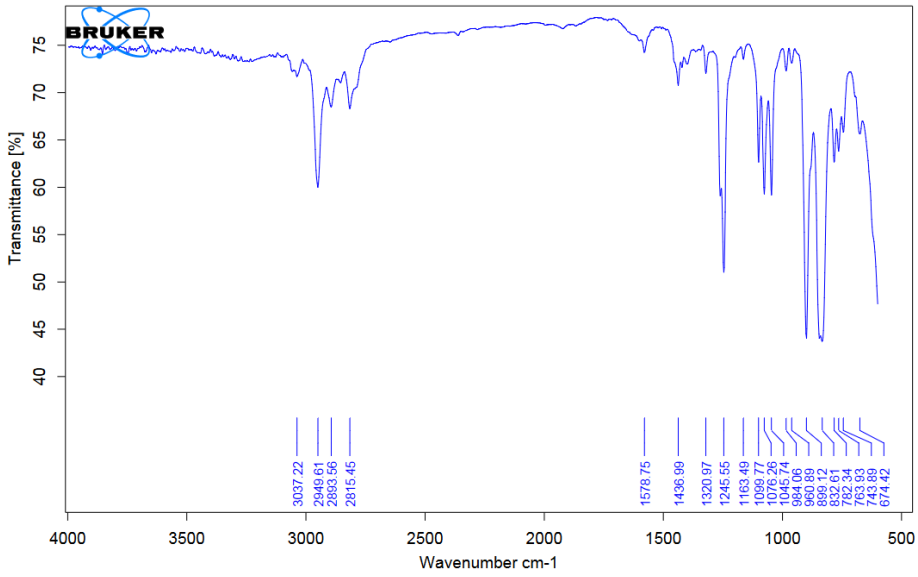

Figure A 31. IR spectrum (KBr plates, drop-cast) of **(BiCN$_2$TMS)$_2$**, with major peaks annotated.

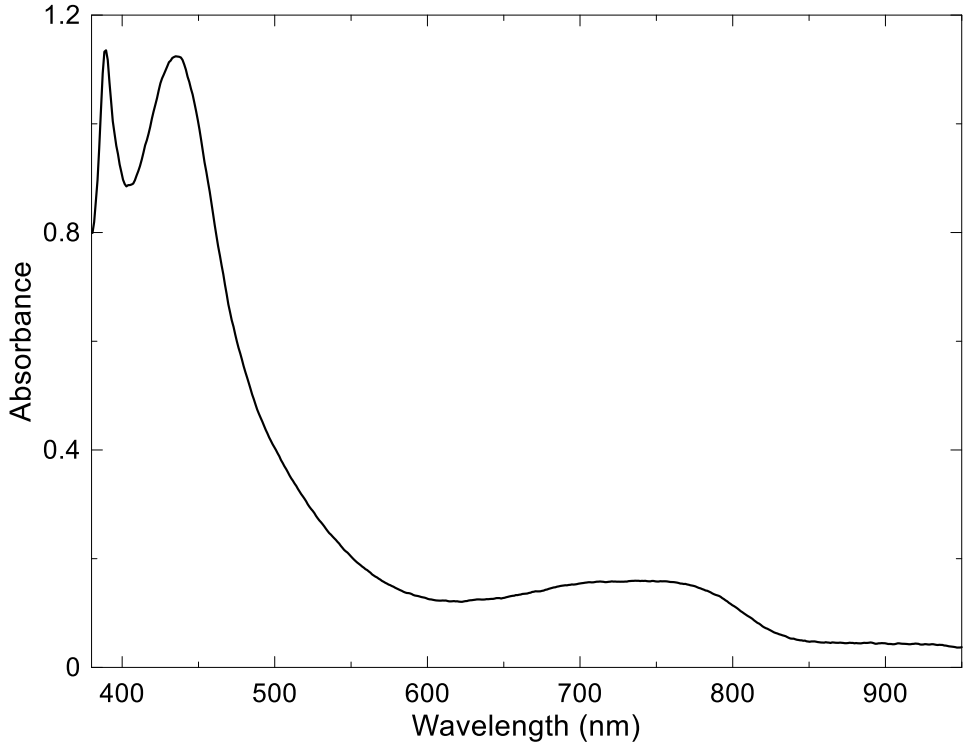

Figure A 32. UV-Vis spectrum (pentane) of **(BiCN$_2$TES)$_2$**.

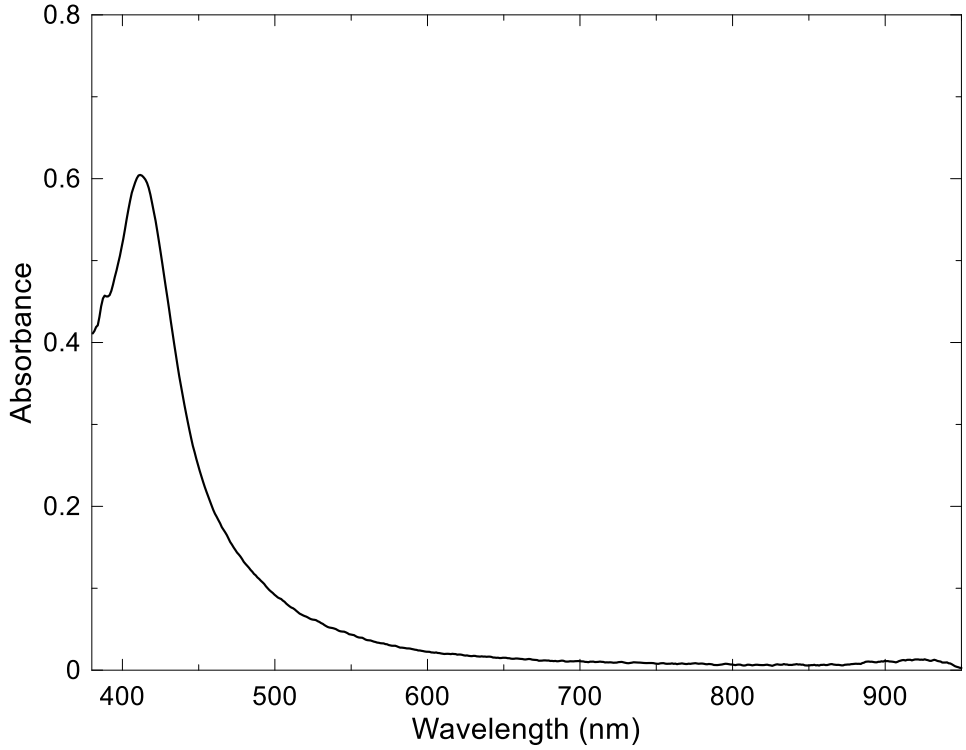

Figure A 33. UV-Vis spectrum (pentane) of **(BiCN$_2$TMS)$_2$**.

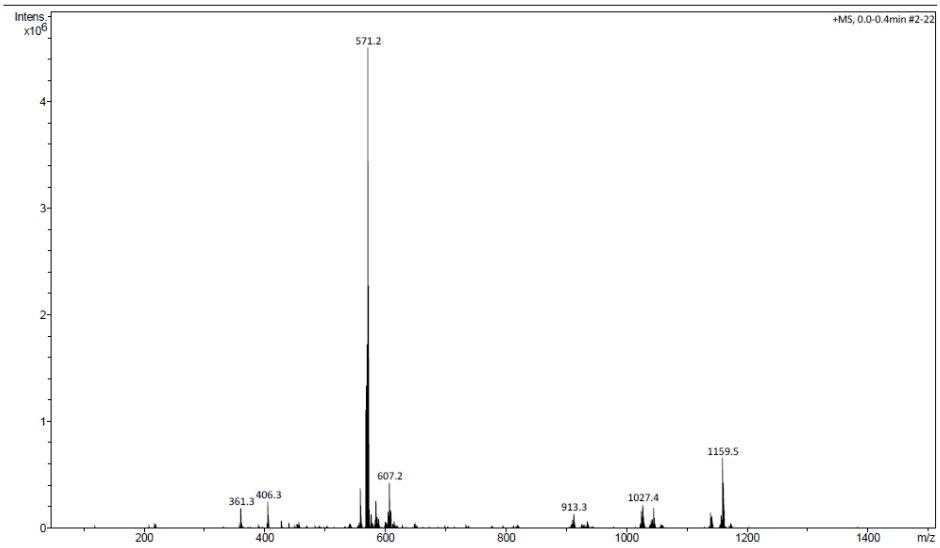

Figure A 34. Full mass spectrum of **(BiCN$_2$TES)$_2$**. Spectrum was run in DCM, using APCI ionization.

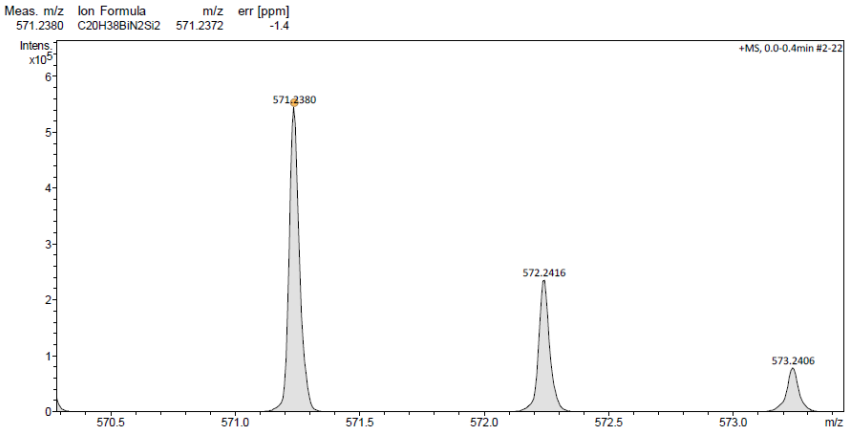

Figure A 35. High-resolution mass spectrum of the peak at m/z of 571.2, corresponding to 2Bi. Spectrum was run using APCI ionization and toluene as the solvent.

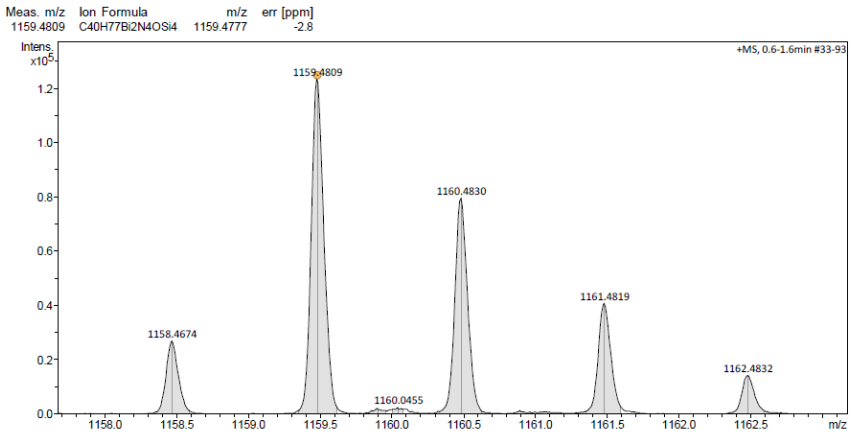

Figure A 36. High resolution mass spectrum of the peak at m/z of 1159.5, corresponding to **(BiCN$_2$TES)$_2$** coordinated to H_3O^+.

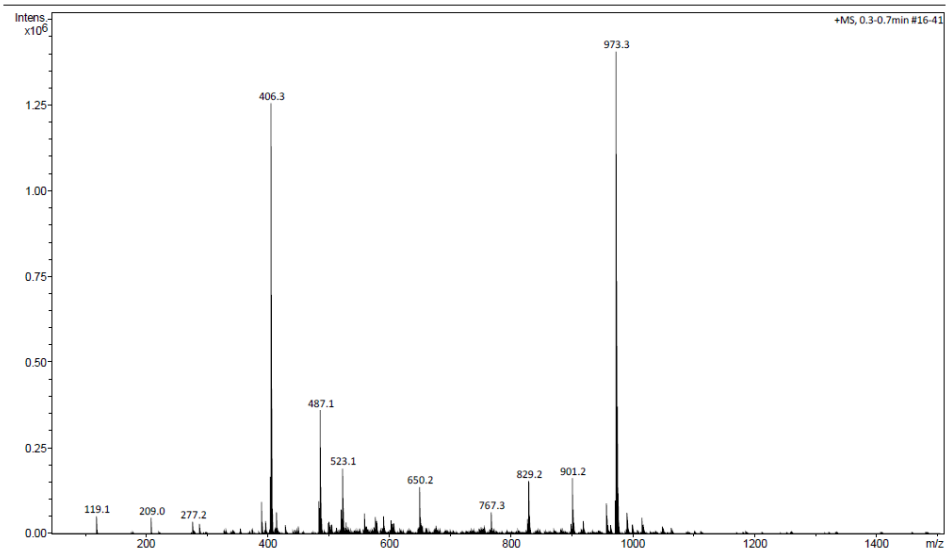

Figure A 37. Full mass spectrum of **(BiCN$_2$TMS)$_2$**. Spectrum was run in DCM, using APCI ionization.

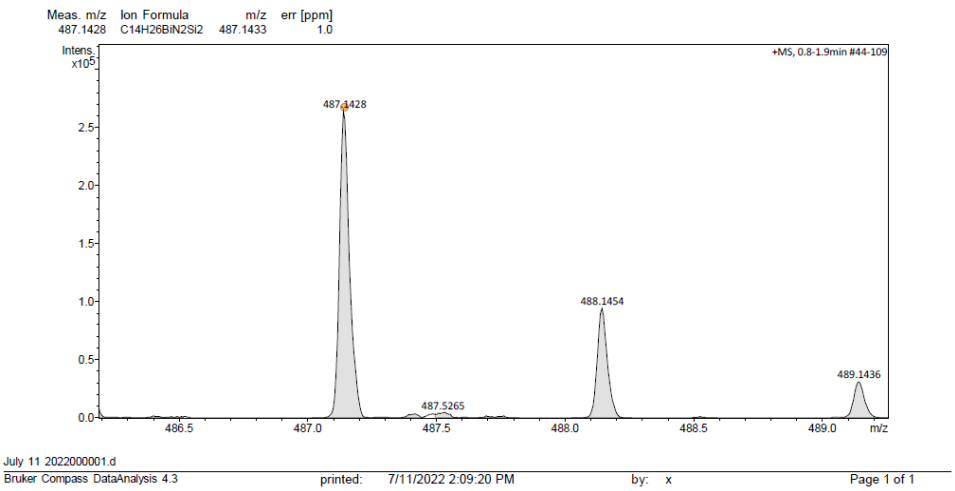

Figure A 38. High-resolution mass spectrum of the peak at m/z of 487.1, corresponding to **1Bi**. Spectrum was run using APCI ionization and DCM as the solvent.

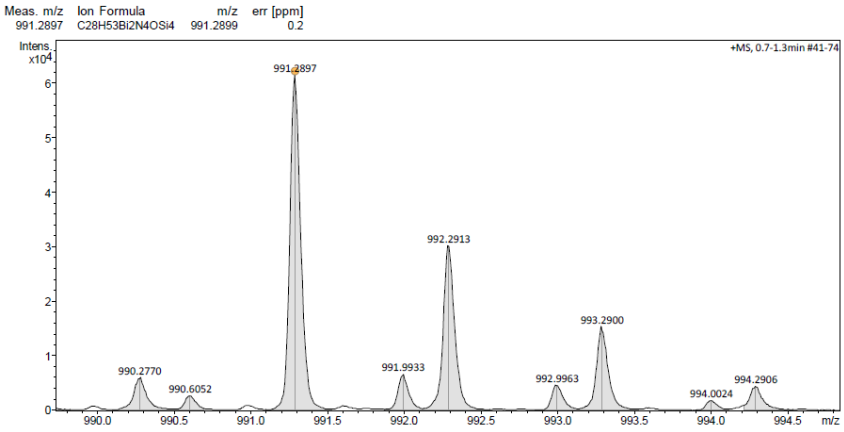

Figure A 39. High resolution mass spectrum of the peak at m/z of 991.3, corresponding to **(BiCN$_2$TMS)$_2$** coordinated to H_3O^+.

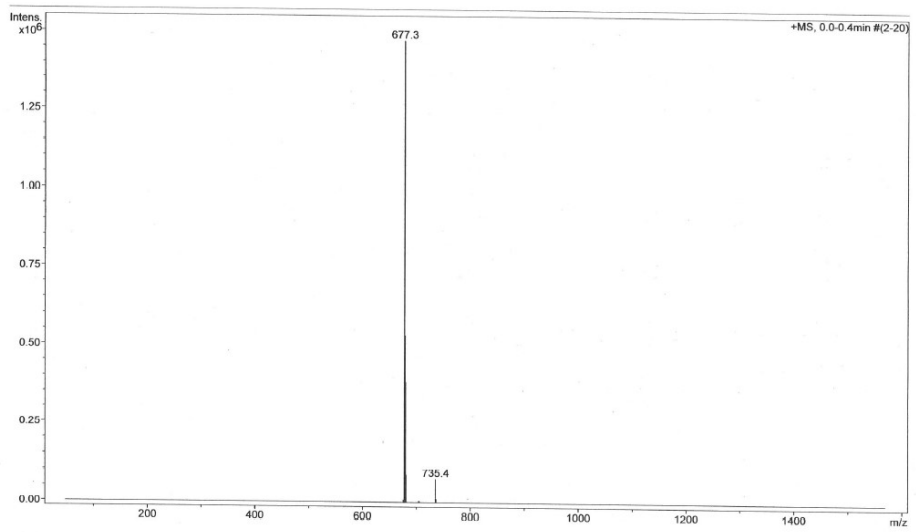

Figure A 40. Full mass spectrum of **3Bi^{red}** compound run in acetonitrile, using ESI ionization.

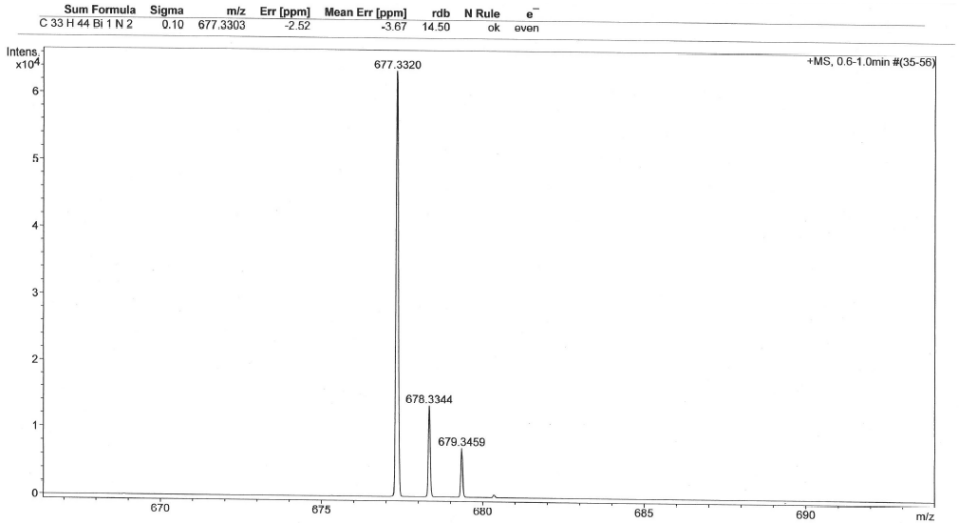

Figure A 41. High-resolution ESI mass spectrum of the peak at 677.3 m/z for **3Bi^{red}**, showing this compound has picked up a methyl group from acetonitrile.

Appendix B: Spectra for Chapter 3

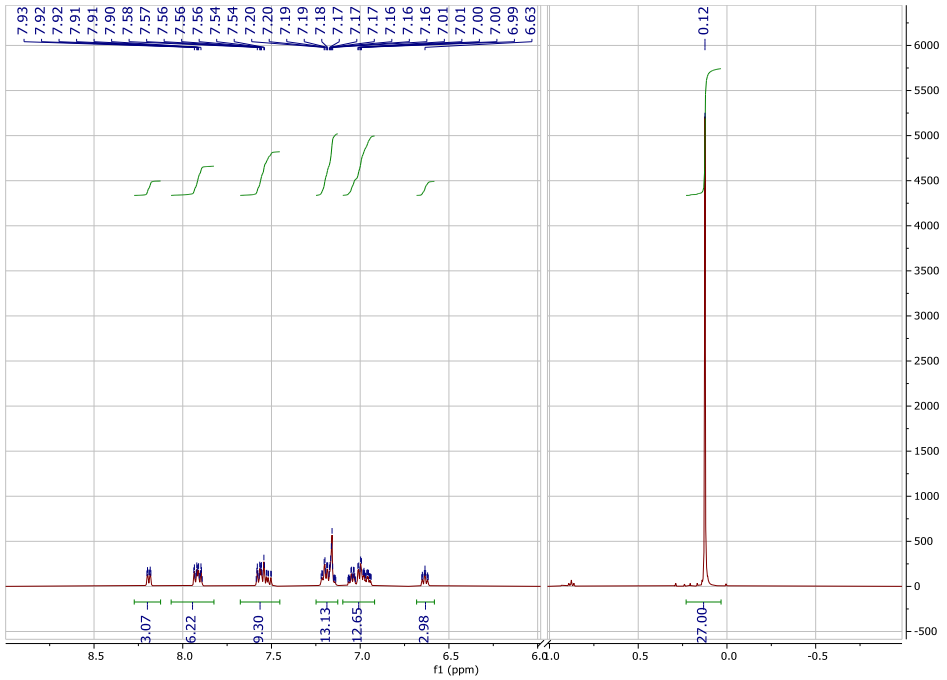

Figure B 1. ^{1}H NMR (C_6D_6, 500 MHz), of tris(Ph_3PNTMS)Bi.

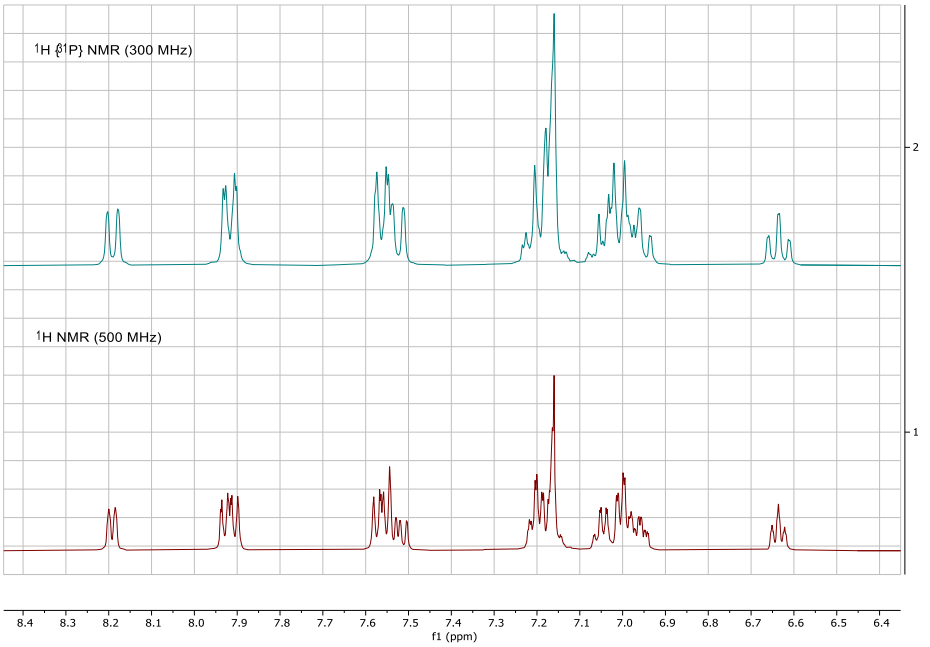

Figure B 2. Stacked ^{1}H NMR's (C_6D_6) of the aromatic region of tris(Ph_3PNTMS)Bi. Top one is ^{31}P decoupled and run at 300 MHz, bottom one is a normal ^{1}H NMR spectrum run at 500 MHz.

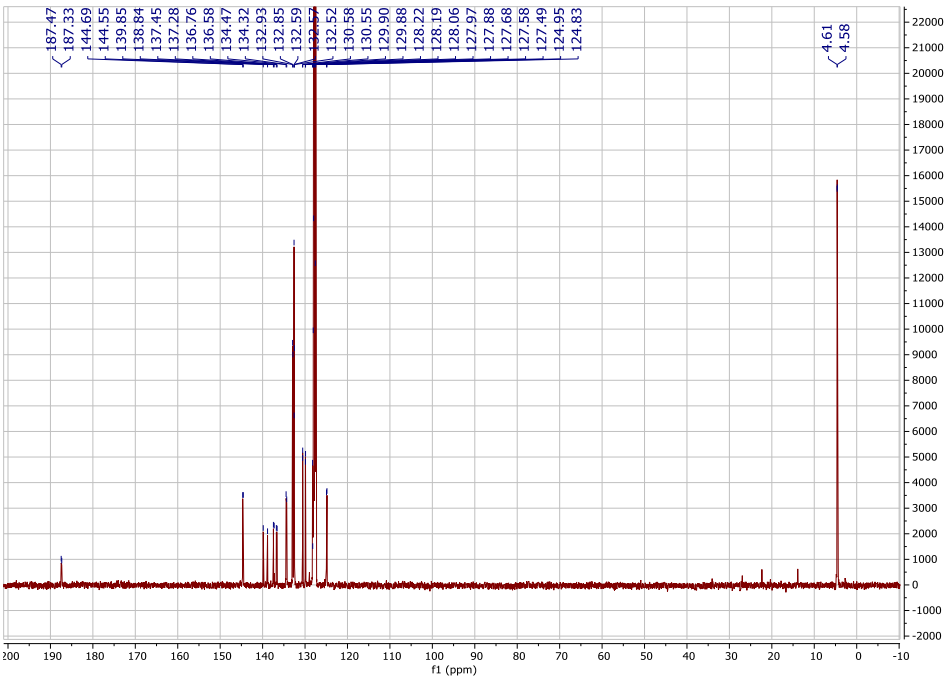

Figure B 3. ^{13}C NMR (C_6D_6, 125 MHz), of tris(Ph_3PNTMS)Bi.

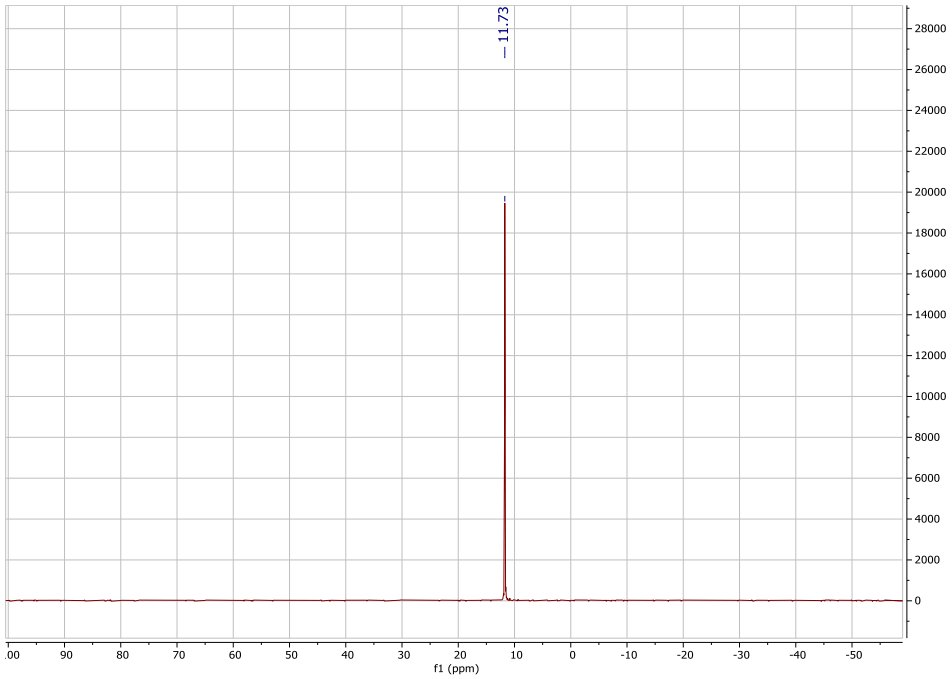

Figure B 4. $^{31}P^{48}$ NMR (C_6D_6, 202 MHz), of tris(Ph_3PNTMS)Bi.

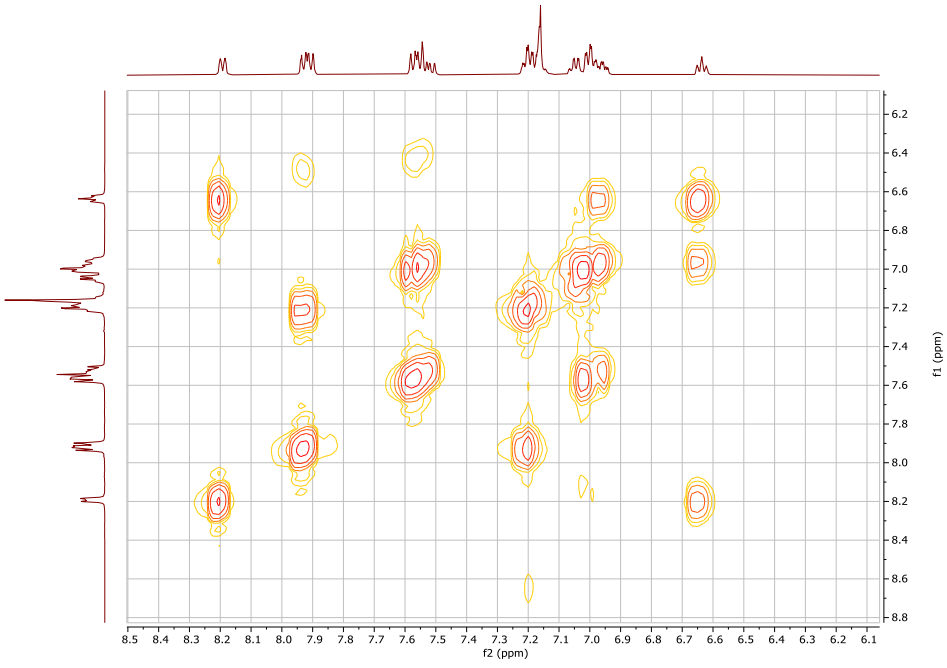

Figure B 5. ^{1}H COSY (C_6D_6, 500 MHz), of tris(Ph_3PNTMS)Bi, zoomed in on the aromatic region.

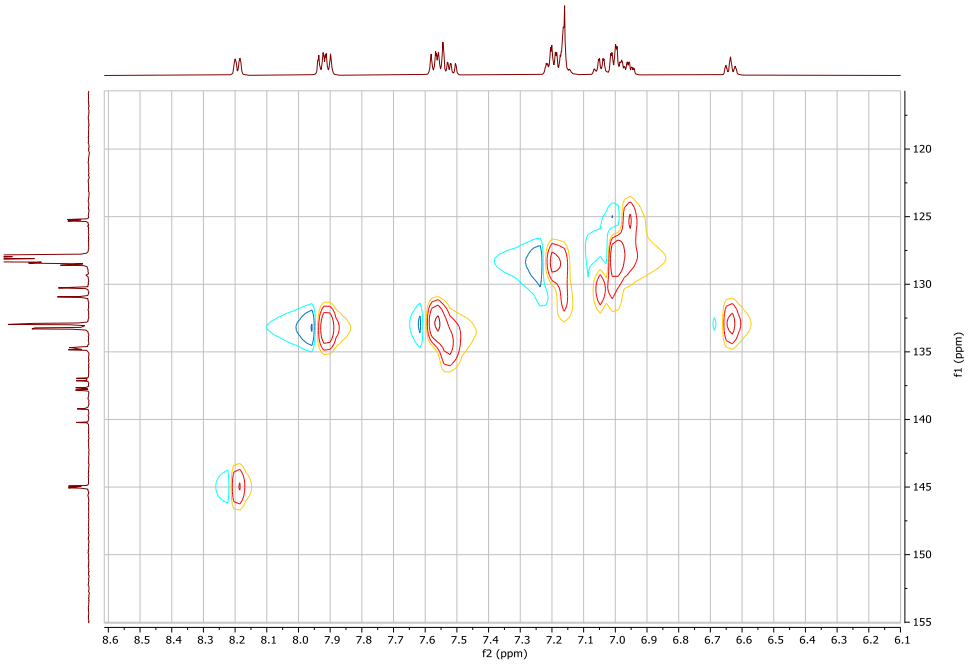

Figure B 6. ^{1}H-^{13}C HSQC (C_6D_6, 500 MHz), of tris(Ph_3PNTMS)Bi, zoomed in on the aromatic region.

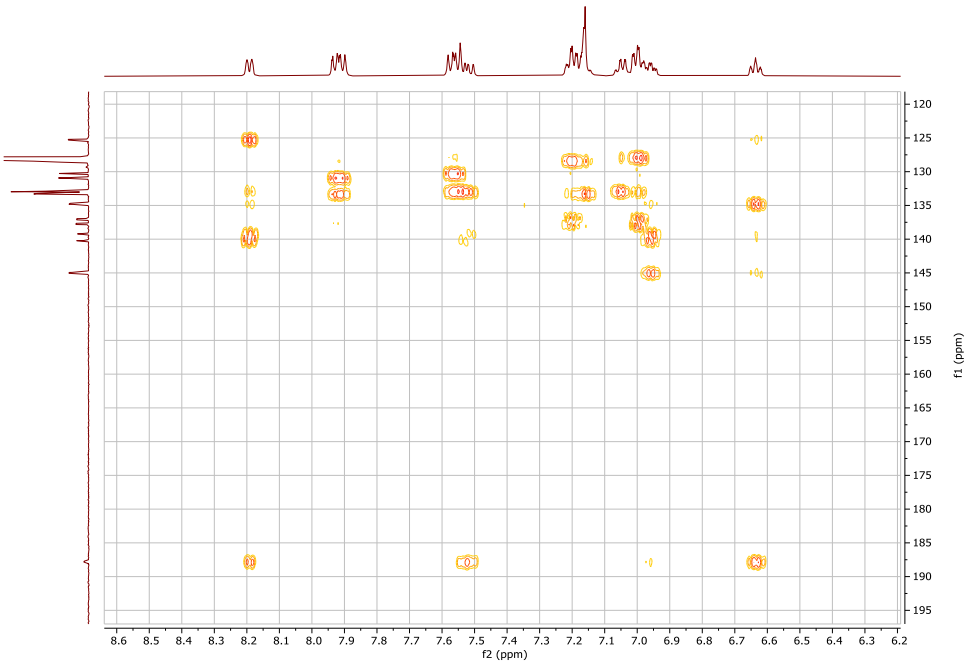

Figure B 7. ^{1}H-^{13}C HMBC (C_6D_6, 500 MHz), of tris(Ph_3PNTMS)Bi, zoomed in on the aromatic region.

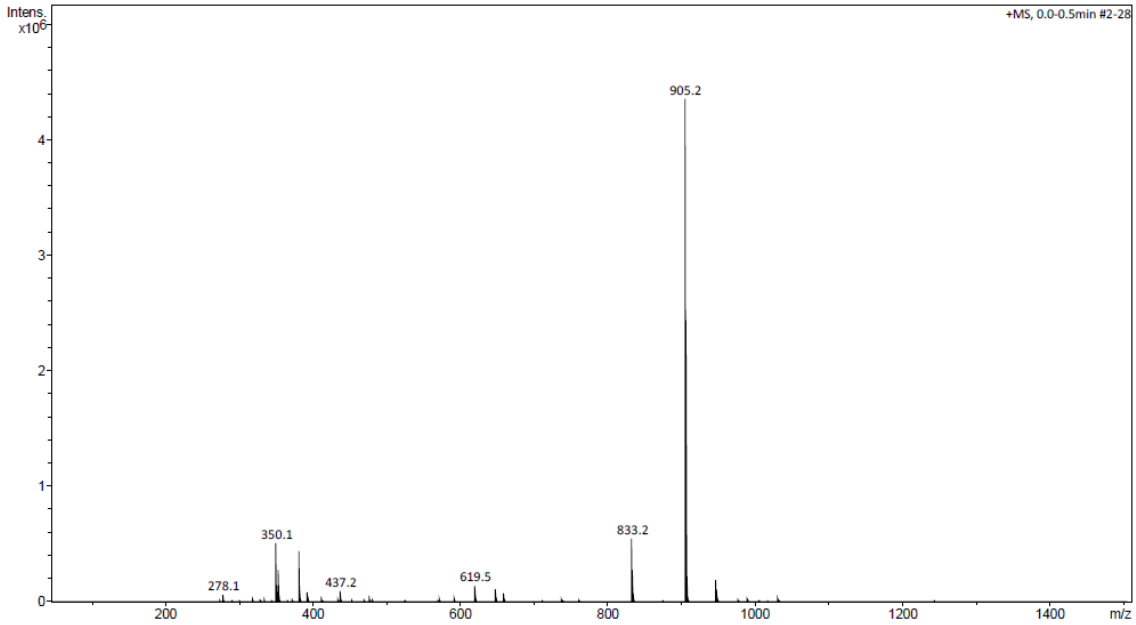

Figure B 8. Full mass spectrum (ESI, toluene) of tris(Ph_3PNTMS)Bi.

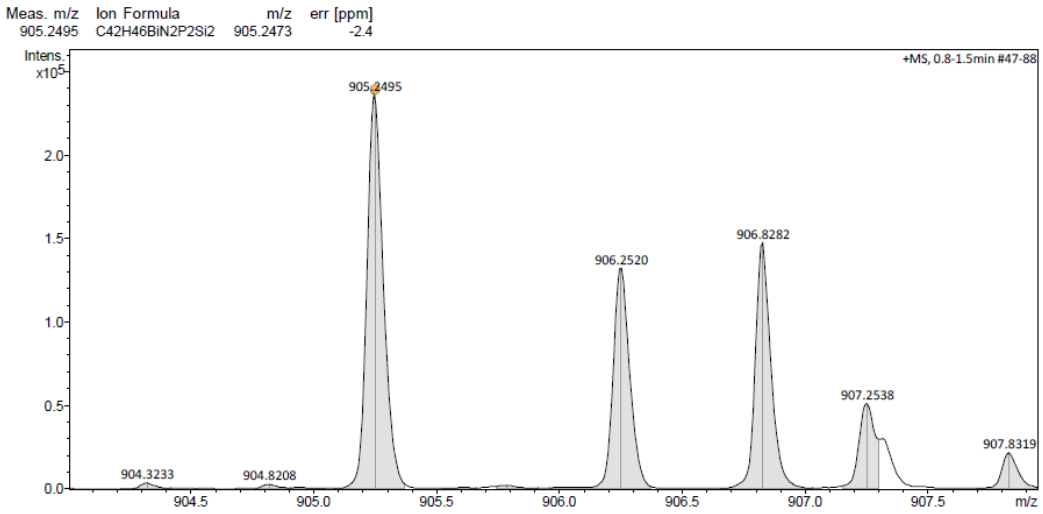

Figure B 9. Zoomed-in mass spectrum (ESI, DCM) of tris(Ph_3PNTMS)Bi for the peak at 905.2495, corresponding to the desired compound.

Appendix C: Computational Details

Computations were performed using Gaussian 16. The functional used was PBE1PBE, using the def2tzvp basis set, with gd3 empirical dispersion. The fluoronium transfer

energy structures were modelled in DCM solvent, while those for H_2 loss and for dimerization were modelled in the gas phase. Large molecules were run using the def2svp basis set, to reduce computational costs. The Cartesian coordinates of each compound are provided in a separate .txt file, and the basis set used for each molecule can also be found in that file.

Appendix D: Copyright Permissions

JOHN WILEY AND SONS LICENSE
TERMS AND CONDITIONS

Nov 02, 2022

This Agreement between Toren Hynes ("You") and John Wiley and Sons ("John Wiley and Sons") consists of your license details and the terms and conditions provided by John Wiley and Sons and Copyright Clearance Center.

License Number	5417090713661
License date	Oct 27, 2022
Licensed Content Publisher	John Wiley and Sons
Licensed Content Publication	CHEMPLUSCHEM
Licensed Content Title	Mesomeric Tuning at Planar Bi centres: Unexpected Dimerization and Benzyl C−H Activation in [CN2]Bi Complexes
Licensed Content Author	Saurabh S. Chitnis, Jason D. Masuda, Toren Hynes
Licensed Content Date	Sep 27, 2022
Licensed Content Volume	0
Licensed Content Issue	0

Licensed Content Pages	1
Type of use	Dissertation/Thesis
Requestor type	Author of this Wiley article
Format	Electronic
Portion	Full article
Will you be translating?	No
Title	MESOMERIC TUNING AT BI CENTRES & THE REUSE OF A WASTE PRODUCT FROM CAGE SYNTHESIS
Institution name	Dalhousie University
Expected presentation date	Nov 2022
Order reference number	1
Requestor Location	Toren Hynes 7 Hartlin Settlement Road Hartlin Settlement, NS B0J2L0 Canada Attn: Dalhousie University
Publisher Tax ID	EU826007151

Terms and Conditions

TERMS AND CONDITIONS

This copyrighted material is owned by or exclusively licensed to John Wiley & Sons, Inc. or one of its group companies (each a"Wiley Company") or handled on behalf of a society with which a Wiley Company has exclusive publishing rights in relation to a particular work (collectively "WILEY"). By clicking "accept" in connection with completing this licensing transaction, you agree that the following terms and conditions apply to this transaction (along with the billing and payment terms and conditions established by the Copyright Clearance Center Inc., ("CCC's Billing and Payment terms and conditions"), at the time that you opened your RightsLink account (these are available at any time at http://myaccount.copyright.com).

Terms and Conditions

- The materials you have requested permission to reproduce or reuse (the "Wiley Materials") are protected by copyright.

- You are hereby granted a personal, non-exclusive, non-sub licensable (on a stand-alone basis), non-transferable, worldwide, limited license to reproduce the Wiley Materials for the purpose specified in the licensing process. This license, **and any CONTENT (PDF or image file) purchased as part of your order,** is for a one-time use only and limited to any maximum distribution number specified in the license. The first instance of republication or reuse granted by this license must be completed within two years of the date of the grant of this license (although copies prepared before the end date may be distributed thereafter). The Wiley Materials shall not be used in any other manner or for any other purpose, beyond what is granted in the license. Permission is granted subject to an appropriate acknowledgement given to the author, title of the material/book/journal and the publisher. You shall also duplicate the copyright notice that appears in the Wiley publication in your use of the Wiley Material. Permission is also granted on the understanding that nowhere in the text is a previously published source acknowledged for all or part of this Wiley Material. Any third party content is expressly excluded from this permission.

- With respect to the Wiley Materials, all rights are reserved. Except as expressly granted by the terms of the license, no part of the Wiley Materials may be copied, modified, adapted (except for minor reformatting required by the new Publication), translated, reproduced, transferred or distributed, in any form or by any means, and no derivative works may be made based on the Wiley Materials without the prior permission of the respective copyright owner.**For STM Signatory Publishers clearing permission under the terms of the STM Permissions Guidelines only, the terms of the license are extended to include subsequent editions and for editions in other languages, provided such editions are for the work as a whole in situ and does not involve the separate exploitation of the permitted figures or extracts,** You may not alter, remove or suppress in any manner any copyright, trademark or other notices displayed by the Wiley Materials. You may not license, rent, sell, loan, lease, pledge, offer as security, transfer or assign the Wiley Materials on a stand-alone basis, or any of the rights granted to you hereunder to any other person.

- The Wiley Materials and all of the intellectual property rights therein shall at all times remain the exclusive property of John Wiley & Sons Inc, the Wiley Companies, or their respective licensors, and your interest therein is only that of having possession of and the right to reproduce the Wiley Materials pursuant to Section 2 herein during the continuance of this Agreement. You agree that you own no right, title or interest in or to the Wiley Materials or any of the intellectual property rights therein. You shall have no rights hereunder other than the license as provided for above in Section 2. No right, license or interest to any trademark, trade name, service mark or other branding ("Marks") of WILEY or its licensors is granted hereunder, and you agree that you shall not assert any such right, license or interest with respect thereto

- NEITHER WILEY NOR ITS LICENSORS MAKES ANY WARRANTY OR REPRESENTATION OF ANY KIND TO YOU OR ANY THIRD PARTY, EXPRESS, IMPLIED OR STATUTORY, WITH RESPECT TO THE MATERIALS OR THE ACCURACY OF ANY INFORMATION CONTAINED IN THE MATERIALS, INCLUDING, WITHOUT LIMITATION, ANY IMPLIED WARRANTY OF MERCHANTABILITY, ACCURACY, SATISFACTORY QUALITY, FITNESS FOR A PARTICULAR PURPOSE, USABILITY, INTEGRATION OR NON-INFRINGEMENT AND ALL SUCH WARRANTIES ARE HEREBY EXCLUDED BY WILEY AND ITS LICENSORS AND WAIVED BY YOU.

- WILEY shall have the right to terminate this Agreement immediately upon breach of this Agreement by you.

- You shall indemnify, defend and hold harmless WILEY, its Licensors and their respective directors, officers, agents and employees, from and against any actual or threatened claims, demands, causes of action or proceedings arising from any breach of this Agreement by you.

- IN NO EVENT SHALL WILEY OR ITS LICENSORS BE LIABLE TO YOU OR ANY OTHER PARTY OR ANY OTHER PERSON OR ENTITY FOR ANY SPECIAL, CONSEQUENTIAL, INCIDENTAL, INDIRECT, EXEMPLARY OR PUNITIVE DAMAGES, HOWEVER CAUSED, ARISING OUT OF OR IN CONNECTION WITH THE DOWNLOADING, PROVISIONING, VIEWING OR USE OF THE MATERIALS REGARDLESS OF THE FORM OF ACTION, WHETHER FOR BREACH OF CONTRACT, BREACH OF WARRANTY, TORT, NEGLIGENCE, INFRINGEMENT OR OTHERWISE (INCLUDING, WITHOUT LIMITATION, DAMAGES BASED ON LOSS OF PROFITS, DATA, FILES, USE, BUSINESS OPPORTUNITY OR CLAIMS OF THIRD PARTIES), AND WHETHER OR NOT THE PARTY HAS BEEN ADVISED OF THE POSSIBILITY OF SUCH DAMAGES. THIS LIMITATION SHALL APPLY NOTWITHSTANDING ANY FAILURE OF ESSENTIAL PURPOSE OF ANY LIMITED REMEDY PROVIDED HEREIN.

- Should any provision of this Agreement be held by a court of competent jurisdiction to be illegal, invalid, or unenforceable, that provision shall be deemed amended to achieve as nearly as possible the same economic effect as the original provision, and the legality, validity and enforceability of the remaining provisions of this Agreement shall not be affected or impaired thereby.

- The failure of either party to enforce any term or condition of this Agreement shall not constitute a waiver of either party's right to enforce each and every term and condition of this Agreement. No breach under this agreement shall be deemed waived or excused by either party unless such waiver or consent is in writing signed by the party granting such waiver or consent. The waiver by or consent of a party to a breach of any provision of this Agreement shall not operate or be construed as a waiver of or consent to any other or subsequent breach by such other party.

- This Agreement may not be assigned (including by operation of law or otherwise) by you without WILEY's prior written consent.

- Any fee required for this permission shall be non-refundable after thirty (30) days from receipt by the CCC.

- These terms and conditions together with CCC's Billing and Payment terms and conditions (which are incorporated herein) form the entire agreement between you and WILEY concerning this licensing transaction and (in the absence of fraud) supersedes all prior agreements and representations of the parties, oral or written. This Agreement may not be amended except in writing signed by both parties. This Agreement shall be binding upon and inure to the benefit of the parties' successors, legal representatives, and authorized assigns.

- In the event of any conflict between your obligations established by these terms and conditions and those established by CCC's Billing and Payment terms and conditions, these terms and conditions shall prevail.

- WILEY expressly reserves all rights not specifically granted in the combination of (i) the license details provided by you and accepted in the course of this licensing transaction, (ii) these terms and conditions and (iii) CCC's Billing and Payment terms and conditions.

- This Agreement will be void if the Type of Use, Format, Circulation, or Requestor Type was misrepresented during the licensing process.

- This Agreement shall be governed by and construed in accordance with the laws of the State of New York, USA, without regards to such state's conflict of law rules. Any legal action, suit or proceeding arising out of or relating to these Terms and Conditions or the breach thereof shall be instituted in a court of competent jurisdiction in New York County in the State of New York in the United States of America and each party hereby consents and submits to the personal jurisdiction of such court, waives any objection to venue in such court and consents to service of process by registered or certified mail, return receipt requested, at the last known address of such party.

WILEY OPEN ACCESS TERMS AND CONDITIONS

Wiley Publishes Open Access Articles in fully Open Access Journals and in Subscription journals offering Online Open. Although most of the fully Open Access journals publish open access articles under the terms of the Creative Commons Attribution (CC BY) License only, the subscription journals and a few of the Open Access Journals offer a choice of Creative Commons Licenses. The license type is clearly identified on the article.

The Creative Commons Attribution License

The Creative Commons Attribution License (CC-BY) allows users to copy, distribute and transmit an article, adapt the article and make commercial use of the article. The CC-BY license permits commercial and non-

Creative Commons Attribution Non-Commercial License

The Creative Commons Attribution Non-Commercial (CC-BY-NC)License permits use, distribution and reproduction in any medium, provided the original work is properly cited and is not used for commercial purposes.(see below)

Creative Commons Attribution-Non-Commercial-NoDerivs License

The Creative Commons Attribution Non-Commercial-NoDerivs License (CC-BY-NC-ND) permits use, distribution and reproduction in any medium, provided the original work is properly cited, is not used for commercial purposes and no modifications or adaptations are made. (see below)

Use by commercial "for-profit" organizations

Use of Wiley Open Access articles for commercial, promotional, or marketing purposes requires further explicit permission from Wiley and will be subject to a fee.

Further details can be found on Wiley Online Library http://olabout.wiley.com/WileyCDA/Section/id-410895.html

Other Terms and Conditions:

v1.10 Last updated September 2015

Questions? customercare@copyright.com or +1-855-239-3415 (toll free in the US) or +1-978-646-2777.
